Barkhausen noise in magnetic thin films

BARKHAUSEN NOISE

IN

MAGNETIC THIN FILMS

N.J. WIEGMAN

BARKHAUSEN NOISE

IN

MAGNETIC THIN FILMS

BARKHAUSEN NOISE IN MAGNETIC THIN FILMS

PROEFSCHRIFT

ter verkrijging van de graad van doctor in de
technische wetenschappen aan de Technische
Hogeschool in Eindhoven, op gezag van de
rector magnificus, prof.ir. J. Erkelens, voor
een commissie aangewezen door het College
van Dekanen, in het openbaar te verdedigen op
dinsdag 6 november 1979 te 16.00 uur

door

Nelie Jansje Wiegman

geboren te Wieringen

DIT PROEFSCHRIFT IS GOEDGEKEURD
DOOR DE PROMOTOREN

Prof.dr. *F.N. Hooge*

en

Prof.dr.ir. *S. Middelhoek*

Aan *Luit*
mijn ouders
Janie en Cornelie

CONTENTS.

1. INTRODUCTION.

1.1. BARKHAUSEN NOISE

The macroscopic behaviour of a ferromagnetic mate-
rial in a magnetic field is represented graphically by the
hysteresis loop which is a plot of the magnetization I/μ_o
against field H. On a microscopic scale the reversal of
the magnetization takes place, however, by two different
effects namely the displacement of the magnetic domain
walls and by the rotation of the magnetization inside the
domains. It is partially an irreversible process so far
as it is caused by the irreversible displacement of the
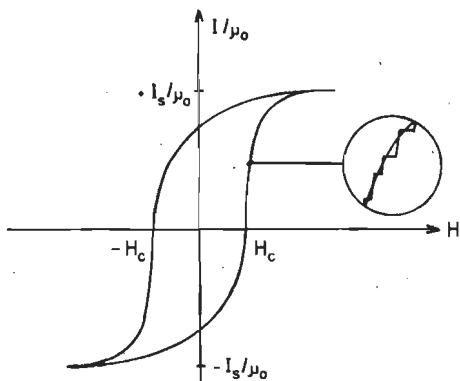
Fig. 1.1. The hysteresis loop with Barkhausen jumps in the region of irreversible wall
displacement.

domain walls. So the magnetization is not a smooth func-
tion of the magnetic field but shows a structure composed
of many individual steps (fig. 1.1.). The first experi-
mental verification of this discontinuous process was
made by Barkhausen in 1919 [1.1] . To explain the Bark-

1

hausen effect we consider the movement of a plane domain
wall in a crystal. The one-dimensional irreversible dis-
placement of a plane domain wall can be described with
the aid of a function $\gamma_w(x)$, which represents the sur-
face energy of the wall as a function of the position
of the wall [1.2], see fig. 1.2. The variation of γ_w
with x is due to the presence of magnetically active dis-
locations, inclusions and voids, of which some can pin
the domain walls (see sec. 5.2.1.). The function $\gamma_w(x)$
depends on the temperature via the magnetic material con-
stants (viz. spontaneous magnetization, anisotropy con-
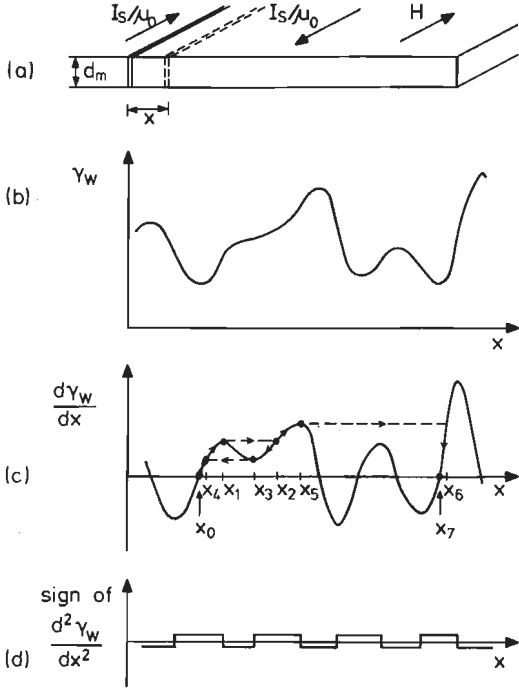
Fig. 1.2. (a) The displacement of a 180° domain wall, (b) the wall energy $\gamma_w(x)$, (c) the
gradient of the wall energy, and (d) the sign of the second derivative of $\gamma_w(x)$, all as a
function of the position of the wall.

stants and saturation magnetostriction) and also on the
distribution of the pinning centres in the sample.

Let us consider the displacement of a plane 180°
wall (the magnetization at both sides of the wall being

2

anti-parallel) in a non-uniform material. The energy per unit of wall area is $\gamma_w(x)$, see fig. 1.2(a) and (b). In the absence of a magnetic field the wall is at rest at some minimum x_0 ($d\gamma_w/dx=0$ and $d^2\gamma_w/dx^2>0$), x_0 being indicated in fig. 1.2(c). If a slowly increasing magnetic field H is applied so that the wall is reversibly displaced to a position x, the energy γ_H per unit area of wall supplied by the magnetic field is

$$\gamma_H = -2I_s H(x-x_0) \qquad [J\,m^{-2}] \qquad (1.1)$$

From the condition of minimizing the total energy γ, with $\gamma = \gamma_w + \gamma_H$,

$$d\gamma/dx = d\gamma_w/dx - 2I_s H = 0 \qquad (1.2)$$

we find for an applied field H an equilibrium position x at which

$$d\gamma_w/dx = 2I_s H \qquad (1.3)$$

In the region of reversible wall displacement ($x_0 < x < x_1$) the restoring force of the wall $(d\gamma_w/dx)_x$ counterbalances the pressure $2I_s H$ of the field. The wall displaces reversibly according to formula (1.3) if $d^2\gamma_w/dx^2 > 0$. In the position x_1 the gradient $d\gamma_w(x)/dx$ of the wall energy $\gamma_w(x)$ is at a maximum because $d^2\gamma_w/dx^2$ becomes negative; without increasing the field the wall then moves irreversibly to x_2. This irreversible wall displacement is called a Barkhausen jump. On slowly reducing the field strength to zero after the wall has reached x_2, a reversible wall motion from x_2 to x_3 takes place. Then x_4 is reached with an irreversible wall jump and the last wall motion from x_4 to x_0 is reversible again. On increasing the field the wall moves from x_2 to x_6 and on decreasing the field again, this wall is reversibly displaced to x_7. The new equilibrium position x_7 is then reached when the field strength is zero.

    To summarize: in the case of an increasing field H, starting from an equilibrium position the domain wall displacement is reversible for $d^2\gamma_w/dx^2 > 0$, while the wall

3

begins to move irreversibly if $d^2\gamma_w/dx^2$ becomes negative just beyond the equilibrium position (fig. 1.2(c) and (d)). This model can be applied to all cases of wall motion in which we may neglect the interaction between different walls and the interaction between different wall segments of one wall.

Many papers have been written about the Barkhausen effect. Stierstadt [1.3] wrote an excellent review of the papers on this subject published until about 1965. The more recent work has been reviewed by Rudyak [1.4], especially the Russian literature, and by McClure and Schröder [1.5]. Lambeck [1.6] discussed the Barkhausen effect in thin films. He reported the behaviour of evaporated thin films of Ni, Fe, Co, 80-20 Ni-Fe and 50-50 Ni-Fe. Using the magneto-optic Kerr-effect (sec. 2.7) and the inductive method he investigated the Barkhausen effect, particularly the magnetic after-effect as a function of temperature. As to the Barkhausen effect he paid attention to the size of the wall jumps as a function of temperature. In the last few years some other brief papers concerning the Barkhausen effect in thin films have been published [1.7-1.12]. As far as we know, no systematic investigation has as yet been published carried out into the characteristics of the Barkhausen effect in thin magnetic films at a constant temperature. The present thesis contains an analysis of the Barkhausen effect in 80-20 Ni-Fe films at room temperature, covering a wide range of thicknesses (400-2800 Å), anisotropy fields (360-1760 A/m) and coercive fields (44-280 A/m).

The investigations performed on the Barkhausen effect can be classified from two points of view. In sec. 1.2 this is done according to the type of measurement carried out, independent of the kind of sample used. We will discuss the possibilities and restrictions of the various methods and the information that can be obtained from them. In sec. 1.3 we shall pay attention to the types

of sample used regardless of the type of measurement. The different geometries of the samples will be discussed and an outline will be given of the detailed knowledge available on their magnetization behaviour. The specific choice of the samples and methods of investigation in the present thesis are discussed in sec. 1.4.

1.2. MEASURING TECHNIQUES

A large number of measurements have been performed in different investigations, which only provide a superficial insight into the behaviour of the Barkhausen effect and the influence of some magnetic and non-magnetic quantities on this effect. This is due largely to the type of samples used. The measuring technique itself allows for a much better insight to be gained, as will be discussed below.

During the magnetization reversal one measures the variation of the magnetization, i.e. the Barkhausen jumps, as a function of the applied magnetic field. The signal to be analysed is shown in fig. 1.3. In principle the investigations can be carried out using three different methods.

(1) The signal is analysed as a function of the applied field, along the hysteresis loop. In doing so the number of Barkhausen pulses (sometimes of different size) is usually plotted as a function of the field [1.3, 1.5, 1.11] . It is possible to determine the temperature dependence [1.13, 1.14] and the structure dependence [1.15] . Sometimes the effects of temperature [1.16] and stress [1.17] are investigated along one branch of the loop or at a constant field. In chapter 4 the number of Barkhausen jumps has been determined of some of our films in terms of the field. The number of pulses of various sizes as a function of the pulse size has also been studied with the

5

field as the parameter.

(2) The second method concerns the Fourier analysis of the Barkhausen signal (see sec. 2.4). One measures the power, integrated over the time it takes to traverse one hysteresis loop, the noise signal being measured as a function of frequency. The experimental noise spectra are approximately given by

$$E(f) \approx \frac{e(f)}{1 + (f/f_o)^n} \qquad [v^2 s^2] \qquad (1.4)$$

in which f_o is the cut-off frequency of the spectrum. The level of the spectrum in the low frequency range $(f < f_o)$ is given by $e(f)$. In some samples $e(f)$ is constant while in other samples $e(f)$ is a slowly decreasing function of frequency. The noise spectrum is a decreasing function of frequency with an f^{-n} dependence in the higher frequency range $(f > f_o)$. The value of n varies in most investigations between 1.5 and 2 [1.5, 1.18-1.20]. The measured slope in the
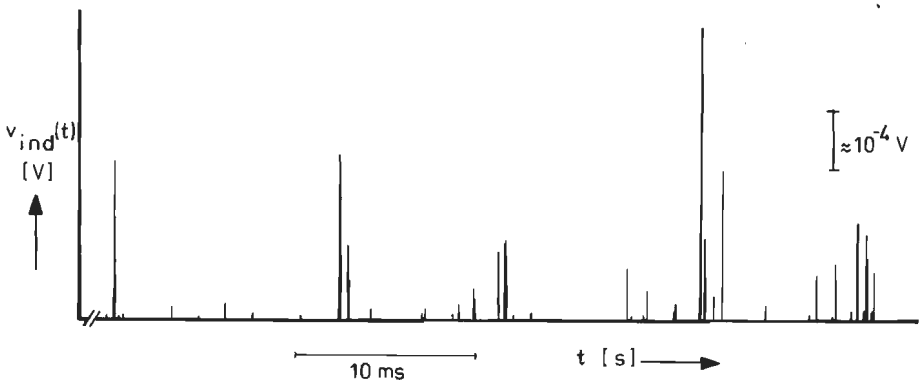
Fig. 1.3. The Barkhausen signal during a small part of the reversal time.

higher frequency range $(f > f_o)$ gives information about any relationship between the parameters of a single pulse, such as the amplitude, time duration and time preceding or following the pulse [1.21, 1.37] However, all phase information contained in the signal

6

is lost in this measuring method.
(3) The third method is a statistical analysis of the be-
    haviour in the time domain concerning all frequency-
    density functions (one- and more-dimensional) of the
    parameters of the signal such as form, amplitude,
    duration and the time preceding or following a pulse
    (see chapter 3). Considering the signal as generated
    by a statistically determined process, one can cal-
    culate the energy spectrum of the noise [1.21] , using
    the frequency-density functions of the pulse parame-
    ters. So one can check the statistical measurements
    by using both methods (2) and (3). Only a very small
    number of papers that deal with this third method
    have been published [1.21]. However, a large amount
    of papers has been written about the pulse-size distri-
    bution and the pulse-duration distribution of differ-
    ent samples [1.5]. Method (3) enables the relations
    between the parameters of a pulse to be examined
    (secs. 3.6 and 3.7). Furthermore, if we use the avail-
    able possibilities for affecting the behaviour of
    the wall jumps in a well-known way, we can obtain
    information about the parameters that determine the
    frequency spectrum. Thus we gain an insight into the
    effect of the physical process on the noise spectrum.

1.3. SAMPLES

    The type of samples on which the Barkhausen effect
has been investigated can be divided into four groups.
(1) Most of the samples used are macroscopic ones, for
    example strips, cores, (laminated) toroids and espe-
    cially wires [1.19-1.24]. Therefore they exhibit a
    three-dimensional magnetic domain structure. The
    Barkhausen effect is generated by microscopic magnet-
    ization changes. It is not possible to establish a
    relation between the Barkhausen effect and the micro-

scopic magnetization behaviour in macroscopic samples, because of the poor knowledge available on the microscopic magnetization behaviour in these samples. Macroscopic influences on the Barkhausen effect, however, such as demagnetization, stress and temperature can be investigated very well [1.13-1.17, 1.22, 1.24-1.28]; on the other hand it is very difficult to assess the influence of these effects separately. Magnetization changes in all three dimensions occur very often in these samples. Only one measurement has been performed in three dimensions by Gründl et al. [1.29]. In the experiments one measures in general only the variations of the magnetization along a single axis. Most investigators are using samples having a small demagnetizing factor owing to a large ratio between length and cross-sectional area. An additional advantage is that usually the resulting large shape anisotropy also causes the magnetization changes to be dominant along the longitudinal axis of the samples.

The large number of wall jumps in bulk samples also presents a difficulty: it is highly probable that physically independent wall jumps generated in different sections of the sample occur at the same time, which give the same signal as that obtained from physically dependent wall jumps. This probability of pulse overlapping can be diminished by applying a very slowly increasing magnetic field and by reducing the size of the sample.

(2) The second group of samples consists of picture frame single crystals. Here no demagnetizing effects occur. The crystals, if cut and polished very accurately, exhibit a two-dimensional domain structure. The number of domain walls during the reversal of the magnetization is small and their magnetization behaviour is very simple [1.30, 1.31].

By using a measuring equipment with dI/dt = constant during the reversal, $\gamma_w(x)$ in these samples can be measured. A disadvantage, however, is that these crys-

tals are not easily accessible for inductive measurements of the wall jumps. Optical measurements of the wall motion are often disturbed by the presence of closure domain structures at the surface of the crystal. Only a small number of investigations into the Barkhausen noise have been performed on picture frame crystals. The results concern properties of $\gamma_w(x)$ instead of properties of the Barkhausen effect itself [1.32-1.34] and must not be compared directly with Barkhausen noise measurements on other samples. When measuring the Barkhausen noise of these samples by the conventional method (see secs. 2.4 and 2.5), the reversal takes place in a few large, mostly reproducible wall jumps. Therefore a statistical study of the general features of the Barkhausen effect cannot be deduced from measurements on picture frame crystals.

(3) Magnetic films constitute another group of samples with a two-dimensional domain structure. The number of Barkhausen investigations has been small so far, as discussed in sec. 1.1, see also [1.35]. A difficulty of these measurements on thin films is due to the poor signal-to-noise ratio caused by the small rotation of the polarization direction of the light, when using the magneto-optic Kerr effect (see sec. 2.7). When using the inductive method (see sec. 2.3). the amount of magnetic material is so small (of the order of 10^{-11} m^3) that it complicates the measurements.

In this thesis we shall confine our investigations to thin metallic films in which the magnetization direction lies in the plane of the film. The micromagnetic behaviour has been the subject of many investigations and is a matter of common knowledge. A review of the properties of these films is given in sec. 2.2. Apart from an extensive knowledge of the behaviour of their domains and walls the use of magnetic films offers other advantages. When the films are thin

9

($d_m \leqslant 5000$ Å) no eddy currents will affect the wall
motion, so that this is determined by spin relaxation
effects only. In the thickness range $d_m < 2000$ Å the
demagnetizing effects are negligible (see sec. 2.2).
In uniaxial thin films the magnetization changes occur
almost entirely along the easy axis. With a pick-up
coil all the magnetization changes can be measured.
(4) Some papers have been published reporting results ob-
tained from powders of small particles [1.35, 1.36].

1.4. SCOPE OF THIS THESIS

In bulk samples the macroscopic magnetic behaviour
can be deduced from the hysteresis curve, whereas a de-
tailed knowledge about the microscopic magnetic behaviour
is mostly absent. The Barkhausen signal is a measure of
the changes of the magnetization on a microscopic scale,
which are not reproducible. The signal consists of pulses
generated by the domain wall jumps. During the reversal
of the magnetization the number of pulses is very large.
Therefore only statistical methods can be used for an
analysis of this signal. If we are able to relate the re-
sults of this statistical analysis to the microscopic mag-
netization behaviour of the domains and domain walls,
then the Barkhausen effect can indeed be used as a method
to obtain information about the microscopic behaviour.
Up to now a systematical study of these connections has
not been reported; the present thesis does cover such a
study. Any relationship between the behaviour of jumping
domain walls and the results of a statistical analysis
of the Barkhausen effect can only be found from certain
types of samples. The microscopic magnetization behaviour
must then be known and the number of Barkhausen jumps
during one reversal must be so large that statistical
methods are applicable. For that reason we choose for
this investigation thin uniaxial Ni-Fe films, as will

be briefly explained in the following.

The Barkhausen effect is caused by the interaction between magnetic domain walls and pinning centres in the material (see sec. 1.1). Some other effects also affect the domain wall motion to disturb the measurement of the Barkhausen effect. These disturbing effects are for example the demagnetizing field, eddy currents, magnetization changes in more than one dimension, overlapping pulses, and the interaction between different domain walls and between different wall segments of one wall. We can avoid most of these effects by the use of thin uniaxial magnetic films with the easy axis of the magnetization in the plane of the film (see sec. 1.3(a)). In many investigations the microscopic magnetization behaviour of these films was studied thoroughly. To relate the results of measurements of the Barkhausen effect to the structure and dynamical behaviour of the domain walls a simple domain structure with a small number of non-interacting walls must be available. However, the number of detectable jumps must be large enough to allow statistical methods of analysis to be used. If the magnetization behaviour can be easily influenced in a well-known way the potentialities of the investigation will increase substantially. Nearly all these aims can be achieved in the thin films we used in our investigation.

We have used all three measuring methods (sec. 1.2). The noise spectrum has been measured with analog measuring equipment. Furthermore the noise signal has been digitized and the shape of the signal recorded on a disc memory. All sorts of measurements described earlier can now be performed very easily. The one- and two-dimensional frequency-density functions have been plotted. The variation of the signal along the hysteresis loop has been measured. The noise spectra can also be calculated from the recorded time series, but for most samples these results are less accurate than those obtained using the analog

11

experimental equipment. Therefore, the calculation has
only been applied to check the two methods using some
appropriate samples. The complete experimental program
has been applied to 52 specimens of 23 different films.
Since we can affect the Barkhausen effect by applying
different fields and films with different thicknesses, the
influence of the physical parameters on the density-
functions and on the noise spectrum can be determined.
In this way a more detailed model for the Barkhausen
effect can be developed.

Lieneweg [1.21] performed measurements of the energy
spectra and determined the frequency-density functions of
the same samples. His measurements show a relationship
between the pulse area (= pulse size) and the duration of
a jump. He used Heiden's theory [1.37] on the influence
on the noise spectrum of a relation between the pulse
parameters. Thus he was able to explain the noise spectra
he measured, but it was not possible for him to relate
his results to the micromagnetic properties of his bulk
samples, consisting of 81-19 Ni-Fe wires. From our meas-
urements, however, it becomes evident that there is a re-
lationship between the results of the statistical analy-
sis of the Barkhausen effect and the micromagnetic behav-
iour as shown in chapters 3 and 5.

The probability of pulse overlapping caused by the
appearance of two physically independent jumps at the same
instant increases with decreasing reversal time (i.e.
time necessary to reverse the magnetization of the sam-
ple) and increases with increasing sample size. In bulk
materials pulse overlapping produced in this way occurs
very often, while in thin films this is scarcely present
at the same magnetizing frequency. In our films only a
small number (about 500) of fast wall jumps occurs dur-
ing the reversal of the magnetization (the sum of the
time durations of the jump ranges between 0.1 and 1% of
the reversal time). In thin films each detected pulse is

caused by one complicated jump of one domain wall
(fig. 1.4). Mostly this pulse can be regarded as a col-
lection of physically strongly coupled single wall jumps:
if a domain wall section jumps away from a pinning centre
and begins to move, this moving wall section causes a
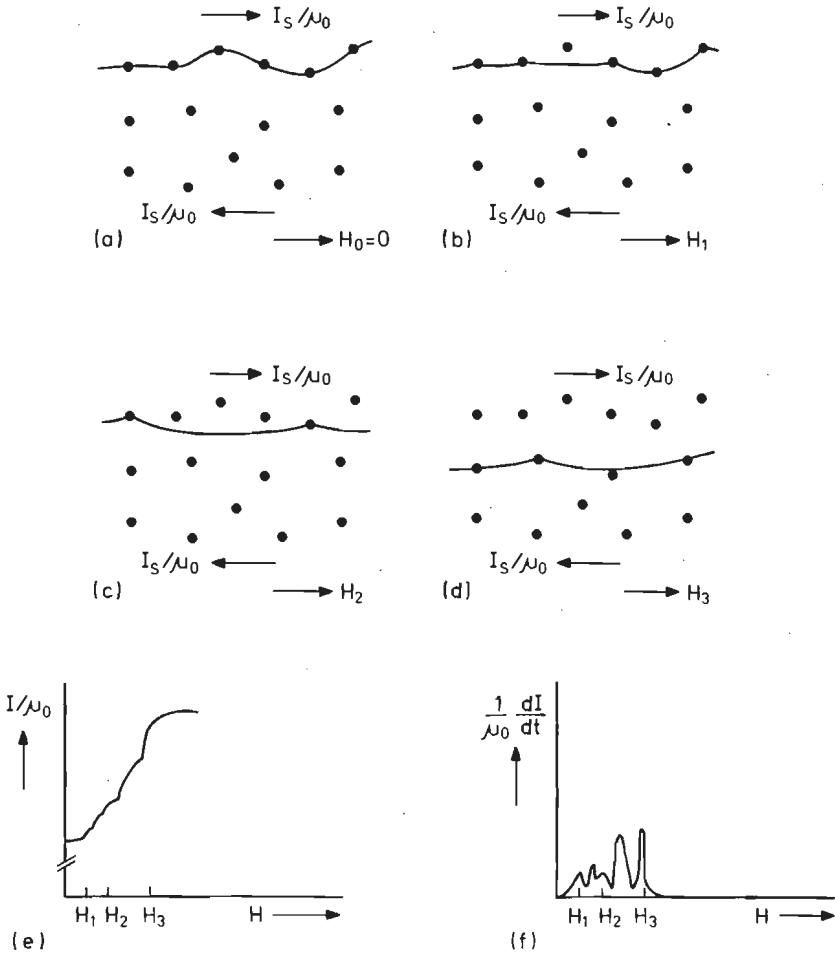
Fig. 1.4.   (a) - (d) Wall motion in a non-uniform sample; (e) the magnetization and (f) the
Barkausen jump $(1/\mu_0)dI/dt$ as a function of the increasing field H.

neighbouring wall section to start moving too, and so on
(fig. 1.4). These single wall jumps are physically
strongly coupled. They generate one pulse in the measur-
ing equipment and, therefore, will be regarded in this

thesis as a single wall jump.

In chapter 2 the properties of our samples and the
experimental methods are described. In chapter 3 the accu-
racy of the measurement of the Barkhausen effect in the
time domain is considered. The form and accuracy of the
one- and two-dimensional frequency-density functions of
the parameters of the Barkhausen pulses are discussed.
The general features of the Barkhausen effect are dis-
cussed in chapter 4, where the reversal of the magnetiza-
tion as a function of the applied field is dealt with.
Measurements of the number and size of the Barkhausen
jumps and the statistics of the pulse parameters are
presented. In chapter 5 the theoretical relation be-
tween the pulse size and pulse duration is derived and
a comparison with the measurements is given. On the basis
of the measured frequency-density functions we can calcu-
late the Barkhausen noise spectra. This is done in
chapter 6, where also a comparison is made between the
calculated and measured noise spectra.

REFERENCES
1. 1   H. Barkhausen, Physik. Z. 20, 1919, p.401-403.
1. 2   E. Kneller, "Ferromagnetismus", Springer, Berlin, 1962, p. 365.
1. 3   K. Stierstadt, Springer Tracts in Modern Physics, 40, 1966, p. 1-106.
1. 4   V.M. Rudyak, Sov. Phys. USP, 13 (4), 1971, p. 461-479.
1. 5   J.C. McClure Jr., K. Schröder, C.R.C. Crit. Rev. Sol. St. Sc. 6 (1), 1976, p. 45-83.
1. 6   M. Lambeck, "Barkhausen Effekt und Nachwirkung in Ferromagnetika", W. de Gruyter & Co,
       Berlin, 1971.
1. 7   N.J. Wiegman, Proc. 4e Int. Conf. Noise in Solid St. Dev. Noordwijkerhout (The Netherlands),
       1975, p. 44-47.
1. 8   N.J. Wiegman, Paper F1.2, 8e Int. Coll. Magn. Thin Films, York (England), 1976, p. 117.
1. 9   N.J. Wiegman, Appl. Phys. 12, 1977, p. 157-161.
1.10   N.J. Wiegman, to be published.
1.11   N.J. Wiegman, R. ter Stege, Appl. Phys. 16, 1978, p. 167-174.
1.12   N.J. Wiegman, to be published.
1.13   K. Stierstadt, E. Pfrenger, Z. Phys. 179, 1964, p. 182-198.
1.14   K. Stierstadt, W. Boeckh, Z. Phys. 186, 1965, p. 154-167.
1.15   P. Deimel, B. Röde, G. von Trentini, J. Magn. and Magn. Mat. 4, 1977, p. 235-241.
1.16   K. Stierstadt, H. – J. Geile, Z. Phys. 180, 1964, p. 66-79.
1.17   K. Stierstadt, E. Preuss, Z. Phys. 199, 1967, p. 456-464.
1.18   H. Bittel, Physica 83B, 1976, p. 6-13.
1.19   M. Celasco, F. Fiorillo, IEEE, Vol. MAG. 10, 1974, p. 115-117.
1.20   L.G.M.M. Lammers, N.J. Wiegman, Phys. Stat. Sol. (a), 35, 1976, p. K45-K47.
1.21   U. Lieneweg, W. Grosse-Nobis, Int. J. Magn. 3, 1972, p. 11-16.

1.22   U. Lieneweg, IEEE Vol. MAG. **10**, 1974, p. 118-120.
1.23   P. Mazzetti, G. Montalenti, J. Appl. Phys. **34**, 1963, p. 3223-3225.
1.24   F. Parzefall, K. Stierstadt, Z. Physik., **224**, 1969, p. 126-134.
1.25   L. Storm, C. Heiden, W. Grosse-Nobis, IEEE. Vol. MAG. **2**, 1966, p. 434-438.
1.26   P. Mazzetti, G. Montalenti, Proc. Int. Conf. Magn., 1964, Nottingham, p. 701-706.
1.27   V. Hajko, A. Zentko, T. Tima, Acta Phys. Slov. **23**, 1973, p. 20-28.
1.28   U. Lieneweg, J. Magn. and Magn. Mat. **4**, 1977, p. 242-246.
1.29   A. Gründl, P. Deimel, B. Röde, H. Daniel, ICM 1976, Amsterdam.
1.30   H.J. Williams, H. Shockley, C. Kittel, Phys. Rev. **80**, 1950, p. 1090-1094.
1.31   G. Hellmiss, Wiss. Ber. AEG-Telefunken **43**, 1970, p. 77-89.
1.32   W. Grosse-Nobis, J. Magn. and Magn. Mat. **4**, 1977, p. 247-253.
1.33   W. Grosse-Nobis, Proc. 4e int. conf. Noise in Solid St. Dev., Noordwijkerhout, (The Netherlands) 1975, p. 36-39.
1.34   J.A. Baldwin Jr., G.M. Pickles, J. Appl. Phys. **43**, 1972, p. 4746-4749.
1.35   See 1.3 p.64.
1.36   V.V. Chekanov, G.I. Yaglo, Sov. Phys. Sol. St., **16**, 1974, p. 1021-1022.
1.37   C. Heiden, Phys. Rev., **188**, 1969, p. 319-326.

2. SAMPLES AND EXPERIMENTAL METHODS.

2.1. INTRODUCTION

In sec. 2.2 of this chapter we consider the general
properties of the samples measured during this investiga-
tion. In sec. 2.2.1 the macroscopic data of the samples
are given. In chapters 4, 5 and 6 we sometimes refer to
features of the wall structure and of the magnetization
behaviour during a reversal, etc. All what can be said
about this behaviour is available in the literature and
is described in secs. 2.2.2 and 2.2.3, as far as this is
used in the present thesis.

Furthermore, in this chapter, the measuring equip-
ment is described. The Barkhausen signal is measured in
this investigation using the inductive method. In sec.
2.3 the pick-up coil circuits are described with which
the Barkhausen jumps during the reversal are measured.
The Barkhausen effect of the thin films has been inves-
tigated both by measuring the noise spectrum of the in-
duced voltage (sec. 2.4) and by recording the noise sig-
nal as function of time (sec. 2.5). The magnetization
behaviour of these films can be observed on a macroscopic
scale by tracing the hysteresis loop (sec. 2.6) and on a
microscopic scale by observing the domain structure
through a microscope (sec. 2.7).

2.2. THE SAMPLES

The properties of our thin films will be described only briefly because there is a large number of papers concerning these films. The general behaviour of thin films is described in many papers and books [2.1-2.6] .

2.2.1. Macroscopic data of the samples

For our measurements of the Barkhausen effect thin magnetic polycrystalline Ni-Fe films have been used. Prof. S. Middelhoek of the Delft University of Technology has kindly supplied the samples. The films had been evaporated on a glass substrate with a thickness of 1 mm. The Ni-Fe samples possess a pronounced shape anisotropy. Therefore, without external fields, the magnetization is in the plane of the film. When the films are evaporated in a homogeneous magnetic field, the easy axis for the magnetization in the whole film coincides with the direction of the applied field: the thin films exhibit uniaxial anisotropy [2.1] . Our films satisfy these conditions.

The thickness and the composition of the Ni-Fe alloy are known from measurements by Middelhoek. The thickness d_m of the films, which were available for our measurements, ranged between 400 and 2800 $\mathring{A}$. As a result of the thinness of the films, walls with their planes parallel to the surface cannot exist. The domain configuration at the surface is representative for the whole film; it has a two-dimensional structure [2.1-2.3] . The Ni-Fe films have a composition of about 74 to 83% nickel. In this range the curves for the crystal anistropy constant K_1 and the magnetostriction coefficient λ pass through zero. At a composition of 74-26 Ni-Fe K_1 is zero while λ is zero at a composition of about 83-17 Ni-Fe [2.7, 2.8] . The Ni-Fe films exhibit small local anisotropy variations. Some of the films contain an additional amount of 10 per cent Co to obtain a high value of the anisotropy constant [2.9] .

When a field is applied along the easy direction
the observed hysteresis loop can be considered to be a
rectangular loop (fig. 2.1a) [2.3] . In this case the
magnetization in the film reverses by wall motion,
showing Barkhausen jumps (fig. 2.1b). The expected form
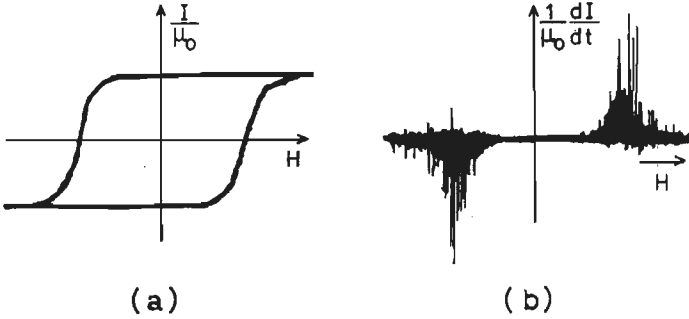
Fig. 2.1. Schematic view of the reversal of the magnetization along the easy axis:
(a) hysteresis loop, (b) Barkhausen jumps.

of the hysteresis loop in the hard direction is shown in
fig. 2.2. If the magnetization is reversed by uniform
rotation the hysteresis loop is a straight line. Experi-
mentally, however, open loops are obtained, which means
that irreversible processes also occur during the reversal
in the hard direction. The irreversible processes are due
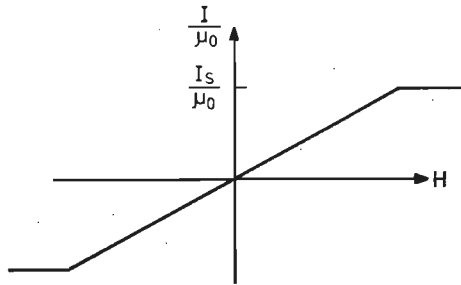
Fig. 2.2. The hysteresis loop along the hard axis.

to the splitting up of the film into an equal number of
clockwise and anti-clockwise rotating domains [2.4] . In
our investigation of the Barkhausen effect the applied

18

magnetic field H is always parallel to the easy axis of the film.

Since the films with a surface area of about 1 cm^2 are thin, the demagnetizing factor in the plane of the film is negligible. The square film is often approximated by an oblate ellipsoid [2.10] , so that the demagnetizing factor N_D of the film is given by [2.8]

$$N_D = \frac{\pi}{4} \cdot \frac{d_m}{a} \qquad (2.1a)$$

where a is the length of the side of the film. For the completely saturated film the demagnetizing field H_{DS} then becomes

$$H_{DS} = -N_D \frac{I_s}{\mu_o} = -\frac{\pi}{4} \frac{d_m}{a} \frac{I_s}{\mu_o} \quad [Vs] \qquad (2.1b)$$

where I_s/μ_o ($\approx 1/\mu_o$ Am^{-1}) is the saturation magnetization. An 80-20 Ni-Fe film with d_m = 1000 Å and a = 1 cm has the following values of N_D and H_{DS}:

$$N_D = 8 \times 10^{-6} \text{ and } H_{DS} = -6 \text{ Am}^{-1} \text{ (} \approx 0.075 \text{ Oe).}$$

This approximation is not valid at the edges of the saturated film, where the demagnetization increases, thus producing small reversed domains (spikes). Owing to the presence of the spike domains the demagnetizing field at the film edges is strongly reduced [2.9] .

During most of the magnetization reversal the hysteresis loop in the easy direction has a differential susceptibility.

$$\chi_{diff} = \frac{1}{\mu_o} \cdot \frac{dI}{dt} = constant \qquad (2.2)$$

which ranges between 7×10^3 and 7×10^4 for our films. The reversible susceptibility, χ_{rev}, is much smaller. As described by Heiden and Storm [2.12] the size of a Barkhausen jump as measured in the pick-up coil must be corrected for the influence of the demagnetizing field. The

correction factor is given by [2.12] as:

$$\frac{1}{1 + N_D X_{ref}}$$ (2.3)

Since $N_D \, X_{rev} \ll 1$ in our samples this effect had no influence on our measurements.

A table containing data of all our measured films is shown in appendix 1. Some macroscopic properties of the films, for example the coercive field H_c, the anisotropy field H_K and the film thickness d_m are given there.

2.2.2. The magnetization process

We will now outline the domain growth and domain structure during the reversal. We observed this growth with the Kerr-effect (sec. 2.7) in our samples. It was found to be approximately the same for all samples.

In the measurements the samples were placed in an external field, which varied linearly with time (see sec. 2.4). This field was always parallel to the easy axis of the films. The value of dH/dt was chosen so small that during a wall jump the applied field could be considered constant. By tracing the major hysteresis loop in this way we measured the quasi-static remagnetization behaviour of the samples.

Owing to the shape of the samples, the demagnetizing field at the edges (normal to the easy axis) of the film was very strong when the film was completely saturated. Therefore, up to very large fields, very small reversed domains were present at the film edges. The saturation along the easy axis of the film occurred just at a field H_{sat} of the order of $0.1 \, I_s / \mu_o$ ($\approx 10^6 / 4 \pi$ Am^{-1}). Upon a small reduction of the applied field from H_{sat} the very small reversed spike domains appeared again. This strongly reduced the demagnetizing field at the edges. The spikes were nucleated at a field H_N at inhomogeneities at the

edges of the film (fig. 2.3a). The volume of the reversed
spike domains formed a negligible part of the total volume
of the film. Upon reducing the applied field to zero and
reversing the field direction, then, at a field $H_{c,min}$,
i.e. the minimum coercive field for wall motion in the
film, the reversal of the magnetization started. On in-
creasing the applied field from $H_{c,min}$ some spikes grew
slowly, while the area of most of them remained constant.
Upon further increasing the magnetic field suddenly, a
fast growth of one or more spikes was observed, which
resulted in reversed domains extending from one side of
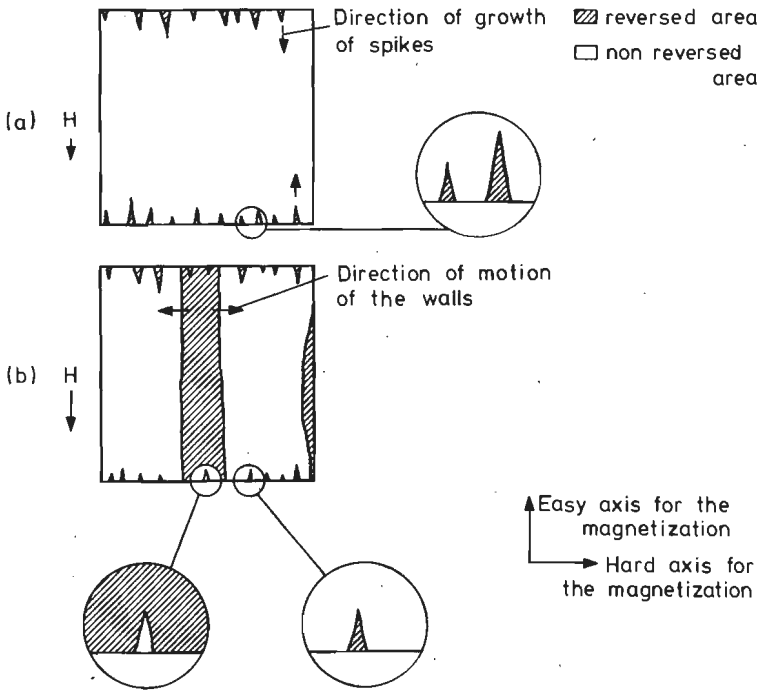
Fig. 2.3. Remagnetization behaviour of the films: (a) spike domains at the edges of the
film and (b) long reversed domains.

the film to the other. Subsequently the reversed area of
the film increased rapidly by lateral wall motion
(fig. 2.3b). In the reversed domains at the edges of the
film small spikes with the original magnetization direc-
tion were present. A new domain could grow in the non-

reversed area from a spike at one of the edges of the
film as long as the film was not completely reversed.
If a non-reversed domain is completely reversed by the
movement of the adjacent walls then these walls disappear.
So with increase of the reversed area of the film the num-
ber of domain walls decreases. The domains grew continu-
ously until almost the whole film was reversed. At $H_{c,max}$,
i.e. the maximum coercive field for wall motion in the
film, the domain growth was virtually completed: only very
small spikes remained. These spikes did not disappear
until the value of the applied field had become very high.
This occurs at the saturation field H_{sat}. The fields
$H_{c,min}$ and $H_{c,max}$ varied between about 20 and 500 Am^{-1}.
All the domain walls were practically parallel to the
easy axis of the film (fig. 2.3).

The total length of the domain walls varied strongly
during the reversal, as will be clear from the previous
description of the reversal process. During the steep
portion of the hysteresis loop the total wall length
mostly varied within about 50% in a single sample. For
the different samples the total wall length at $H \approx H_c$
varied between 2 and 7 times the length of the film side
along the easy axis.

In a few samples the growth of domains from the
spikes was very difficult. In that case the spike growth
only began at a large value of the applied field ($=H_{c,min}$).
The minimum driving field for wall motion in the remaining
part of the sample is much smaller. Thus, when the spike
growth had begun, the jumps at the beginning of the rever-
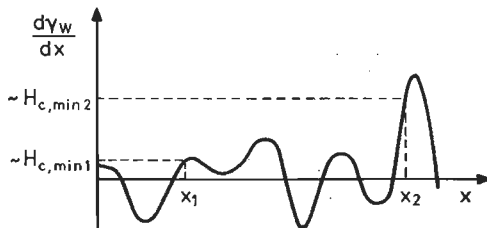
Fig. 2.4. Influence of the minimum coercive field $H_{c,min}$ on the size of the first Bark-
hausen jump.

sal process were very large. This can be explained by using
the potential energy model of sec. 1.1. In fig. 2.4 this is
shown for two values of $H_{c,min}$, namely $H_{c,min1}$ and $H_{c,min2}$
with $H_{c,min2} \gg H_{c,min1}$. The corresponding equilibrium
positions of the wall are denoted by (see eq. (1.3)) x_1 and
x_2, respectively. This situation occurs in samples in
which the macroscopic magnetization behaviour is not uni-
form throughout the entire sample: different parts of the
sample have different hysteresis loops. In this thesis we
refer to such a sample as a macroscopically inhomogeneous
one.

For the field H_{RB} at which the proper reversal begins
we do not take the value of the applied field H at which
the spikes begin to grow, but the value of H at which the
fast growth of the spikes begins. The same procedure has
been followed for the determination of the field H_{RE} at
which the proper reversal is finished. This is shown sche-
matically in fig. 2.5.
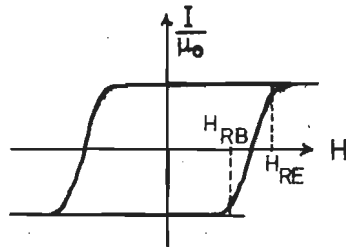
Fig. 2.5. Definition (schematic) of H_{RB}, and H_{RE}.

Mostly the domain growth and structure is in every
reversal reproducible in outline, but the process is not
reproducible in detail. In our measuring equipment we are
not able to identify an inductively measured pulse (see
sec. 2.3), representing a wall displacement, with the
actual wall (section) that has been moved.

2.2.3. The domain walls

In this section we shall describe the different wall
types which occur in thin films. All this information is

available from the literature [2.1-2.5]. Except for the
presentation of the different types of wall, we shall
also discuss the cause of their origin. Our intention is
to show that only the value of the film thickness d_m
determines which type of wall will be present.

In thin Ni-Fe films different types of wall, such
as Bloch, Néel and cross-tie walls occur at different
film thicknesses [2.1, 2.5, 2.11] . Fig. 2.6a shows the
Bloch wall: the magnetization turns around an axis per-
pendicular to the plane of the wall. At the intersection
of the wall with the surface of the specimen, free poles
occur, which lead to stray fields. In bulk specimens the
positive and negative poles are very far apart in compar-
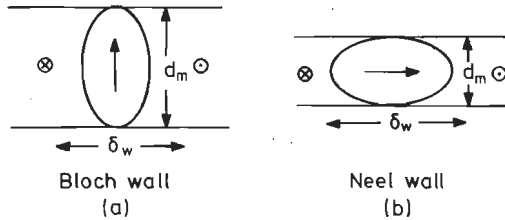
Fig. 2.6.   (a) Cross-section of the Bloch wall; (b) cross-section of the Néel wall.

ison to the wall width,   so that the stray field energy
is relatively small and can usually be neglected. In thin
films, however, the situation is quite different, the
poles are at a distance equal to the film thickness and
high stray fields occur. The result is that the wall
energy in thin 80-20 Ni-Fe films consists mainly of the
energy resulting from these stray fields and the exchange
energy. Therefore the anisotropy energy can be neglected.
Starting with thick films, the stray field energy contri-
bution due to the surface charges of the Block wall in-
creases for decreasing film thickness. At a certain thick-
ness this stray field energy reaches such a high value
that another type of wall, the so-called Néel wall, be-
comes more favourable. This Néel wall (fig. 2.6b) occurs
in very thin films ($d_m < 400$ Å), and is characterized by

the fact that the magnetization in the wall turns around an
axis perpendicular to the plane of the film, in contrast
to the Bloch wall. Just as in the case of Bloch walls the
Néel wall energy consists mainly of the energy resulting
from the stray fields and the exchange energy (except for
extremely) thin films ($d_m < 50$ Å)). Unlike the Bloch wall
energy the Néel wall energy decreases with decreasing
thickness. This occurs until in extremely thin films the
stray field energy contribution disappears. The resulting
wall energy and wall width for Néel walls in very thin
films corresponds to the values calculated for a Bloch
wall in the same material, but in bulk form. From many
observations on domain walls it appears that still an-
other type of wall occurs in thin Ni-Fe films, namely the
so-called cross-tie wall. This type of wall consists of a
chain of crosses, the legs of which are Néel walls (see
fig. 2.7). The cross-tie wall does not represent the
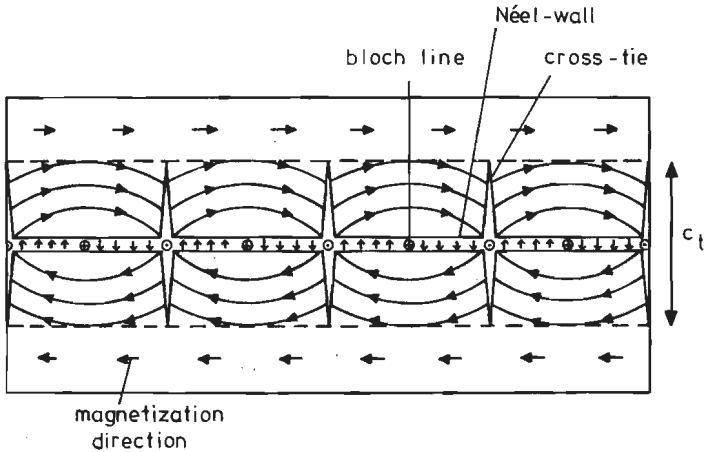
Fig. 2.7. Magnetization distribution round a cross-tie wall.

transition between Bloch and Néel walls, but is rather a
lower energy mode of the Néel wall for all thicknesses.
The cross-tie density of this wall is strongly dependent
on the anisotropy field H_K of the film |2.5| : it is pro-
portional to H_K. At $d_m \approx 900$ Å the cross-tie wall and the
Bloch wall have the same energy, and therefore at this

thickness a transition between Bloch and cross-tie walls
will occur. In fig. 2.8 the surface energies γ_w of the
Bloch, the Néel and the cross-tie walls are plotted as
functions of the thickness d_m. In the cross-tie wall,
the energy of the Bloch lines which separate the posi-
tive and negative Néel wall segments have been neglected.
The influence of the Bloch line energy for very thin
films is shown by the dashed line in fig. 2.8.
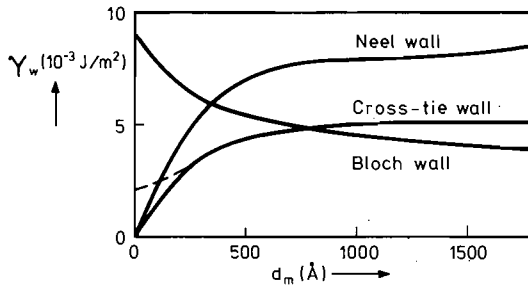
Fig. 2.8. Energy per unit area of a Bloch wall, a Néel wall and a cross-tie wall (solid line: without considering the energy of the Bloch lines; dashed line: including the energy of a small number of Bloch lines) as a function of the film thickness d_m (after [2.11]).

From the previous discussion it is evident that the
transition of one wall type to the other at decreasing
thickness is due to the facts that the contributions to
the domain wall energy of the exchange energy, the stray
field energy and the anisotropy energy vary with film
thickness in a different way. Thus at a certain film
thickness the domain wall structure with a minimum energy
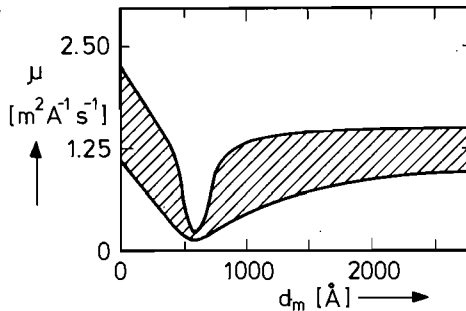
Fig. 2.9. Band containing the wall mobility μ of about 50 films as a function of the film-thickness d_m (modified from [2.13]).

26

is determined only by the value of the film thickness
(and the anisotropy constant).

The domain wall mobility μ [2.13] is also substan-
tially dependent on the film thickness d_m. Fig. 2.9 shows
μ as a function of d_m. In the thickness range where the
cross-tie wall occurs a strong variation of the wall mo-
bility is measured.

The thickness range of our films lies between 400 and
2800 Å. It thus covers the total thickness range in which
cross-tie walls are present, and the thickness range of
about 900 to 2800 Å, where Bloch walls are stable. Films
with Néel walls ($d_m < 400$ Å) were not available.

2.3. PICK-UP COIL CIRCUIT

For thin magnetic films (thickness 400-2800 Å) it is
not possible to locate the pick-up coil so close to the
sample as is necessary for measuring the total flux of
the sample only. Because of the presence of the substrate
(thickness 1 mm) the total flux measured is the sum of
the film flux and the much larger air flux. A calculation
of the air flux Φ_{air} and the film flux Φ_{film} of the pick-
up coils gives the following values for a 80-20 Ni-Fe film
with a thickness of 1000 Å:

$$\Phi_{film} / \Phi_{air} < 5 \% \qquad (2.4)$$

The air flux can be compensated by a proper coil arrange-
ment [2.14] . Therefore a second coil is mounted, which
is connected to the pick-up coil in such a way that the
voltage due to the air flux is compensated. It is diffi-
cult to match the coils exactly and therefore a small
coil is added, which can be rotated through 180°. Another
disturbance is attributed to variously distributed capac-
itances of the coils. This signal can be compensated by
an adjustable aluminium sheet close to one of the coils,
which induces a voltage in the coils which sign is oppo-

site to that of the signal due to the capacitances (see fig. 2.10).

In all our measurements the pick-up coil was oriented so that it measured the changes of the magnetization directed along the easy axis of the films. A consequence of the large size of the pick-up coil with respect to that of the samples is that the flux of the thin film is not linked entirely with the pick-up coil because part of the flux lines close within the pick-up coil cross-section [2.15] . This effect has also to be taken into account in the calibration of the equipment. The "transfer" factor of the pick-up coil was determined by comparing the measured and calculated values of the change of the magnetic moment at a complete reversal of the magnetization. In our pick-up coil about 75% of the flux of the magnetic film is picked-up.
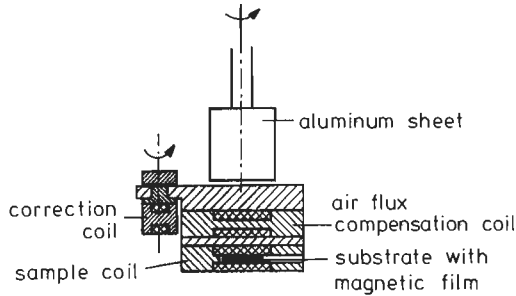
Fig. 2.10. Cross-section of the pick-up coil circuit.

The difference in the measured air flux of the pick-up coil (1375 turns) and the air flux compensation coil is very small. The coils can be connected in series as well as in parallel and their circuit diagrams are shown in fig. 2.11. The impedance of the cable and the first amplifier are designated as C_A and R_A, while R_p is used to obtain a critically damped system. Because $C_A \gg C_s$, where C_s is the capacitance of the coil, the resonance frequency f_o of the undamped system in the series and parallel circuits satisfies $(f_o)_p \approx 2(f_o)_s$. In the low frequency range it is the series circuit that has the most

favourable signal-to-noise ratio, whereas in the higher
frequency range (below $(f_o)_p$) the parallel circuit is the
most favourable one. The frequency at which the signal-
to-noise ratio of both coil circuits are equal depends on
the first amplifier. The higher frequency range is the
most difficult region for measurements of the Barkhausen
noise. Furthermore the series resonance frequency just

(a)

(b).
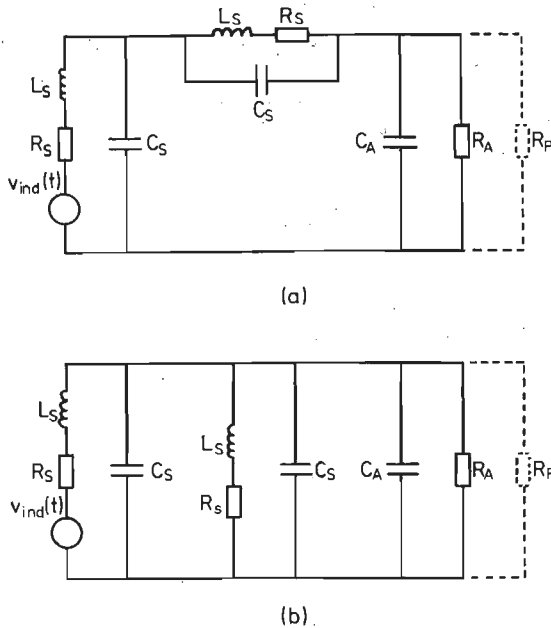
Fig. 2.11. Circuit diagram of (a) the serial pick-up coil circuit and (b) the parallel pick-up
coil circuit.

lies within the measuring range. Therefore we used the
parallel pick-up coil circuit in all our measurements.
The consequence of the use of the parallel pick-up coil
circuit is that the flux of the magnetic film to be picked-
up is reduced by a factor of two: the pick-up coil cir-
cuit has a "transfer-factor" of about 0.5x0.75=0.38.

In our measurements we used two different pick-up
coil circuits, which can be specified by their capacitance
C_s, inductance L_s and resistance R_s. The noise spectra
(sec. 2.4) were measured in the frequency range 10 Hz to

100 kHz. For the measurement of the noise spectrum the
pick-up coil circuit P.U.I can be characterized by
$L_s \approx 5$ mH, $C_s \approx 40$ pF, $R_s \approx 100\,\Omega$, $C_{cable} \approx 100$ pF and
$(f_o)_p \approx 200$ kHz. For the analysis of the Barkhausen noise
signal in the time domain (sec. 2.5) we recorded the digi-
tized signal as a function of time on a disc memory.
In the latter measurements we used a damped pick-up
circuit P.U.II with a fast response, so that the meas-
uring coil has hardly any influence on the shape of the
induced voltage pulses [2.16] . P.U.II has the following
specifications: $L_s \approx 5.5$ mH, $C_s \approx 3$ pF, $R_s \approx 123\,\Omega$,
$C_{cable} \approx 10$ pF and $R_p \approx 4.4$ kΩ . The resonance frequen-
cy of the undamped system is $(f_o)_p \approx 510$ kHz. The low
value of the coil capacitance is realized by dividing the
space available for the turns into six parts and by plac-
ing an insulating foil between each pair of two layers
of turns [2.17] .

2.4. THE MEASUREMENTS OF THE NOISE SPECTRUM

For the measurement of the Barkhausen effect the
pick-up coil circuit containing the magnetic film was
placed in a magnetic field generated with the aid of a
Helmholtz coil pair (see fig. 2.12). In Helmholtz coils
the field is highly uniform. The field generated by a
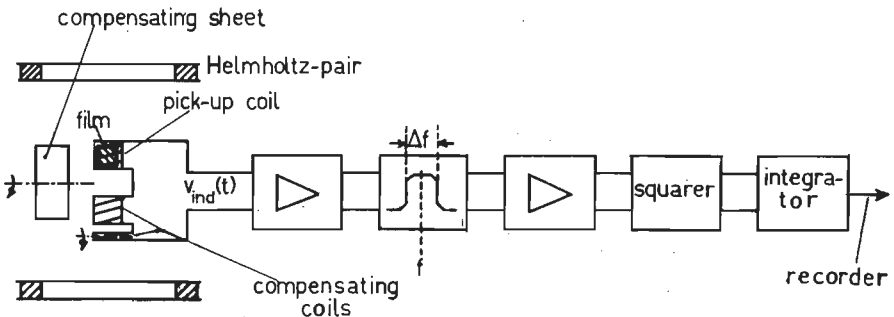
Fig. 2.12. Schematic diagram of the equipment for the measurement of the noise spectrum.

Wavetek function generator (model 142) was swept linearly
in time along the hysteresis loop at a magnetizing fre-
quency $f_{FIELD} = (T_{FIELD})^{-1}$ of 5×10^{-2} Hz or lower. The
maximum field value of 560 A/m was so high that the films
were nearly saturated. This field was directed parallel
to the easy axis of the film. A second Helmholtz pair
was placed perpendicular to the first pair. With these
coils, which are omitted in fig. 2.12, it was possible
to apply a field in the hard direction of the film. The
driving magnetic field generated as just described is
also used in the analysis of the Barkhausen noise in the
time domain (sec. 2.5) and in the domain observations
(sec. 2.7). In the latter, however, the magnetizing fre-
quency was lower by a factor of about 10.

Spectra of the Barkhausen noise were obtained by the
usual methods as shown in fig. 2.12. The Barkhausen noise
signal measured in the pick-up coil circuit P.U.I (see
sec. 2.3) was supplied to the first amplifier. This is
either a Brookdeal 9431 (20 kΩ, 25 pF) nanovolt amplifier
with an equivalent input noise resistance R_{eq} of about
40 Ω (above 1 kHz) or a Brookdeal 9453 (100 MΩ, 20 pF)
low noise amplifier with $R_{eq} \approx 1$ kΩ (above 300 Hz). A
selective amplifier PAR 189 (or PAR 210 A) with a rela-
tive bandwidth Δf around the central frequency f with
$\Delta f/f \geqslant 0.01$ was mostly used as bandpass filter. A Tele-
dyne Philbrick 4353 squaring element (in combination with
two operational amplifiers 1027 of Philbrick) was used for
the determination of the power of the induced voltage. The
noise spectral density integrated over several hysteresis
loops was measured with an integrating circuit, using a
Philbrick operational amplifier 142603. In the figures
(see chapter 6) we have plotted the ensemble average E(f)
over 40 to 60 hysteresis loops of this integrated noise
spectral density, converted to a film thickness of 1000 Å:

$$E(f) = \frac{1}{\Delta f} \left(\frac{1000}{d_m}\right)^2 \int_0^{T_{field}} \{v_{ind}(t)\}^2 \, dt \qquad [v^2 s^2] \qquad (2.5)$$

with $\Delta f = \pi/2 \; (f/Q)$ the noise bandwidth,

   Q the quality factor of the selective amplifier,

   d_m (in $\mathring{A}$) the film thickness,

   e denotes the ensemble average,

   $v_{ind}(t)$ the voltage induced in the pick-up coil
            circuit.

The Nyquist and $1/f$ noise of the measuring equipment has
been integrated too. In every measurement the dc-offset of
the integrator was adjusted so that the integrated back-
ground noise was just counterbalanced by the integrated
dc-offset voltage of the integrator. With this noise elim-
ination, method it is even possible to measure a sample,
which only produces a Barkhausen noise power equal to
about one per cent of the background noise power.

   The experimental results of these measurements are
shown and discussed in chapter 6.

2.5. THE MEASUREMENT IN THE TIME DOMAIN

   By measuring noise spectra, one obtains information
only about the energy of the induced voltage as a function
of frequency. All phase information of the noise signal is
lost. We obtain a good approximation of the real situation
if we regard the noise signal as a stationary sequence of
independent pulses (see sec. 4.3) with for a single pulse
a relation between the pulse parameters: amplitude, dura-
tion and the time period preceding or following the pulse.
The relationship between the pulse parameters is described
by the joint frequency-density function of all pulse para-
meters. The measured frequency-density functions of the
pulse parameters enable us under a few assumptions to cal-
culate the noise spectrum [2.18] (see chapter 6). By com-
paring the calculated and the measured noise spectra the
assumptions made will be checked. Furthermore the frequen-
cy-density functions give information about the origin of

any relationship between the parameters of the physical process of the Barkhausen noise.

In fig. 2.13 the magnetizing field H and the Barkhausen jumps $1/\mu_o (dI/dt)$ are plotted as functions of time. The same figure shows the I/μ_o-H loop of a thin film. The rectangular hysteresis loop which is characteristic for thin 80-20 Ni-Fe films, results in a small reversal time of the magnetization. At a magnetizing frequency of 5×10^{-2} Hz (see sec. 2.4) the reversal time varies between 0.1 sec. and 1 sec. Owing to the large value of the wall mobility μ the wall jumps will be very fast. With our fast pick-up coil P.U.II (see sec. 2.3) we can measure pulse time durations which exceed about one microsecond. Therefore for the investigation in the time domain we have chosen for a digital analysis of the Barkhausen noise with a sampling frequency of 1 MHz. In general the content of the Barkhausen noise spectrum for
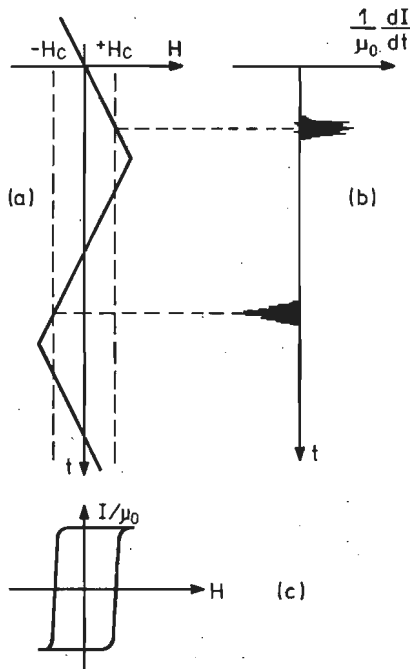
Fig. 2.13. The magnetizing field H (a) and the Barkhausen noise (b) as a function of time; (c) the I/μ_0 - H loop of a thin film.

$f > \frac{1}{2} f_{sampling}$ is smaller than 5% of the total content of the spectrum. Thus according to the sampling theorem, information up to 0.5 MHz can be obtained with this equipment.

Using as the first amplifier a Brookdeal 9453 low noise amplifier (bandwidth 1 MHz) and after further amplification, the induced voltage is applied to a combination of a 8 bits Analog- to- Digital Convertor (Datel ADC G 8B 3C) and a Sample- and- Hold circuit (Teledyne Philbrick 4855), sampling the noise signal at a frequency of 1 MHz. This means that during one reversal of the magnetization 10^5 to 10^6 data are needed to record the information contained in the signal. To investigate the statistical nature of the Barkhausen noise the number of hysteresis loops needed ranges between 10 and 30 implying an analysis of a number of data varying between 2×10^6 and 2×10^7. This presents two practical problems:(1) how to send on-line an 8 bits signal of 1 MHz over a distance of 500 m to a computer and(2) how to store such a number of data in view of the long processing time of the computer.

The two problems were solved simultaneously by making use of the special shape of the signal during the reversal. A characteristic Barkhausen noise signal is shown in fig. 1.3. Only during a small part of the reversal time does the signal differ from zero. Using this property of the signal we can reduce the amount of data during one reversal to a number between 2×10^3 and 10^4, as shown in the following part of this section: a reduction by a factor of 10^2.

The reduction of information is carried out in the "Barkhausen Computer Interface" [x] (fig. 2.14) [2.19]. To reduce the influence of the background noise we detect

[x] Published in: R. ter Stege, N.J. Wiegman, "Equipment for the investigation of the statistical properties of the Barkhausen effect", J. Phys. E: Sci. Instrum. 11, 1978, p. 791-794.

the signal only if it exceeds some adjustable reference
band around zero. This band is variable in steps of 40 mV
(one of the 128 levels of the ADC). To this reference level
we will refer in the following description as zero. Every
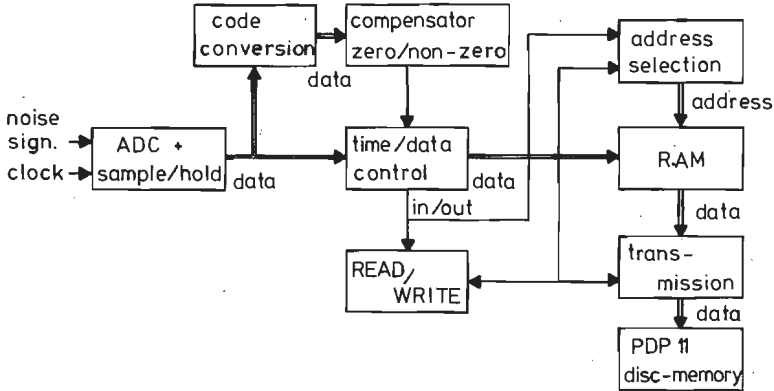
Fig. 2.14. Block diagram of the "Barkhausen Computer Interface".

microsecond a sample is taken. When the sampled value is
different from zero, this value is sent to a Random Access
Memory (10K words of 9 bits) organized as a first-in first-
out memory. If the sampled value is zero, a counter is
started, which counts the number of samples with zero
value. In the Barkhausen Computer Interface the time coun-
ter consists of four 2^8 counters in series. At the moment
that the sample differs again from zero the counter is
stopped. An extra bit is added to the counted number of
samples (consisting of four or less words of 8 bits) indi-
cating that these words represent a time duration and not
a sampled signal value. Then, using a time/data control
unit with a buffer memory, these numbers of nine bits are
transported to the RAM. The next number in the RAM consists
of the first non-zero sampled value of the signal after
this time interval as also are the following numbers. The
memory capacity of the RAM (10K words of 9 bits) is such
that all information about one reversal of the magnetiza-
tion can be stored in the memory. A flat cable of 70 m
length connects the transmission unit of the Barkhausen

35

Computer Interface with a Digital Equipment PDP 11 comput-
er. At the moment that a zero sampled value is detected,
no data are fed to the RAM. At the same moment the read-
out procedure of the first-in first-out RAM is started.
Information is transmitted to the PDP 11 with a maximum
velocity of 5000 words per second up to the moment at
which a non-zero value of the signal is detected. The
PDP-11 computer stores the received data in a disk memory;
after the measurement the stored information is copied on
a tape memory. Via another PDP-11 computer the data are
transmitted to a Burrough B7700 computer. This computer
carries out the statistical analysis of the Barkhausen
noise.

This equipment enables us to analyse the Barkhausen
effect in the time domain up to frequencies of 500 kHz,
i.e. to determine the frequency-densities of the pulse
(jump) parameters (see chapter 3), to calculate the
noise spectrum from the density functions (see chapter 6)
and to investigate the features of the Barkhausen effect
along the hysteresis loop (sec. 4.2). Furthermore it gives
a method to investigate the stationarity of the signal
(sec. 4.3).

2.6. HYSTERESIS LOOP TRACER

The basic circuit of a hysteresis loop tracer for
materials with a small flux change during reversal was
first proposed by Crittenden [2.14]. A block diagram of
our hysteresis loop tracer is shown in fig. 2.15. The
driving fields are generated by two pairs of Helmholtz
coils which axes are perpendicular to each other. This
enables hysteresis loop recording in the presence of a
dc-field perpendicular to the driving field. The current
through the coils comes from a function generator or from
the main supply (50 Hz) via a variable transformer. An

insulating transformer is used to prevent short-circuits.
The film which lies in a revolving film holder, is brought
into a pick-up coil, which output is proportional to
$d\Phi/dt$. The performance of this large pick-up system is
in principle the same as that of the small pick-up coil
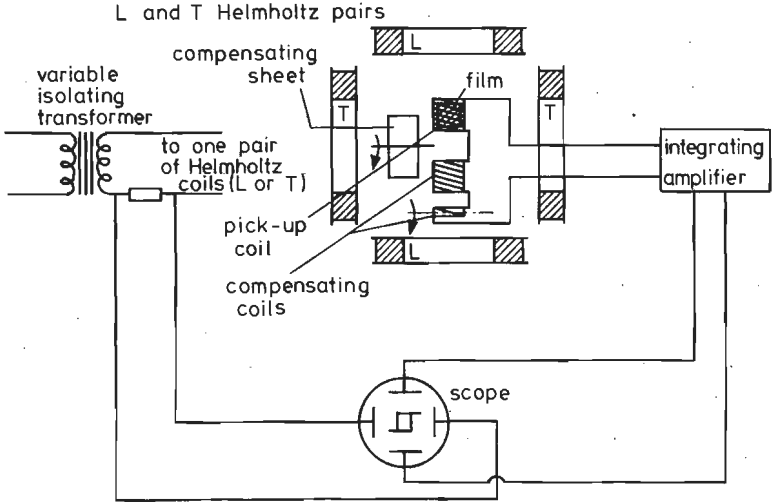
Fig. 2.15. Block diagram of the hysteresis loop tracer.

circuits described in sec. 2.3. The amplified output sig-
nal of the pick-up coil can either be observed directly
on the screen of an oscilloscope, or be fed into the in-
put of an integrator. The output signal of the integra-
tor, which is proportional to the component of the magnet-
ization parallel to the axis of the pick-up coil, is fed
to the vertical amplifier of an oscilloscope. The voltage
on the horizontal input of the oscilloscope is obtained
from a resistance in the driving circuit and is propor-
tional to the field. In fig. 2.1 the output signal of the
pick-up coil before integration (b) and after it (a) is
shown. Barkhausen jumps appear in the non-integrated sig-
nal of the film in the easy direction.

2.7. OBSERVATION OF THE DOMAIN STRUCTURES

For the observation of the domains in the film the
Kerr magneto-optic effect is used [2.2] . When linearly
polarized light is reflected by a ferromagnetic sample,
the plane of polarization is rotated through an angle
which depends on the magnetization direction in the sam-
ple. An analyzer can be adjusted in such a way that the
light reflected from one kind of domains is extinguished.
We adopted the longitudinal effect: the magnetization was
in the plane of the film and parallel to the plane of in-
cidence (fig. 2.16).
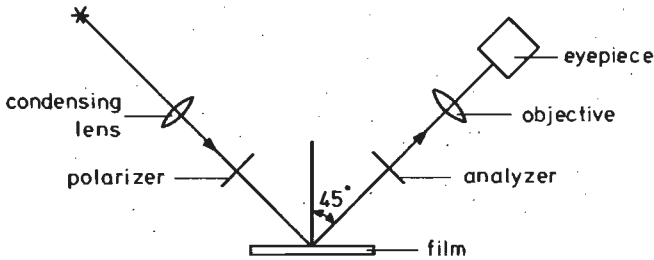
Fig. 2.16. Diagrammatic representation of the observation of domains with the magneto-
optic Kerr effect.

The difference in angle of light rotation of domains
magnetized in opposite directions is very small. It is
about 5 minutes for the longitudinal effect. Magnification
of the effect by a factor of about 10 is obtained by evap-
orating a thin layer of SiO_2 on the film, because of the
multiple beam interference thus obtained. This coating
was also used in our experiments.

REFERENCES
2. 1   M. Prutton, "Thin Ferromagnetic Films", Butterworths, London, 1964.
2. 2   R. Carey, E.D. Isaac, "Magnetic Domains and techniques for their observation",
       Ac. Press, New York, 1966.
2. 3   S. Middelhoek, in J. Smit (ed.), "Magnetic properties of materials",
       McGraw-Hill, New York, 1971, p. 263 - 339.

2. 4   S. Middelhoek, IBM J. Res. & Dev. **6**, 1962, p. 394 - 406.
2. 5   S. Middelhoek, J. Appl. Phys. **34**, 1963, p. 1054 - 1059.
2. 6   S. Middelhoek, D. Wild, IBM J. Res. & Dev. **11**, 1967, p. 93 - 105.
2. 7   E.L. Boyd, IBM J. Res. & Dev. **4**, 1960, p. 116.
2. 8   E. Kneller, "Ferromagnetismus", Springer, Berlin, 1962.
2. 9   E.M. Bradley, J. Appl. Phys. **33**, 1962, p. 1051S - 1057S.
2.10   F.B. Humphrey, F.W. Reynolds, G.R. Stillwell, Proc. of the Fifth National Symposium
       on Vacuum Technology, San Fransisco 1958, p. 204 - 211.
2.11   S. Middelhoek, "Ferromagnetic domains in thin Ni-Fe films", Thesis, University of
       Amsterdam, 1961.
2.12   C. Heiden, L. Storm, Z. Angew. Phys. **21**, 1966, p. 349 - 354.
2.13   S. Middelhoek, IBM J. Res. & Dev. **10**, 1966, p. 351 - 354.
2.14   E.C. Crittenden Jr, A.A. Hudimac, R.I. Strough, Rev. Sc. Instr. **22**, 1951, p. 872 - 877.
2.15   H.J. Oguey, Rev. Sc. Instr. **31**, 1960, p. 701 - 709.
2.16   R.S. Tebble, I.C. Skidmore, W.D. Corner, Proc. Phys. Soc. London, **A63**, 1950,
       p. 739 - 761.
2.17   R. Feldtkeller, "Theory der Spulen und Überträger", Hirzel Verlag, Stuttgart, 1963.
2.18   U. Lieneweg, W. Grosse-Nobis, Int. J. Magn. **3**, 1972, p. 11 - 16.
2.19   R. ter Stege, N.J. Wiegman, J. Phys. E: Sci. Instrum. **11**, 1978, p. 791 - 794.

3. MEASUREMENT OF THE FREQUENCY-DENSITY
   FUNCTIONS.

3.1. INTRODUCTION

During the reversal of the magnetization the voltage, induced in the pick-up coil circuit by a wall jump has the shape as shown in fig. 3.1. The signal can be described
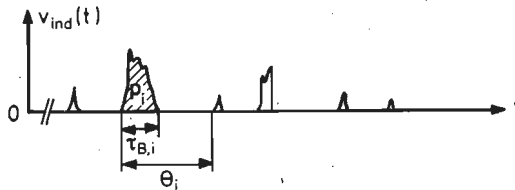
Fig. 3.1. The voltage, $v_{ind}(t)$, induced in the pick-up coil system by the Barkhausen jumps.

mathematically by four parameters, i.e. the pulse size p, the pulse duration τ_B, the time period θ during and follow-ing a pulse and the time t at which the wall motion starts, as defined in fig. 3.1. In our equipment the applied mag-netic field H varies linearly with the time t. So instead of

$$t_i = \sum_{j=0}^{i-1} \theta_j \qquad [s]$$

we can use equally well the quantity H_i, i.e. the applied field at which the i-th jump begins. This will be done in chapter 4. The statistical behaviour of these parame-ters has been measured with the Barkhausen Computer Inter-face [3.1.] Results of these measurements will be discuss-ed in the next sections [3.2, 3.3] .

40

In sec. 3.2 the sensitivity of the measurements in
the time domain is considered. In sec. 3.3 some general
comments are made on the frequency-density functions of
the pulse parameters, namely on the notation and meas-
uring method. In our investigation we have determined all
one- and two-dimensional frequency-density functions of
the pulse parameters p, τ_B and θ. In this chapter the form
of the two-dimensional frequency-density function of p and
τ_B (sec. 3.4), and of the one-dimensional frequency-den-
sity functions of p, τ_B and θ (secs. 3.5 to 3.7) is dis-
cussed at length. We have observed that there was no rela-
tion between p and θ or between τ_B and θ (see sec. 3.7).
All frequency-density functions are determined per hyste-
resis loop, which is always traced with the same frequency
(0.05 Hz) and the same value of dH/dt (112 $Am^{-1}s^{-1}$).

3.2. THE SENSITIVITY OF THE MEASUREMENT IN THE TIME DOMAIN

The general behaviour of the Barkhausen effect has
been investigated by a time domain analysis [3.1] . The
background noise of the equipment is almost completely
eliminated by using a symmetrical reference voltage around
zero (see sec. 2.5). By this method pulses with an ampli-
tude h smaller than the reference voltage are not detected.
In the investigation a sampling frequency of 1MHz was used
which permits a minimum pulse duration of 1 μs to be detect-
ed. In view of the presence of the background noise of the
equipment we have chosen the value of 2 μs (i.e. two sam-
pled values exceed the reference voltage) for the minimum
detectable value ($\tau_{B,det})_{min}$ of τ_B. Summarizing one can
say that a pulse is only detected if both h and τ_B exceed
their previously given minimum detectable values. If the
value of $\theta_i - \tau_{B,i}$, i.e. the time interval between success-
ive jumps (see fig. 3.1), is less then 1 μs , then these
jumps are detected as one wall jump. Thus for the time
period θ following a pulse we have to do with a minimum

41

detectable value $(\theta_{det})_{min}$ of 3 μs. This gives a systematic error at small p and τ_B values: the number of pulses measured there is too small.

For the different samples the amplification differs from measurement to measurement. The background noise increases with amplification and it is necessary to increase the reference voltage too. As a consequence at the output of the Analog Digital Convertor the minimum detectable amplitude $(h_{det})_{min}$ varies between 40 and 280 mV for the different samples. The pulse size p is defined as

$$ p = \frac{1000}{d_m} \int_{1\,jump} |v_{ind}(t)| \, dt \qquad (d_m \text{ in } \text{Å}) \quad [vs] \qquad (3.1) $$

The pulse size in eq. (3.1) is normalized on a film thickness of 1000 Å and thus proportional to the jump area. In the films a two-dimensional domain structure is present, therefore to compare experimental results of different films the surface areas of the wall jumps were considered in our measurements. The minimum detectable value of p, $(p_{det})_{min}$, depends on $(h_{det})_{min}$ and τ_B. It is given by

$$ (p_{det})_{min} = \frac{1000}{d_m A_v} (h_{det})_{min} \tau_B \qquad \text{for } \tau_B \geqslant (\tau_{B,det})_{min} \qquad (3.2) $$

where A_v denotes the amplification of the equipment. With increasing τ_B the value of $(p_{det})_{min}$ increases also. We shall return to this in secs. 3.4 and 3.5, where the density functions $z(p, \tau_B)$ and $z(p)$ are discussed. The sum of the pulse sizes is also considered there. In the table 3.1 we present the range of variation of $(p_{det})_{min}$

TABLE 3.1

	range of minimum detectable values at $\tau_B = 2$ μs
p	1.5×10^{-11} to 8.8×10^{-11} Vs
A_{jump}	2.0×10^{-9} to 1.2×10^{-8} m^2

and of the minimum detectable jump area $(A_{jump,det})_{min}$ $[m^2]$, both at a pulse duration of 2 μs. We calculate A_{jump} from the change of the magnetic moment m during a jump which is given by

$$m = \frac{2 I_s V_{jump}}{\mu_o} = \frac{\int\limits_{1\,jump} |v_{ind}(t)|\,dt}{\mu_o \times (N/l) \times 0.5 \times 0.75} \qquad [A m^2] \quad (3.3)$$

In eq. (3.3), I_s is the saturation polarization (≈ 1 Wbm^{-2}), V_{jump} the jump volume, N/l ($=10^5 m^{-1}$) the number of turns per metre of the pick-up coil and 0.5x0.75 the transfer factor of the pick-up coil system (sec. 2.3). The jump area is

$$A_{jump} = \frac{V_{jump}}{d_m \times 10^{-10}} \qquad (d_m \text{ in } \mathring{A}) \quad [m^2] \quad \cdot(3.4a)$$

or using the eqs. (3.1) and (3.3)

$$A_{jump} = \frac{p/1000}{2 I_s \times (N/l) \times 0.5 \times 0.75 \times 10^{-10}} \qquad (3.4b)$$

The maximum detectable value of p, $(p_{det})_{max}$, is determined by the maximum input voltage of the ADC, which is 5 Volt. For $\tau_B > (\tau_{B,det})_{min}$ this gives

$$(p_{det})_{max} = \frac{5 \times 1000}{d_m A_v} \tau_B \qquad (d_m \text{ in } \mathring{A}) \qquad (3.5)$$

By varying the amplification A_v we can shift $(p_{det})_{max}$; thus pulses with a large p can be measured accurately and without the previously mentioned systematic errors.

3.3. THE METHOD OF MEASURING THE FREQUENCY-DENSITY FUNCTION

All frequency-density functions of the pulse parameters are denoted by z in this thesis, for example we use

$z(p \ \tau_B \ \theta \ H)$, $z(p)$, etc.

In fig. 3.2 the Barkhausen signal is shown as a function of the applied magnetic field H(t). The frequency density $z(p_i \ \tau_{B,j} \ \theta_k \ H_l)$ is equal to

$$z(p_i \tau_{B,j} \theta_k H_l) = \frac{N(p_i \tau_{B,j} \theta_k H_l)}{\Delta p_i \ \Delta \tau_{B,j} \ \Delta \theta_k \ \Delta H_l} \qquad \left[V^{-1} s^{-3} A^{-1} m \right] \qquad (3.6)$$

in which $N(p_i \ \tau_{B,j} \theta_k H_l)$ is the number of pulses per hysteresis loop having values of p, τ_B, θ and H satisfying the restrictions that

p lies in the interval Δp_i around p_i (3.7a)
τ_B lies in the interval $\Delta \tau_{B,j}$ around $\tau_{B,j}$ (3.7b)
θ lies in the interval $\Delta \theta_k$ around θ_k (3.7c)
and H lies in the interval ΔH_l around H_l.   (3.7d)
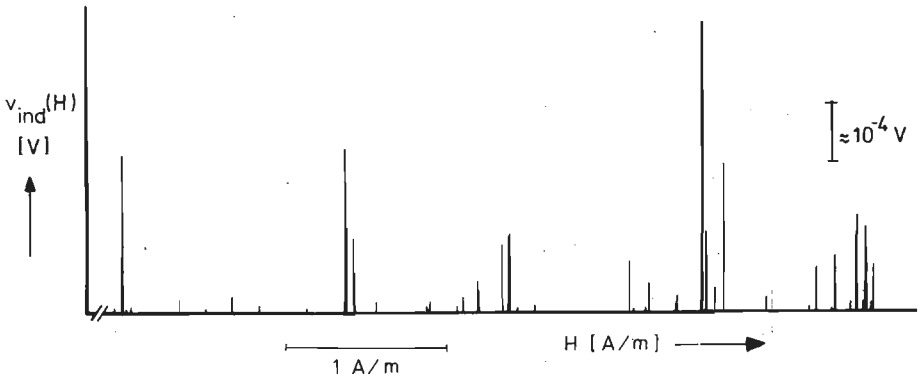
Fig. 3.2. Barkhausen signal during a small part of the reversal.

Only if we are interested in the behaviour of the Barkhausen noise along the hysteresis loop, hence as function of field H, do we start from eq. (3.6) and do we determine the density function $z(p \ H)$, $z(\tau_B \ H)$ etc. This will be done in chapter 4 [3.3] . Mostly, however, the statistics of the Barkhausen effect are determined for one complete hysteresis loop. The field dependence is disregarded. Hence we shall use $z(p \ \tau_B \ \theta)$ defined as

$$z(p\,\tau_B\,\theta) = \sum_l z(p\,\tau_B\,\theta\,H_l)\,\Delta H_l \qquad \left[v^{-1}\,s^{-3}\right] \quad (3.8)$$

The one- and two-dimensional frequency-density functions $z(p)$, $z(p\,\tau_B)$ and $z(p\,\theta)$, etc. follow from eq. (3.8), for example:

$$z(p\,\tau_B) = \sum_k z(p\,\tau_B\,\theta_k)\,\Delta\theta_k \qquad \left[v^{-1}\,s^{-2}\right] \quad (3.9a)$$

and

$$z(\tau_B) = \sum_i z(p_i\,\tau_B)\,\Delta p_i \qquad \left[s^{-1}\right] \quad (3.9b)$$

The total number of pulses per hysteresis loop is

$$N_{tot} = \sum_i \sum_j \sum_k \sum_l z(p_i\,\tau_{B,j}\,\theta_k\,H_l)\,\Delta p_i\,\Delta\tau_{B,j}\,\Delta\theta_k\,\Delta H_l \qquad (3.10)$$

In the determination of the frequency-density functions several hysteresis loops are traced. For one measurement the number of loops is such that about 10^4 pulses are available for the determination of the frequency-density functions.

In our measuring range the parameters p, τ_B and θ vary over several decades (2 to 5) and the frequency-density functions decrease strongly with increasing value of the parameters. For example the one-dimensional frequency-density functions of p, τ_B and θ can be represented in the greater part of the measuring range by functions of the form

$$z(x) = \Lambda\,(x/x^*)^{-\lambda} \qquad \text{with } 0.75 < \lambda < 2.4 \quad (\lambda \neq 1) \qquad (3.11)$$

where x stands for p, τ_B or θ and Λ and λ have constant values and $x^* = 1$. We want to take full account of the pulses at higher x values. Therefore we apply the following measuring method. In measuring $z(x)$ we divide the measuring range of x in intervals of increasing length, so that these intervals have equal lengths on a logarithmic scale. Therefore, with increasing x, the number of pulses measured in an interval decreases slower than in

the case where intervals with a fixed length would have been used. Choosing

$$x_{i+1} = c \, x_i \qquad \text{with} \quad c = \text{constant} \qquad (3.12)$$

we find for the length Δx_i of the i-th interval

$$\Delta x_i = x_{i+1} - x_i = (c-1) \, x_i \qquad (3.13)$$

so that the lengths of successive intervals grow by a factor of

$$\Delta x_{i+1} / \Delta x_i = c \qquad (3.14)$$

We use the symbol n_i for the number of pulses counted in the i-th interval. If eq. (3.11) holds then n_i satisfies ($\lambda \neq 1$)

$$n_i = \int_{x_i}^{x_{i+1}} z(x) \, dx = \frac{\Lambda(c^{1-\lambda}-1)}{1-\lambda} \, x_i^{1-\lambda} \qquad (3.15)$$

The density $z_{m,i}$ of pulses measured so in the i-th interval is

$$z_{m,i} = n_i / (c-1) \, x_i \qquad (3.16)$$

We plot this measured value $z_{m,i}$ at $\sqrt{c} \, x_i$, on logarithmic scale at the middle of the interval, being the geometric mean of x_i and x_{i+1}. Thus we obtain

$$z_m(\sqrt{c} \, x_i) = z_{m,i} = \Lambda \, x_i^{-\lambda} \frac{(c^{1-\lambda}-1)}{(1-\lambda)(c-1)} \qquad (3.16a)$$

From eq. (3.11) follows the theoretical value of z at the value $x = \sqrt{c} \, x_i$:

$$z(\sqrt{c} \, x_i) = \Lambda \, (\sqrt{c} \, x_i)^{-\lambda} \qquad (3.17)$$

Comparing eqs. (3.16a) and (3.17) gives

$$\frac{z_m(\sqrt{c} \, x_i)}{z(\sqrt{c} \, x_i)} = \frac{c^{\lambda/2}(c^{1-\lambda}-1)}{(1-\lambda)(c-1)} \qquad (3.18)$$

For p we used $c \approx 2$, for τ_B the value $c \approx 1.4$ and for θ the value $c \approx 1.8$. Fig. 3.3 shows the ratio z_m/z. We see that for $0.75 < \lambda < 2.4$ ($\lambda \neq 1$) and $1.4 < c < 2$ the values of $z_m(\sqrt{c}\, x_i)$ agree within 3% with those of $z(\sqrt{c}\, x_i)$ throughout the entire measuring range. For the magnetic field H we used intervals of equal length. The use of the values $z_m(\sqrt{c}\, x_i)$ do not bring along any error in the determination of the slope λ, because in the logarithmic plotting
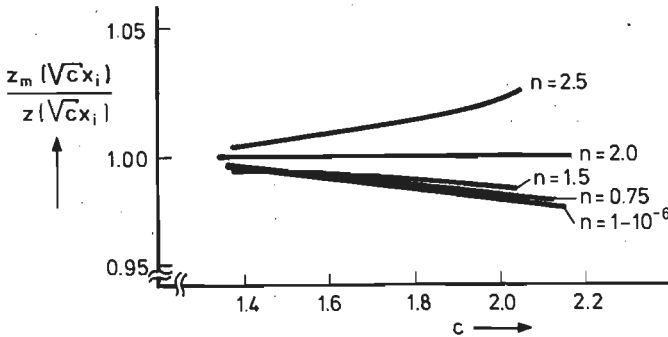
Fig. 3.3. The ratio z_m/z as a function of c with η as parameter.

method the curve of the density function is only shifted a little. So we may conclude that a density function of the form given by eq. (3.11) can be represented very accurately by the described method, while the accuracy is much larger than in the case that intervals of a constant length are used [3.4] as follows from the following discussion. When intervals of a constant length Δx are used than the value of Δx cannot be determined in such a way that it gives a large accuracy for the determination of $z(x)$ over a wide range of x values. Choosing the value of Δx as to give a good definition of $z(x)$ at low x values we get in most intervals numbers of pulses which are so small that statistical methods become inaccurate. Choosing Δx as to give an accurate result in the central part of the x range at the beginning of the x range the intervals are then too large to determine the form of the function $z(x)$ accurately.

3.4. THE TWO-DIMENSIONAL FREQUENCY-DENSITY FUNCTION OF p AND τ_B

The frequency-density function $z(p, \tau_B)$ of the Barkhausen pulses was measured. Both coordinate axes of the $p\,\tau_B$-plane were divided into intervals as described in sec. 3.3. All measured pulses had p and τ_B values, which are situated in only a part of the $p\,\tau_B$-plane (see fig. 3.4). In fig. 3.5 two typical examples of the iso-fre-
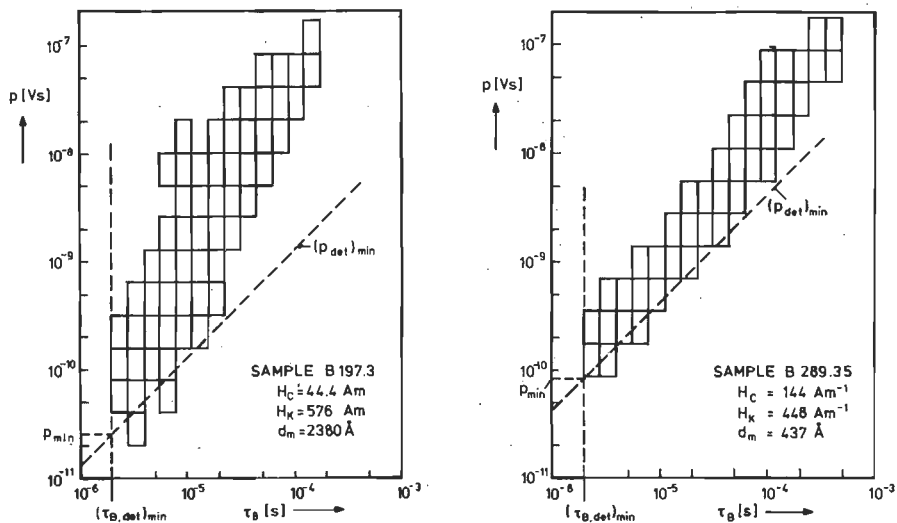
Fig. 3.4. The intervals in the $p\tau_B$ - plane where Barkhausen jumps occur for two different samples. The limits of the measuring range are indicated by the dashed lines.

quency-density lines of the measured density function $z(p, \tau_B)$ are sketched by interpolation between the measured densities in the intervals. Table 3.2 presents the measured number of pulses $N(p, \tau_B)$ per interval and table 3.3 the measured values of the density function $z(p, \tau_B)$ of the samples presented in figs. 3.4 and 3.5. Table 3.2 presents also $N(p)$ and $N(\tau_B)$. Within our measuring range the iso-frequency-density lines do not form closed curves. In the whole measuring range the frequency density increases with decreasing values of the pulse parameters. Below the measuring range the density functions of the Barkhausen jumps must somewhere begin to

(a)

p [Vs]

10^{-7}

$p_w(\tau_B)$

10^{-8}

3×10^{12}

6×10^{13}

$(p_{det})_{min}$

10^{-9}

1.4×10^{15}

$z(p, \tau_B)$

2.5×10^{16}

10^{-10}

5×10^{17}

SAMPLE B 197.3
$H_C = 44.4 \ Am^{-1}$
$H_K = 576 \ Am^{-1}$
$d_m = 2380 \ Å$

p_{min}

10^{-11}

10^{-6} 10^{-5} 10^{-4} 10^{-3}

$(\tau_{B,det})_{min}$ $\tau_B \ [s]$ ⟶

p [Vs]

10^{-7}

$p_w(\tau_B)$

$(p_{det})_{min}$

4×10^{11}

10^{-8}

8×10^{12}

(b)

1.6×10^{14}

3×10^{15}

$z(p, \tau_B)$

10^{-9}

6×10^{16}

10^{-10}

SAMPLE B 289.35
$H_C = 144 \ Am^{-1}$
$H_K = 448 \ Am^{-1}$
$d_m = 437 \ Å$

p_{min}

10^{-11}

10^{-6} 10^{-5} 10^{-4} 10^{-3}

$(\tau_{B,det})_{min}$ $\tau_B \ [s]$ ⟶
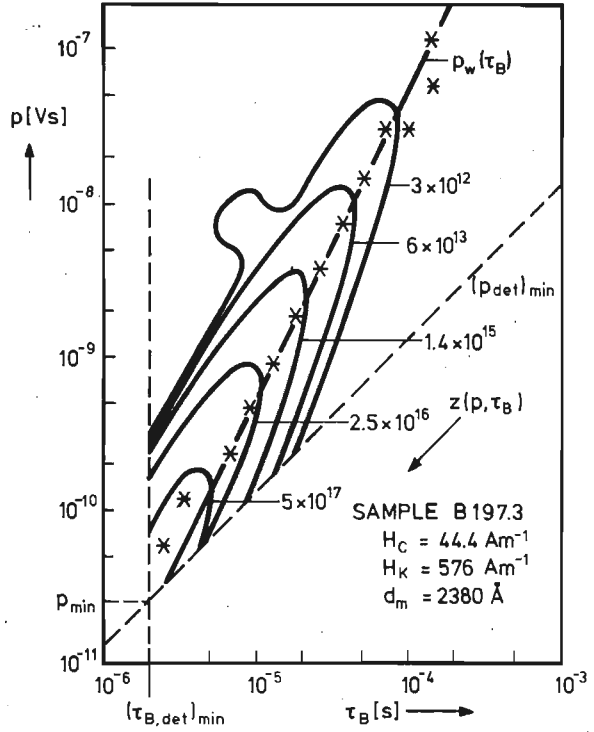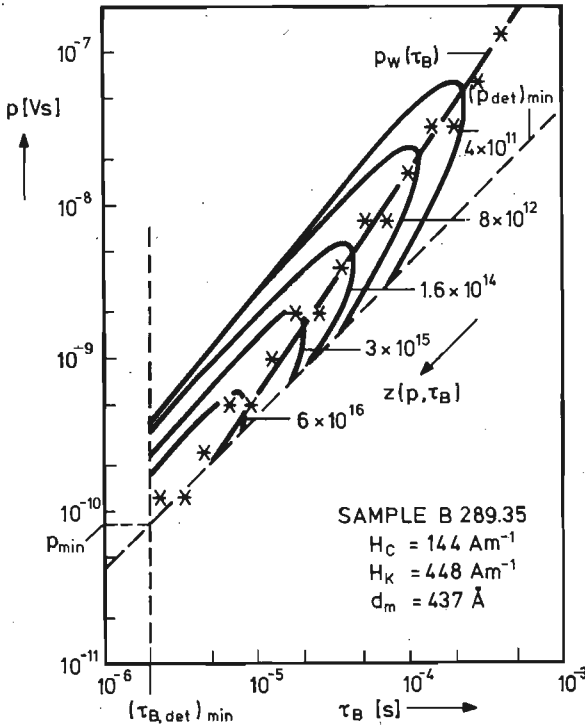
Fig. 3.5. Iso-frequency-density curves of $z(p,\tau_B)$ of two samples: (a) a film with $d_m = 2380 Å$ and (b) a film with $d_m = 437 Å$. The maximum of $z(p,\tau_B)$ for a given τ_B value is indicated by *.

49

TABLE 3.2a: N(p, τ_B) of the sample B197.3

p \ τ_B	2.37 ×10⁻⁶	3.35 ×10⁻⁶	4.73 ×10⁻⁶	6.68 ×10⁻⁶	9.44 ×10⁻⁶	1.33 ×10⁻⁵	1.88 ×10⁻⁵	2.66 ×10⁻⁵	3.76 ×10⁻⁵	5.31 ×10⁻⁵	7.50 ×10⁻⁵	1.06 ×10⁻⁴	1.50 ×10⁻⁴	N(p)
2.88 ×10⁻¹¹		0.10												0.10
5.75 ×10⁻¹¹	359*	26.3		01										385
1.15 ×10⁻¹⁰	70.0	174*	61.7	1.50										307
2.29 ×10⁻¹⁰	2.00	47.2	141*	38.9	4.60	0.10								234
4.56 ×10⁻¹⁰		0.70	39.1	65.4*	40.6	2.70	0.90							149
9.11 ×10⁻¹⁰			2.00	17.1	52.1*	20.5	1.60							93.3
1.82 ×10⁻⁹				0.20	14.6	25.4*	17.9	1.30						59.4
3.62 ×10⁻⁹					0.30	5.50	22.9*	11.9	1.70					42.3
7.24 ×10⁻⁹			0.1		0.20	0.60	5.30	14.2*	7.90	1.20				29.4
1.44 ×10⁻⁸					0.10		0.10	1.50	8.10*	6.20*	1.00			17
2.88 ×10⁻⁸								0.20	1.50	4.10	5.20*	0.90		12
5.75 ×10⁻⁸										0.20	1.10	1.00*	0.70*	3.0
1.15 ×10⁻⁷													0.10	0.10
N(τ_B)	431	248	244	123	113	54.7	48.7	29.1	19.3	11.7	7.30	1.90	0.80	Σ = 1332

TABLE 3.2b: N(p, τ_B) of the sample B289.35

p \ τ_B	2.37 ×10⁻⁶	3.35 ×10⁻⁶	4.73 ×10⁻⁶	6.68 ×10⁻⁶	9.44 ×10⁻⁶	1.33 ×10⁻⁵	1.88 ×10⁻⁵	2.66 ×10⁻⁵	3.76 ×10⁻⁵	5.31 ×10⁻⁵	7.50 ×10⁻⁵	1.06 ×10⁻⁴	1.50 ×10⁻⁴	2.11 ×10⁻⁴	2.99 ×10⁻⁴	4.22 ×10⁻⁴	N(p)
1.25 ×10⁻¹⁰	215*	61.3*															276
2.48 ×10⁻¹⁰	0.64	61.5*	129*	7.00													198
4.96 ×10⁻¹⁰		0.091	16.1	68.8*	45.2*												130
9.89 ×10⁻¹⁰				0.46	39.9*	40.4*	10.6										91.4
1.97 ×10⁻⁹						5.00	34.2*	18.5*	0.73								58.4
3.94 ×10⁻⁹							0.55	11.1	16.4*	3.91							32.0
7.87 ×10⁻⁹									2.73	9.82*	5.36*	0.46					18.4
1.57 ×10⁻⁸										0.18	4.55*	5.27*	0.91				10.9
3.13 ×10⁻⁸											0.18	1.91	4.09*	2.00*			8.18
6.25 ×10⁻⁸												0.091	0.27	1.27	1.00*	0.091	2.72
1.25 ×10⁻⁷															0.48	0.36*	0.82
N(τ_B)	216	123	145	76.3	85.1	45.4	45.4	29.5	19.8	13.9	10.1	7.73	5.27	3.27	1.46	0.45	Σ = 827

50

TABLE 3.3a: $z(p, r_B)$ of the sample B197.3

p \ r_B	2.37×10^{-6}	3.35×10^{-6}	4.73×10^{-6}	6.68×10^{-6}	9.44×10^{-6}	1.33×10^{-5}	1.88×10^{-5}	2.66×10^{-5}	3.76×10^{-5}	5.31×10^{-5}	7.50×10^{-5}	1.06×10^{-4}	1.50×10^{-4}
2.88×10^{-11}		4.25×10^{15}											
5.75×10^{-11}	$1.08^*\times10^{19}$	5.61×10^{17}		1.07×10^{16}									
1.15×10^{-10}	1.51×10^{17}	$1.86^*\times10^{18}$	4.66×10^{17}	8.00×10^{15}									
2.29×10^{-10}	1.51×10^{16}	2.52×10^{17}	$5.33^*\times10^{17}$	$1.04^*\times10^{17}$	8.70×10^{15}	1.34×10^{14}							
4.56×10^{-10}		1.88×10^{15}	7.41×10^{16}	8.77×10^{16}	$3.85^*\times10^{15}$	1.81×10^{15}	4.28×10^{14}						
9.11×10^{-10}			1.90×10^{15}	1.13×10^{16}	2.47×10^{16}	$6.88^*\times10^{15}$	3.80×10^{14}						
1.82×10^{-9}				6.74×10^{13}	3.48×10^{15}	4.29×10^{15}	$2.14^*\times10^{15}$	1.10×10^{14}					
3.62×10^{-9}					3.58×10^{13}	4.65×10^{14}	1.37×10^{15}	$5.04^*\times10^{14}$	5.11×10^{13}				
7.24×10^{-9}				8.44×10^{12}	1.19×10^{13}	2.11×10^{13}	1.59×10^{14}	3.01×10^{14}	$1.19^*\times10^{14}$	1.28×10^{13}			
1.44×10^{-8}						1.50×10^{12}	1.59×10^{12}	6.12×10^{13}	$3.31^*\times10^{13}$	3.78×10^{12}			
2.88×10^{-8}								1.07×10^{12}	6.06×10^{12}	1.10×10^{13}	9.85×10^{12}	$1.20^*\times10^{12}$	
5.75×10^{-8}										2.69×10^{11}	1.05×10^{12}	6.73×10^{11}	$3.34^*\times10^{11}$
1.15×10^{-7}													2.38×10^{10}

TABLE 3.3b: $z(p, r_B)$ of the sample B289.35

p \ r_B	2.37×10^{-6}	3.35×10^{-6}	4.73×10^{-6}	6.68×10^{-6}	9.44×10^{-6}	1.33×10^{-5}	1.88×10^{-5}	2.66×10^{-5}	3.76×10^{-5}	5.31×10^{-5}	7.50×10^{-5}	1.06×10^{-4}	1.50×10^{-4}	2.11×10^{-4}	2.99×10^{-4}	4.22×10^{-4}
1.25×10^{-10}	$2.96^*\times10^{18}$	$6.02^*\times10^{17}$														
2.48×10^{-10}	4.41×10^{15}	3.03×10^{17}	$4.49^*\times10^{17}$	1.72×10^{16}												
4.96×10^{-10}		2.24×10^{14}	2.80×10^{16}	$8.46^*\times10^{16}$	$3.93^*\times10^{16}$											
9.89×10^{-10}				2.81×10^{14}	1.74×10^{16}	$1.26^*\times10^{16}$	2.32×10^{15}									
1.97×10^{-9}					7.78×10^{14}	$3.76^*\times10^{15}$	$1.44^*\times10^{15}$	4.02×10^{13}								
3.94×10^{-9}							2.99×10^{13}	4.32×10^{14}	$4.53^*\times10^{14}$	7.61×10^{13}						
7.87×10^{-9}								3.79×10^{13}	$9.60^*\times10^{13}$	$3.72^*\times10^{14}$	2.23×10^{12}					
1.57×10^{-8}									8.98×10^{11}	1.58×10^{13}	$1.30^*\times10^{13}$	1.58×10^{12}				
3.13×10^{-8}									3.18×10^{11}	2.36×10^{12}	$3.58^*\times10^{12}$	$1.24^*\times10^{12}$				
6.25×10^{-8}										6.61×10^{10}	1.19×10^{11}	3.93×10^{11}	$2.19^*\times10^{11}$	1.41×10^{10}		
1.25×10^{-7}														3.51×10^{10}	$2.00^*\times10^{10}$	

decrease with decreasing p and τ_B, as discussed by
Stierstadt [3.5] . The minimum jump size will be much
smaller, by a factor of at least 10^3, than our minimum
detectable jump size. So the iso-frequency-density lines
will be closed far below our measuring range.

The measurements show that in the Barkhausen process
a most probable pulse size $p_w(\tau_B)$ exists at each given
value of τ_B, just as found by Lieneweg [3.6] from
nickel-iron wires. In each measurement $p_w(\tau_B)$ and τ_B
proved to satisfy an equation of the form [3.2]

$$p_w(\tau_B) = K \tau_B^{\varkappa} \qquad [Vs] \qquad (3.19)$$

In the measurement $p_w(\tau_B)$ is determined by tracing a line
through the measuring points that represent the largest
values of the density $z(p,\tau_B)$ at a given value of τ_B. We
thus obtain an accuracy of $\varkappa$ of about ± 0.1. This is done
because it is difficult to determine the iso-frequency-
density lines and the method used gives an accuracy which
is sufficient for our investigation. A pulse is only de-
tected if both the pulse amplitude h and the pulse time
τ_B exceed $(h_{det})_{min}$ and $(\tau_{B,det})_{min}$, respectively, as dis-
cussed in sec. 3.2. The value of $(p_{det})_{min}$ (see eq.(3.2))
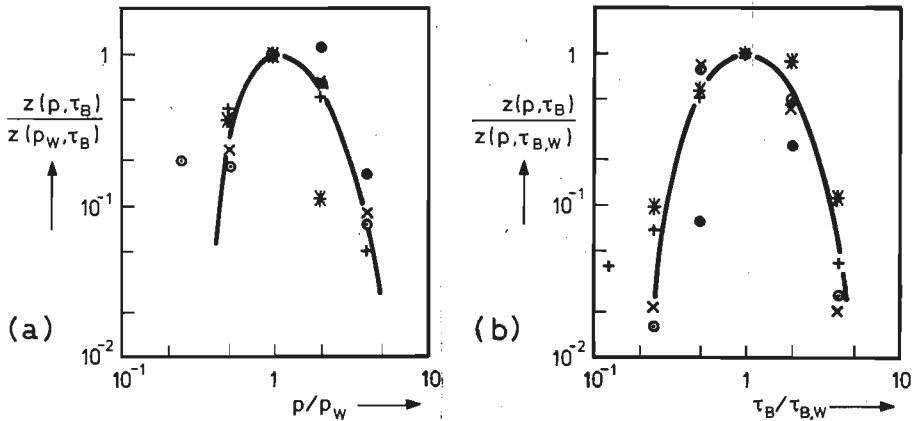
Fig. 3.6.   (a) Density function of the pulse size for different τ_B values:
$\bullet$: $\tau_B = 4.7 \times 10^{-6}$s, $\times$: $\tau_B = 9.4 \times 10^{-6}$s, $\odot$: $\tau_B = 1.9 \times 10^{-5}$s, $+$: $\tau_B = 3.8 \times 10^{-5}$s and
$*$: $\tau_B = 7.5 \times 10^{-5}$s. (b) Density function of the pulse time for different p values:
$\bullet$: p = 1.2×10^{-10}Vs, $\times$: p = 4.6×10^{-10}Vs, $\odot$: p = 1.8×10^{-9}Vs, $+$: p = 7.2×10^{-9}Vs and
$*$: p = 2.9×10^{-8}Vs. Both figures present results of the sample B197.3.

is proportional to τ_B. The value of $p_w(\tau_B)$ is hardly disturbed by the limited measuring range of the equipment owing to the strong relation between p and τ_B.

In fig. 3.6a $z(p, \tau_B)/z(p_w, \tau_B)$ is shown as a function of p with τ_B as parameter and fig. 3.6b shows the density function $z(p, \tau_B)/z(p, \tau_{B,w})$ with p as parameter. All these densities follow the same curve. The quantity $\tau_{B,w}$ is the most probable pulse duration at a given pulse size p. At a given τ_B the spreading of $p(\tau_B)$ values around $p_w(\tau_B)$ is small as can be seen from fig. 3.6a. Thus the mean pulse size at a given value of τ_B, $<p(\tau_B)>$ can be approximated by

$$< p(\tau_B)> \approx p_w(\tau_B) \qquad [vs] \qquad (3.21)$$

For the different samples $<p(\tau_B)>$ is somewhat larger than $p_w(\tau_B)$ but it is considerably smally than $2 p_w(\tau_B)$.

The measured values of $\varkappa$ are plotted in fig. 3.7 as a function of the film thickness d_m. From the plot one can deduce that two values of $\varkappa$ dominate: $\varkappa = 2 \pm 0.1$ and $\varkappa = 1.5 \pm 0.1$. These two different values characterize two different wall jumping processes, which will be further discussed in chapter 5. A small number of samples
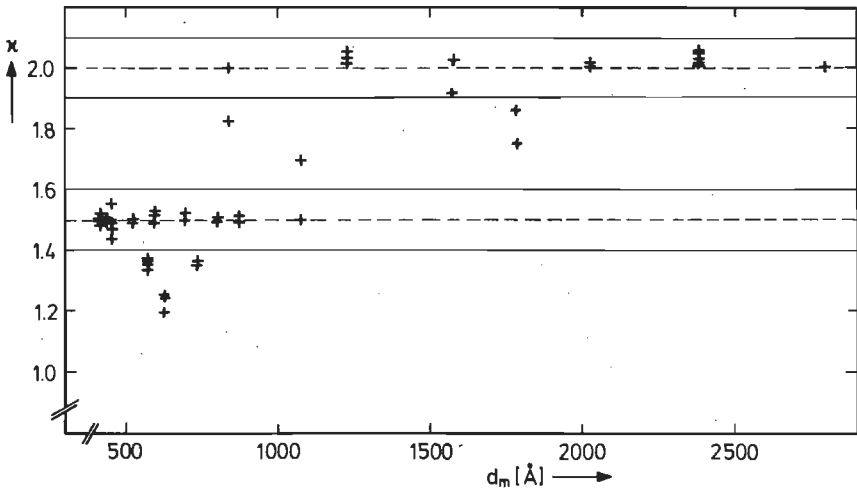
Fig. 3.7. Value of $\varkappa$ as a function of the film thickness d_m for all measured samples.
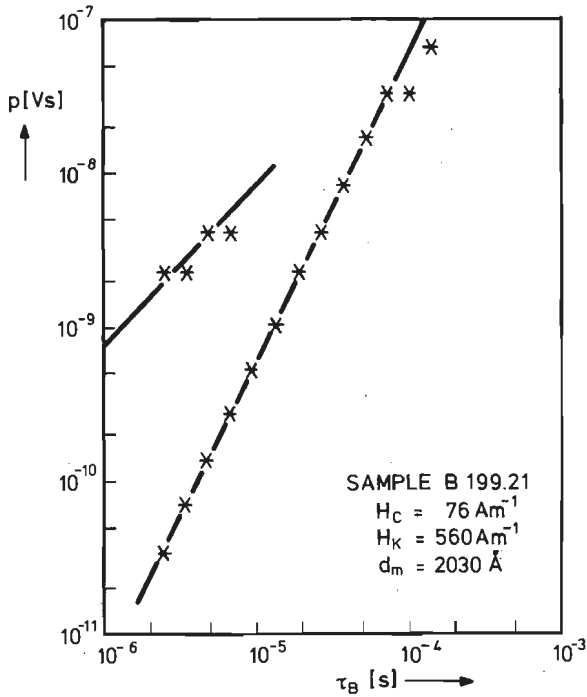
Fig. 3.8. Curves of $p_w(\tau_B)$ for a sample 2030Å thick; * indicates the maximum values of $z(p,\tau_B)$ as a function of p for a given τ_B.

have values of $\varkappa$ between 1.5 and 2. In a few samples, however, two branches for $p_w(\tau_B)$ are measured (fig.3.8). The second branch is only found for large values of p and satisfies

$$p_w(\tau_B) \propto \tau_B \qquad (3.22)$$

The number of jumps and the values of the frequency-density function in this second branch, as well as the spreading are very low. Three samples show $\varkappa$ values around 1.3. In chapter 5 the form of $p_w(\tau_B)$ is derived for different simplified models of domain wall motion and the results of the derivation are compared with the experimental results.

3.5. THE FREQUENCY-DENSITY FUNCTION OF p

The frequency-density function $z(p)$ of the pulse size p can be determined from $z(p\ \tau_B\ \theta\ H)$ (eq. (3.5)) as:

$$z(p) = \sum_j \sum_k \sum_l z(p\ \tau_{B,j}\ \theta_k\ H_l)\ \Delta\tau_{B,j}\Delta\theta_k\Delta H_l \quad \left[V^{-1}s^{-1}\right] \quad (3.25)$$

The measured values of $z(p)$ can be approximated by a curve described by an equation of the form (see fig. 3.9).

$$z(p) = \begin{cases} A_1 \left(\dfrac{p}{p^*}\right)^{-\alpha_1} & p_{min} < p \leqslant p_o \\[3mm] A_2 \left(\dfrac{p}{p^*}\right)^{-\alpha_2} & p_o \leqslant p < p_{max} \end{cases} \quad (3.23)$$

where p_{min} equals $(p_{det})_{min}$ at $\tau_B = (\tau_{B,det})_{min}$ and $p^* = 1Vs$. A_1, A_2, α_1 and α_2 are constants. For all samples the measured value of A_1 is of the order of magnitude of $10^{-4} V^{-1}s^{-1}$ and the values of α_1 range between 1.30 and 2.05, as seen from fig. 3.10. The majority of α_1 values lie between 1.4 and 1.8. In all experiments we find

$$\alpha_2 > 2\alpha_1 \quad (3.24)$$

The measurements show that over about three to four decades the measured frequency-density functions accurately follow eq. (3.24). The curve drawn at first sight through the measured points in the plot of $z(p)$ against p can be traced with an accuracy of about $\pm$ 0.1 with respect to the slope (dashed curves fig. 3.9). It has to be noted that in addition to eq. (3.24) some different functional forms of $z(p)$ reasonably agree with the measurements, for example [3.6]

$$z(p) \approx A\ (p/p^*)^{-\alpha}\ exp(-p/p_o) \quad (3.26a)$$

or

$$z(p) \approx \left\{ \frac{(p/p^*)^{\alpha_1}}{A_1} + \frac{(p/p^*)^{\alpha_2}}{A_2} \right\}^{-1} \quad (3.26b)$$
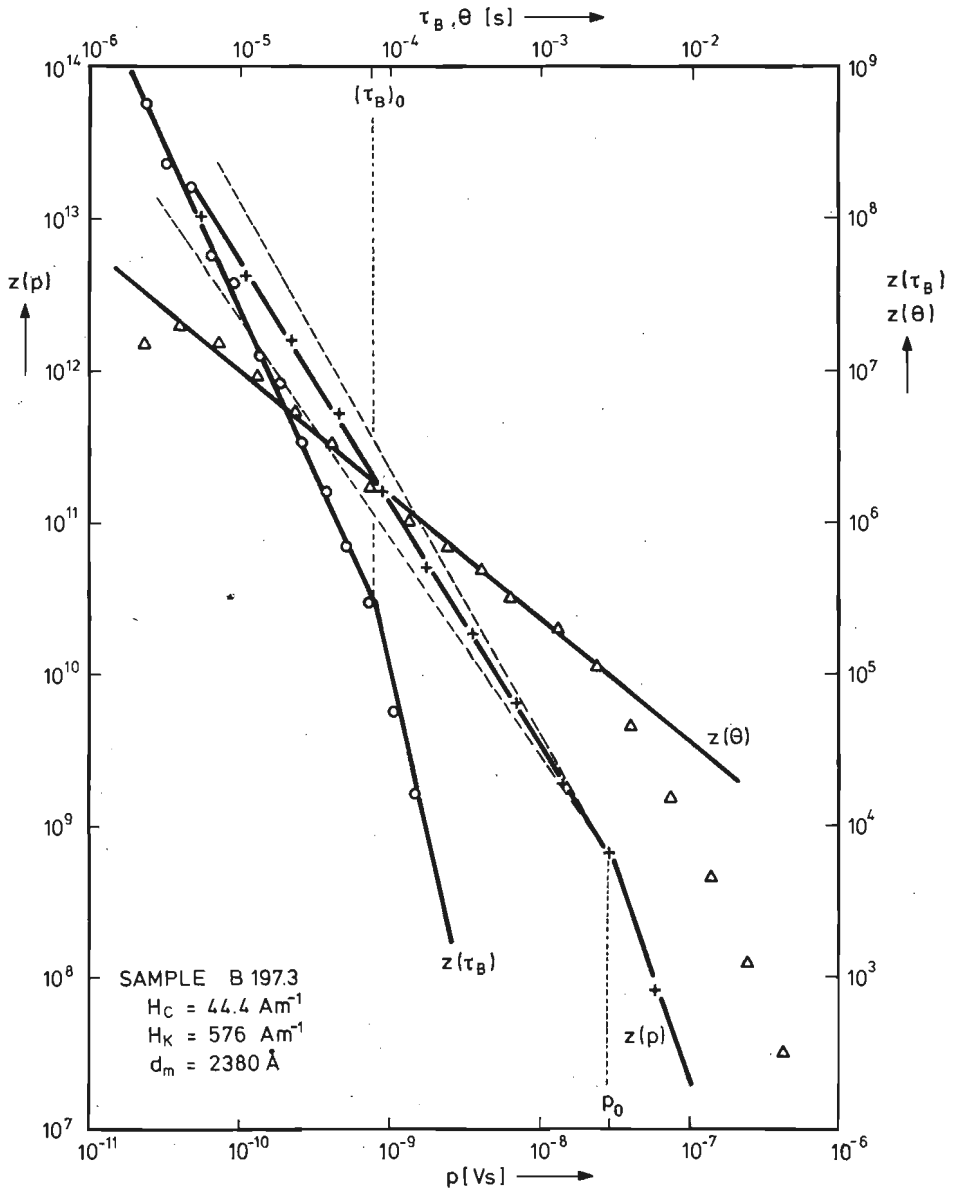
Fig. 3.9.   Shape of the one-dimensional density functions $z(p)$, $z(\tau_B)$ and $z(\theta)$.

However, we will restrict ourselves to the representation of eq. (3.24).

A pulse is only detected if both h and τ_B exceed $(h_{det})_{min}$, resp. $(\tau_{B,det})_{min}$ (see sec. 3.2), taking into
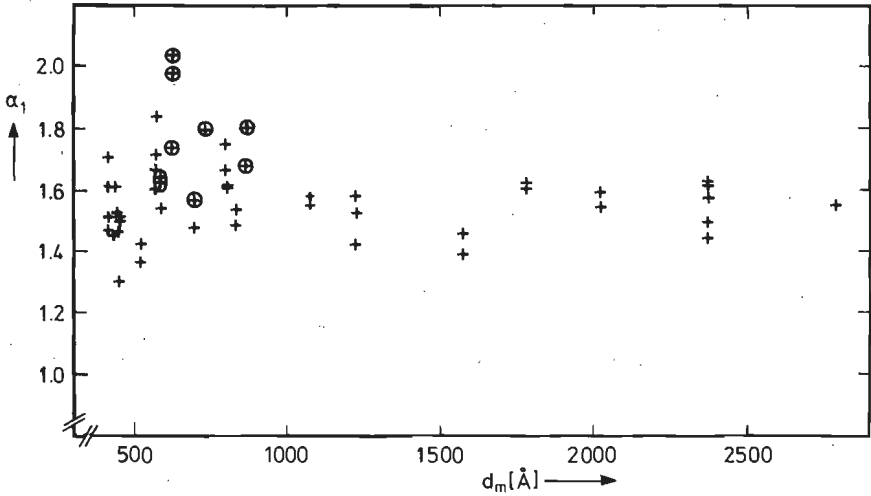
Fig. 3.10. Measured slope α_1 of the density function z(p) plotted as a function of the film thickness d_m; samples with very small values of P_{tot} are indicated by ⊕.

account that $(p_{det})_{min} \propto \tau_B$ (eq (3.2)). So a fraction of the pulses with (see fig. 3.4)

$$p > \frac{1000}{d_m A_v} (h_{det})_{min} \times (\tau_{B,det})_{min} = P_{min} \qquad (3.27)$$

is not counted by the equipment. By this systematic error the measured value of z(p) is too low. In the Barkhausen pulses $p_w(\tau_B)$ grows stronger with τ_B than $(p_{det})_{min}$ does, as described in sec. 3.4. As a consequence only at the beginning of the measuring range do we measure too low a value of z(p), mostly only for the first two measuring points is the error substantial ($\gg 10\%$). So this system-atic error has scarcely any influence on the slope α_1 determined from the experiments; the measured slope α_1 becomes a little too low.

For large values of p the number of pulses measured per interval is so small that application of statistical methods gives inaccurate results. This applies to about the last half decade of the p range in which Barkhausen pulses are measured. Large pulses are detected with cer-tainty (see sec. 3.2), therefore only a measuring error is present here and no systematic error. This discussion

57

is also valid for $z(\tau_B)$ and $z(\theta)$.

With eq.(3.24) we can very easily calculate the meas-
ured total pulse size P_{tot} per hysteresis loop:

$$P_{tot} = \int_{P_{min}}^{P_{max}} p \, z(p) \, dp \qquad \left[Vs\right] \qquad (3.28)$$

where p_{max} is the maximum jump size detected in the sam-
ple. The pulse size p is proportional to the jump area.
In every reversal the magnetization of the whole film is
reversed and this happens twice per hysteresis loop. The
proper value of the total pulse size $(P_{tot})_c$ per hystere-
sis loop can be calculated from eq. (3.4b). The surface
area of the samples varies between 0.8 and 1.1 cm^2 usual-
ly it is 1 cm^2. Using a film surface area of 1 cm^2 and a
transfer factor of the pick-up coil circuit of 0.5x0.75
we find

$$(P_{tot})_c \approx 1.5 \times 10^{-6} \quad Vs \qquad (3.29)$$

In fig. 3.11 the measured value P_{tot} is plotted as a
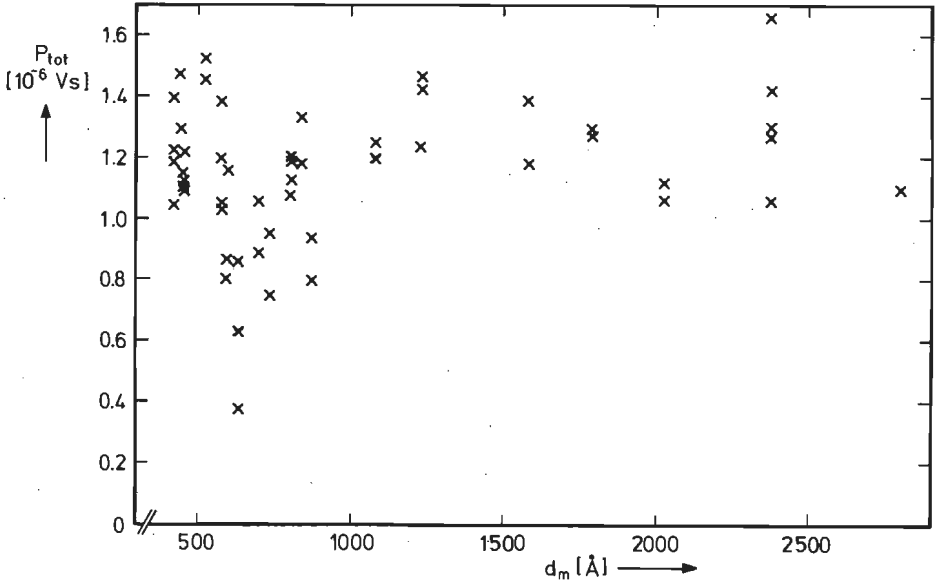
Fig. 3.11. Measured sum of all pulse sizes as a function of d_m.

function of the film thickness d_m. It varies between 0.38×10^{-6} and 1.66×10^{-6} Vs, whereas the majority of P_{tot} values range between 1.0×10^{-6} and 1.4×10^{-6} Vs. The difference between P_{tot} and $(P_{tot})_c$ is sometimes very large. As already discussed the error in α_1 will be small but a large number of small pulses cannot be measured. The question now arises: can the systematic errors give rise to such large differences between P_{tot} and $(P_{tot})_c$? To answer this question we shall examine the influence of these errors on P_{tot}.

In the estimation of the possible error in $z(p)$ the influence of measuring errors will be neglected. We use in the calculation two assumptions:

(1) With decreasing p the density function of p will still increase until p'_{min} ($\ll p_{min}$) where it begins to decrease with a further decrease of p. For $p > p'_{min}$ the actual density function $z'(p)$ follows an equation of the form (3.24).

(2) For values of p around p_o the density of p is measured accurately, and so are A_2 and α_2. No systematic errors occur here.

Then the actual frequency-density function of p, $z'(p)$ is approximated by

$$
z'(p) = \begin{cases}
A'_1 \left(\dfrac{p}{p^*} \right)^{-\alpha'_1} & p'_{min} < p \leqslant p_o \\[2em]
A_2 \left(\dfrac{p}{p^*} \right)^{-\alpha_2} & p_o \leqslant p < p_{max}
\end{cases}
\qquad (3.30)
$$

where $p^* = 1$ Vs. We describe the relationship between A'_1, α'_1 and p'_{min} and the measured quantities A_1, α_1 and p_{min} as follows

$$A'_1 = (1/f_A) A_1 \qquad (3.31a)$$

$$\alpha'_1 = \alpha_1 + \Delta\alpha \qquad (3.31b)$$

$$p'_{min} = (1/f_p) p_{min} \qquad (3.31c)$$

59

where $\Delta\alpha > 0$ and $f_p \gg 1$. With assumption (2), and using eqs.(3.24) and (3.30) we find

$$f_A = p_o^{-\Delta\alpha} > 1 \tag{3.32}$$

and

$$A_2\, p_o^{-\alpha_2} = A_1\, p_o^{-\alpha_1} \tag{3.33}$$

Furthermore the actual total pulse size P_{tot}' is

$$P_{tot}' = \int_{P_{min}}^{P_{max}} p\, z'(p)\, dp \qquad [Vs] \tag{3.28a}$$

The relative error in the measured total pulse size, $(P_{tot}' - P_{tot})/P_{tot}'$, can now be calculated. This calculation is carried out in Appendix 2. The result is shown in fig. 3.12, where the relative error in P_{tot} is plotted as a function of $2 - \alpha_1$ for different values of $\Delta\alpha$ and p_{min}'. The curves of fig. 3.12 show that already a small value of $\Delta\alpha$ (≈ 0.1) and a value of f_p between 10^2 and 10^3 can result in large errors in P_{tot}, particularly if α_1 has a value of about 2. An error of 0.1 in the determination of α_1 is quite reasonable (fig. 3.9). The value of 10^3 for f_p is in agreement with the estimation of Stierstadt [3.5] as already discussed in sec. 3.4. In

curve	$\Delta\alpha$	P_{min}'
—·—·	0	$10^{-14}\sqrt{10}$
——	0.05	$10^{-14}\sqrt{10}$
·······	0.05	$10^{-13}\sqrt{10}$
----	0.1	$10^{-14}\sqrt{10}$
—··—	0.2	$10^{-14}\sqrt{10}$
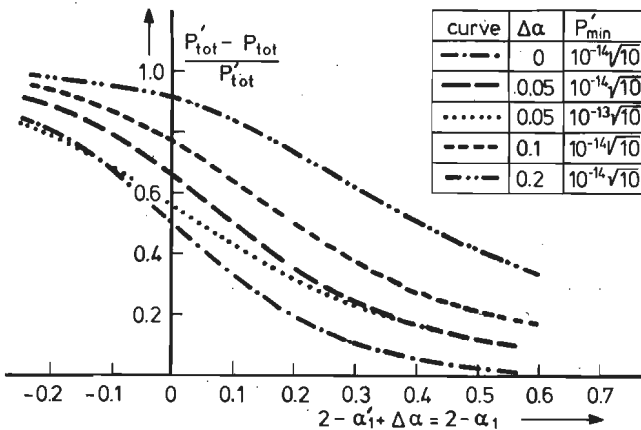
Fig. 3.12. Relative error in P_{tot}: the curves are calculated using eq (A2.6) for $f_p = 10^3$ and $p_0 = 10^{-8}\sqrt{10}$.
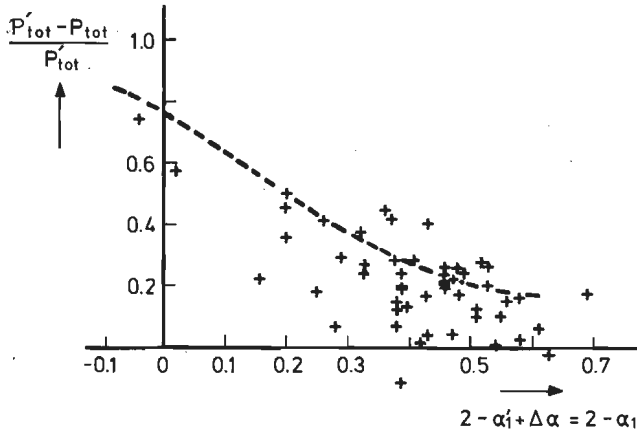
Fig. 3.13. Relative error in P_{tot} for $\Delta\alpha = 0.1$, $p'_{min} = 10^{-14}\sqrt{10}$, $f_p = 10^3$ and $p_0 = 10^{-8}\sqrt{10}$ (dashed curve) and measured values (x) of $(P_{tot})_c - P_{tot}$ $/(P_{tot})_c$ for all our samples.

fig. 3.13 we have plotted the calculated curve of $(P'_{tot} - P_{tot})/P'_{tot}$ for $\Delta\alpha = 0.1$ and $f_p = 10^3$, just as the measured values of $(P_{tot})_c - P_{tot}$ $/(P_{tot})_c$. From this figure we can conclude that the low values of P_{tot} sometimes measured can be accounted for very well by a small error in the experimentally determined value of α_1 and by the fact that a large number of the pulses has p values below the detection limit of the equipment. The systematic errors are thus responsible for the low values of P_{tot} sometimes measured.

3.6. THE FREQUENCY-DENSITY FUNCTION OF τ_B

The measured frequency-density function $z(\tau_B)$ of the pulse duration τ_B can be approximated very well by (fig. 3.9)

$$
z(\tau_B) = \begin{cases} D_1 \left(\dfrac{\tau_B}{\tau_B^*}\right)^{-\delta_1} & (\tau_{B,det})_{min} < \tau_B \leqslant (\tau_B)_o \\[4mm] D_2 \left(\dfrac{\tau_B}{\tau_B^*}\right)^{-\delta_2} & (\tau_B)_o \leqslant \tau_B < (\tau_B)_{max} \end{cases}
\tag{3.34}
$$

where $\tau_B^x = 1s$. D_1, D_2, δ_1 and δ_2 are constants. The value of D_1 is of the order of magnitude of 10^{-4} s^{-1} for the different samples. The values of δ_1 range between 1.55 and 2.40 (fig. 3.14) while for δ_2 we find

$$\delta_2 > 2\delta_1$$

The range of measured values of τ_B is two decades, that of p is three to four decades, and furthermore in general $\delta_1 > \alpha_1$. As a consequence the slope δ_1 determined from the traced curve through the measured points will exhibit a larger inaccuracy than the slope α_1 of the curve of z(p). For the same reason the inaccuracy caused
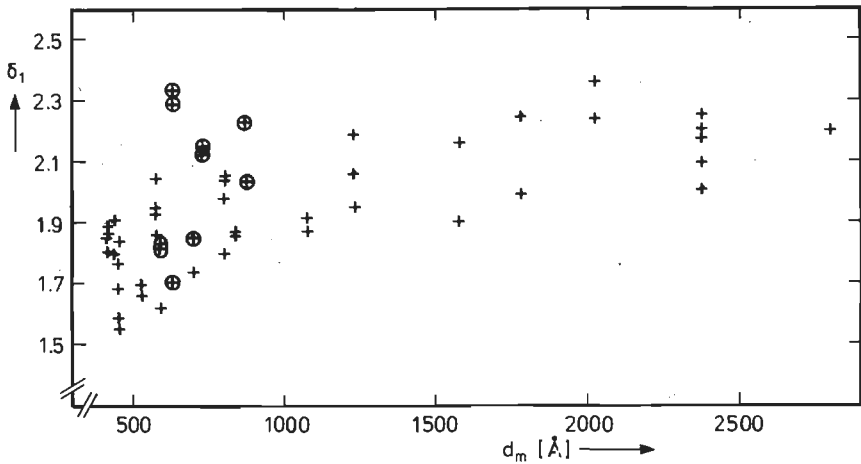
Fig. 3.14. Measured value of δ_1 as a function of the film thickness; samples with very small values of P_{tot} are indicated by ⊕.

by the systematic error is larger in δ_1 than in α_1. The same discussion as in sec. 3.5 on z(p) can now be applied to the accuracy of the measured density functions of τ_B. For the parameter p it was possible to estimate the error of the measured frequency density z(p) by comparing results deduced from the measured function z(p) with other experimental results. In the case of τ_B no comparison with experimental results can be made.

The sum of the pulse durations per hysteresis loop is denoted by T_B:

$$T_B = \sum_j \cdot \tau_{B,j} \, z(\tau_{B,j}) \, \Delta\tau_{B,j} \quad [s] \qquad (3.35)$$

In the presented examples we find for T_B the following
values:

sample B197.3 $T_B \approx 10^{-2}$ s

sample B289.34 $T_B \approx 10^{-2}$ s

3.7. THE FREQUENCY-DENSITY FUNCTION OF θ

In our measurements we also investigated $z(p,\theta)$ and
$z(\tau_B,\theta)$. No relation between p and θ or between τ_B and θ
was observed as can be seen in table 3.4. So we can con-
sider θ to be independent of p and τ_B. That θ, p and τ_B
does not depend on p and τ_B does not imply that the pulses
occur independently of each other. If the occurrance of
pulses were independent one should find for $z(\theta)$ [3.7] :

$$z(\theta) \propto \frac{1}{\theta_0} \exp(-\theta/\theta_0) \qquad (3.36)$$

The density function of θ is measured in our films and
can be approximated by (see fig. 3.9)

$$z(\theta) \approx B \, (\theta/\theta^*)^{-\beta} \qquad \theta > \theta_{min} \qquad (3.37)$$

B and β are constants and $\theta^* = 1s$. The measured value of
β is of the order of $1s^{-1}$ for all samples. For the dif-
ferent samples the measured values of β range between
0.7 and 1.6 (fig. 3.15).

In chapter 5 the wall jumping process is extensively
described. Here we are anticipating the results that will
be deduced there. We shall shortly indicate the parameters
on which p, τ_B and θ depend.

(a) The pulse size p: The pulse size p_i of the i-th jump
depends on the driving field $H_{d,i}$ at the i-th wall
jump and on $\tau_{B,i}$ (see eqs. (5.24), (5,64b) and (5.73)).
The driving field $H_{d,i}$ is discussed in sec. 5.3 and
given by (see eq. (5.16)).

TABLE 3.4a: z(p, θ) of the sample B197.3

p \ θ	4.22×10^{-6}	7.50×10^{-6}	1.33×10^{-5}	2.37×10^{-5}	4.22×10^{-5}	7.50×10^{-5}	1.33×10^{-4}	2.37×10^{-4}	4.22×10^{-4}	7.50×10^{-4}	1.33×10^{-3}	2.37×10^{-3}	4.22×10^{-3}	7.50×10^{-3}	1.33×10^{-2}	2.37×10^{-2}	4.22×10^{-2}	7.50×10^{-2}	
2.88×10^{-11}					2.00×10^{14}														0.10
5.75×10^{-11}	1.08×10^{17}	8.29×10^{16}	5.40×10^{16}	2.72×10^{16}	2.03×10^{16}	1.06×10^{16}	6.25×10^{15}	3.95×10^{15}	2.67×10^{15}	2.16×10^{15}	1.28×10^{15}	7.88×10^{14}	3.33×10^{14}	1.35×10^{14}	5.21×10^{13}	1.86×10^{13}	4.42×10^{12}	3.55×10^{12}	381
1.15×10^{-10}	3.62×10^{16}	3.31×10^{16}	2.35×10^{16}	1.34×10^{16}	7.80×10^{15}	4.94×10^{15}	2.64×10^{15}	1.88×10^{15}	1.35×10^{15}	7.57×10^{14}	5.49×10^{14}	3.35×10^{14}	1.35×10^{14}	4.55×10^{13}	1.46×10^{13}	3.14×10^{12}	8.85×10^{11}	6.50×10^{11}	304
2.29×10^{-10}	1.36×10^{16}	1.43×10^{16}	9.33×10^{15}	5.48×10^{15}	3.20×10^{15}	2.08×10^{15}	1.08×10^{15}	7.28×10^{14}	4.94×10^{14}	3.41×10^{14}	2.18×10^{14}	1.17×10^{14}	4.94×10^{13}	1.70×10^{13}	3.27×10^{12}	6.29×10^{11}	1.76×10^{11}	5.66×10^{10}	232
4.56×10^{-10}	6.57×10^{15}	4.61×10^{15}	2.80×10^{15}	2.16×10^{15}	1.28×10^{15}	6.67×10^{14}	3.80×10^{14}	2.48×10^{14}	1.68×10^{14}	9.79×10^{13}	6.71×10^{13}	3.65×10^{13}	1.64×10^{13}	3.34×10^{12}	7.59×10^{11}	4.51×10^{10}	1.26×10^{10}	7.10×10^{9}	148
9.11×10^{-10}	1.27×10^{15}	1.42×10^{15}	1.30×10^{15}	6.89×10^{14}	4.81×10^{14}	2.28×10^{14}	1.18×10^{14}	7.90×10^{13}	6.21×10^{13}	3.41×10^{13}	1.82×10^{13}	1.17×10^{13}	3.93×10^{12}	6.05×10^{11}	1.20×10^{11}				93
1.82×10^{-9}	9.21×10^{14}	5.53×10^{14}	4.52×10^{14}	2.43×10^{14}	1.68×10^{14}	6.95×10^{13}	3.61×10^{13}	2.21×10^{13}	1.68×10^{13}	1.12×10^{13}	7.03×10^{12}	2.94×10^{12}	7.94×10^{11}	2.14×10^{11}	1.00×10^{10}				59
3.62×10^{-9}	2.39×10^{14}	2.68×10^{14}	1.71×10^{14}	8.51×10^{13}	5.89×10^{13}	2.41×10^{13}	2.11×10^{13}	8.79×10^{12}	6.68×10^{12}	4.29×10^{12}	1.81×10^{12}	7.94×10^{11}	2.70×10^{11}	3.57×10^{10}					42
7.24×10^{-9}	7.18×10^{13}	8.72×10^{13}	5.29×10^{13}	3.84×10^{13}	2.23×10^{13}	1.43×10^{13}	5.29×10^{12}	3.41×10^{12}	1.91×10^{12}	1.03×10^{12}	7.06×10^{11}	3.27×10^{11}	8.96×10^{9}						29
1.44×10^{-8}	4.00×10^{12}	2.24×10^{13}	2.40×10^{13}	1.71×10^{13}	4.80×10^{12}	3.37×10^{12}	2.40×10^{12}	1.07×10^{12}	6.79×10^{11}	3.14×10^{11}	1.52×10^{11}	5.70×10^{10}	1.20×10^{10}	2.24×10^{9}					17
2.88×10^{-8}	6.00×10^{12}	6.75×10^{12}	6.33×10^{12}	3.93×10^{12}	2.40×10^{12}	9.00×10^{11}	5.07×10^{11}	1.07×10^{11}	3.40×10^{11}	1.35×10^{11}	9.50×10^{10}	3.57×10^{10}	1.00×10^{10}						12
6.75×10^{-8}		5.64×10^{11}					6.35×10^{11}	3.58×10^{11}	4.02×10^{10}	6.35×10^{10}	8.95×10^{10}	3.01×10^{10}	1.13×10^{10}	6.35×10^{9}	1.25×10^{10}				3.0
1.15×10^{-7}										2.83×10^{9}									0.10
$N(\theta)$	36	56	70	72	81	79	78	89	112	129	144	148	105	60	32	16	5.9	9.2	$\Sigma \approx 1321$

TABLE 3.4b: z(r_B, θ) of the sample B197.3

r_B \ θ	4.22×10^{-6}	7.50×10^{-6}	1.33×10^{-5}	2.37×10^{-5}	4.22×10^{-5}	7.50×10^{-5}	1.33×10^{-4}	2.37×10^{-4}	4.22×10^{-4}	7.50×10^{-4}	1.33×10^{-3}	2.37×10^{-3}	4.22×10^{-3}	7.50×10^{-3}	1.33×10^{-2}	2.37×10^{-2}	4.22×10^{-2}	7.50×10^{-2}	$N(r_B)$
2.37×10^{-6}	5.05×10^{12}	4.36×10^{12}	2.83×10^{12}	1.55×10^{12}	1.07×10^{12}	5.61×10^{11}	3.34×10^{11}	2.22×10^{11}	1.58×10^{11}	1.05×10^{11}	6.97×10^{10}	4.10×10^{10}	1.71×10^{10}	8.26×10^{9}	2.32×10^{9}	7.20×10^{8}	1.70×10^{8}	1.35×10^{8}	673
4.22×10^{-6}	9.08×10^{11}	9.56×10^{11}	6.42×10^{11}	4.14×10^{11}	2.08×10^{11}	1.43×10^{11}	7.31×10^{10}	5.20×10^{10}	3.29×10^{10}	2.19×10^{10}	1.43×10^{10}	8.22×10^{9}	3.48×10^{9}	1.18×10^{9}	2.51×10^{8}	4.11×10^{7}	1.49×10^{7}	7.43×10^{6}	242
7.50×10^{-6}	5.94×10^{11}	4.28×10^{11}	2.91×10^{11}	1.75×10^{11}	1.12×10^{11}	7.10×10^{10}	3.43×10^{10}	2.21×10^{10}	1.55×10^{10}	1.04×10^{10}	5.93×10^{9}	3.42×10^{9}	1.62×10^{9}	3.39×10^{8}	5.87×10^{7}	4.95×10^{6}	1.86×10^{6}	5.22×10^{5}	189
1.33×10^{-5}	2.30×10^{11}	1.67×10^{11}	1.11×10^{11}	5.43×10^{10}	2.35×10^{10}	1.27×10^{10}	7.52×10^{9}	6.38×10^{9}	3.73×10^{9}	1.98×10^{9}	1.02×10^{9}	3.34×10^{8}	7.05×10^{7}	8.25×10^{6}					117
2.37×10^{-5}	5.28×10^{10}	5.78×10^{10}	4.92×10^{10}	2.30×10^{10}	1.73×10^{10}	7.43×10^{9}	5.01×10^{9}	2.03×10^{9}	8.92×10^{8}	5.66×10^{8}	2.19×10^{8}	5.58×10^{7}	1.16×10^{7}						50
4.22×10^{-5}	1.32×10^{10}	1.49×10^{10}	1.15×10^{10}	1.06×10^{10}	3.47×10^{9}	2.32×10^{9}	1.31×10^{9}	4.40×10^{8}	4.29×10^{8}	2.23×10^{8}	1.04×10^{8}	5.58×10^{7}	1.82×10^{7}	2.79×10^{6}					27
7.50×10^{-5}	1.88×10^{9}	2.61×10^{9}	2.64×10^{9}	1.65×10^{9}	8.36×10^{8}	8.79×10^{8}	2.06×10^{8}	1.49×10^{8}	1.39×10^{8}	4.70×10^{8}	4.11×10^{7}	1.82×10^{7}	2.79×10^{6}						12
1.33×10^{-4}		2.94×10^{7}		9.28×10^{7}	1.57×10^{7}	2.94×10^{7}	1.65×10^{7}	1.86×10^{7}	1.04×10^{7}	8.81×10^{6}	1.65×10^{6}	2.79×10^{6}							1.8
$N(\theta)$	36	56	70	72	81	79	78	89	112	129	144	146	105	60	32	16	6.9	9.2	$\Sigma \approx 1321$

$$H_{d,i} = H_{cp,i} - H_{cl,i} \qquad \left[A\,m^{-1}\right] \qquad (3.38)$$

where $H_{cp,i}$ is the applied field at which the i-th
wall jumps occurs and $H_{cl,i}$ is the local coercive
field during the i-th jump.

(b) The pulse duration τ_B: The pulse duration τ_B of the
Barkhausen jumps depends on the wall jumping process:

(b1) For a pinning dominated process $\tau_{B,i}$ depends on
the distance that the wall segment, after overcoming
pinning point i, traverses in the i-th jump before
this wall(segment) is pinned again (see sec. 5.4).

(b2) For a stiffness dominated process $\tau_{B,i}$ depends on
the length of the moving wall segment $l_{w,i}$ of the
i-th jump (see sec. 5.5.2, eq. (5.59a)).

(c) The time θ: As shown in fig. 3.1 the time θ_i during
and following the i-th pulse is the time interval be-
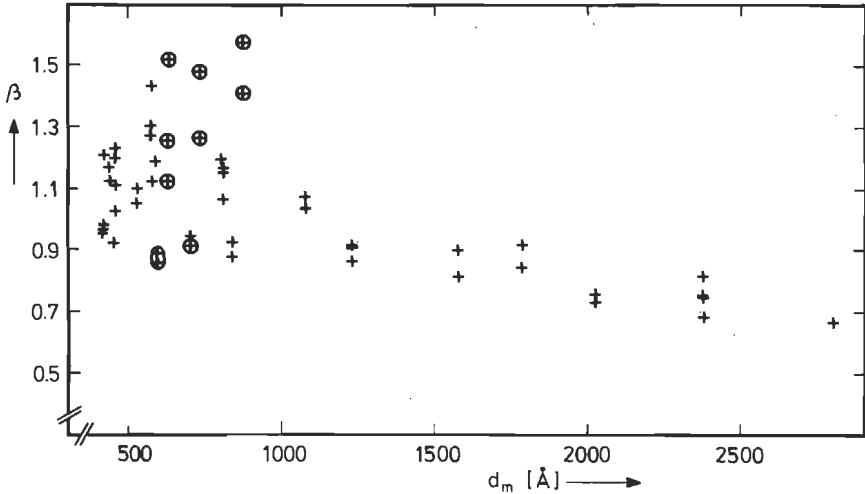
Fig. 3.15. Slope β of the density function $z(\theta)$ as a function of d_m; samples with very small
values of P_{tot} are indicated by ⊕.

tween the beginning of the i-th pulse and the begin-
ning of the (i+1)-th pulse. After overcoming a pinning
point i (at an applied field $H_{cp,i}$) only a stronger
pinning point can pin the wall, thus with $H_{cp} > H_{cp,i}$.
The applied field increases linearly with time (sec.
2.4), thus we can write.

$$\theta_i \propto H_{cp,i+1} - H_{cp,i} = \Delta H_{cp,i} \qquad (3.39)$$

where $H_{cp,i}$ and $H_{cp,i+1}$ represent the values of the applied field at which the i-th, resp. the (i+1)-th jump begins (see sec. 5.2.2). When $H_{cp,max}$ corresponds to the strongest pinning point present in the sample and a pinning point i is overcome then the following pinning point (i+1) is overcome at an applied field H_{cp} with

$$H_{cp,i} < H_{cp} < H_{cp,max} \qquad (3.40)$$

Several walls are present in the film during the reversal (see sec. 2.2.2) and furthermore mostly only a part of the wall moves. So different wall segments in different parts of the film are often responsible for successive wall jumps. The occurrance of successive wall jumps determines θ. Hence θ does not depend on the parameters of a single jump, as is the case for p and τ_B.

Hence from the points (a) to (c) we can conclude that θ_i is independent of p_i and $\tau_{B,i}$ and for $z(\theta)$ measured in our films we find an equation of the form (3.37), so the pulses do not occur independent of each other. This is not surprising because when the reversal goes on the range of possible θ values for a following jump decrease as follows from eqs. (3.39) and (3.40). For the i-th jump

$$0 < \theta_i < H_{cp,max} - H_{cp,i} \qquad (3.41)$$

where $H_{cp,i}$ increases with the applied field during the reversal.

The measurements of $z(\theta)$ are very inaccurate. Two effects influence the accuracy:
(1) The presence of background noise. The background noise sometimes exceeds the reference voltage of the Barkhausen Computer Interface (see sec. 2.5). A large time interval θ is then splitted into a small number of smaller intervals. The presence of background noise results in an increase of

β . In our measurements the influence of the background
noise increases with increasing amplification, hence also
with increasing level of the reference voltage. Fig. 3.16
shows the measured value of β as a function of the ref-
erence voltage.
(2) Jumps with an amplitude lower than the reference volt-
age are not detected. These missing jumps cause a shift
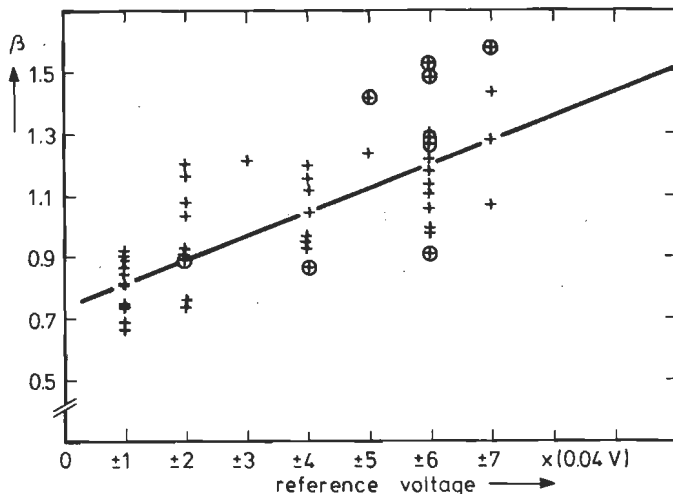
Fig. 3.16. Measured slope β as a function of the reference level of the Barkhausen Com-
puter Interface; samples with very small values of P_{tot} are indicated by ⊕.

from smaller to larger values of the time interval θ. A
decrease of β results. The effect of the errors is that
large intervals are divided into smaller ones and that
small intervals are joined together. The results of the
measurements of z(θ) anywhere have to be used with great
care.

The sum of the values of θ per hysteresis loop is
denoted by Θ :

$$\Theta = \sum_k \theta_k z(\theta_k) \Delta\theta_k \qquad [s] \qquad (3.42)$$

In the presented examples we find for   :
    sample B197.3   Θ ≈ 3.4 s
    sample B289.34   Θ ≈ 0.4 s

The frequency-density functions of τ_B and θ (see fig. 3.9) suggest that sometimes different pulses overlap. This can easily be estimated for a simplified case by assuming that the beginning of the pulses occurs at random points in time. From calculations carried out in appendix 3, we can conclude that the probability of pulse overlapping is small enough to be disregarded.

REFERENCES
3. 1   R. ter Stege, N.J. Wiegman, J. Phys. E: Sci. Instrum. 11, 1978, p. 791 - 794.
3. 2   N.J. Wiegman, to be published.
3. 3   N.J. Wiegman, R. ter Stege, Appl. Phys. 16, 1978, p. 167 - 174.
3. 4   C.H. Vincent, "Random Pulse Trains", IEE, London, 1973, (Peregrimus, London 1973).
3. 5   K. Stierstadt, Springer Tracts in Modern Physics, 40, 1966, p. 12.
3. 6   U. Lieneweg, W. Grosse-Nobis, Int. J. Magn. 3, 1972, p. 11 - 16.
3. 7   H. Bittel, L. Storm, "Rauschen", Springer, Berlin, 1971.

4. GENERAL BEHAVIOUR OF THE BARKHAUSEN EFFECT.

4.1. INTRODUCTION [*]

As was discussed in secs. 1.2 and 1.3, a large number
of publications on the Barkhausen effect deal with the be-
haviour along the hysteresis curve of bulk samples. In some
papers suggestions have been given about a relationship
between certain quantities and the Barkhausen effect: for
example investigations are reported about the relation-
ship between the coercive field and the density function
of the pulse size [4.1, 4.2] , as well as the thickness
dependence of the measured total number of jumps per loop
and of the measured mean pulse size [4.3, 4.4] . In some
of these investigations only a small number of measure-
ments has been performed. In the present chapter measure-
ments of this type are described which are carried out on
thin films. A large number of magnetic films has been
investigated, covering a wider range of values of the
coercive field H_c and film thickness d_m than is the case
in most other investigations.

In our measurements a large number (about 40) of hys-
teresis loops was traced. Each reversal was divided into
several sections, all having equal lengths ΔH. The corre-
sponding sections of the different reversals were taken

together and in each section of the reversal, several quantities of the Barkhausen process were investigated. Thus, in secs. 4.2 and 4.3, each measuring point represents a value averaged over all jumps recorded in an interval ΔH from a number of hysteresis loops. Without further indication all quantities presented in this chapter are averages. All results of the measurements were obtained with the aid of the Barkhausen Computer Interface [4.5].

The behaviour of the jumps as a function of the applied magnetic field H is presented in sec. 4.2. The results are similar to those measured on bulk samples [4.4, 4.6]. In all published statistical calculations of the Barkhausen spectrum [4.7, 4.8] the authors assume the process of domain wall jumping to be stationary. Until now no experimental confirmation of the stationarity has been published. In sec. 4.3 our results on thin films are shown with respect to this stationarity. In sec. 4.4 properties from the measurements in the time domain and from the frequency-density functions of the pulse parameters are summarized. The influence of H_c and d_m is investigated.

When wall jumps occur then the demagnetizing field of the sample varies suddenly. This is also the case for the driving field which decreases then so that the reversal process is retarded. This effect is called the blocking mechanism of the demagnetizing field. In sec. 4.4 we have investigated whether the blocking mechanism caused by the demagnetizing field [4.9] is present in our samples.

4.2. THE MAGNETIZING BEHAVIOUR ALONG THE HYSTERESIS LOOP IN THE EASY DIRECTION

The behaviour of the Barkhausen jumps as a function of the applied field H was investigated on a number of our films. During both reversals the magnetization behaviour shows an identical behaviour, as was to be expected. The results of the different films resemble each other so
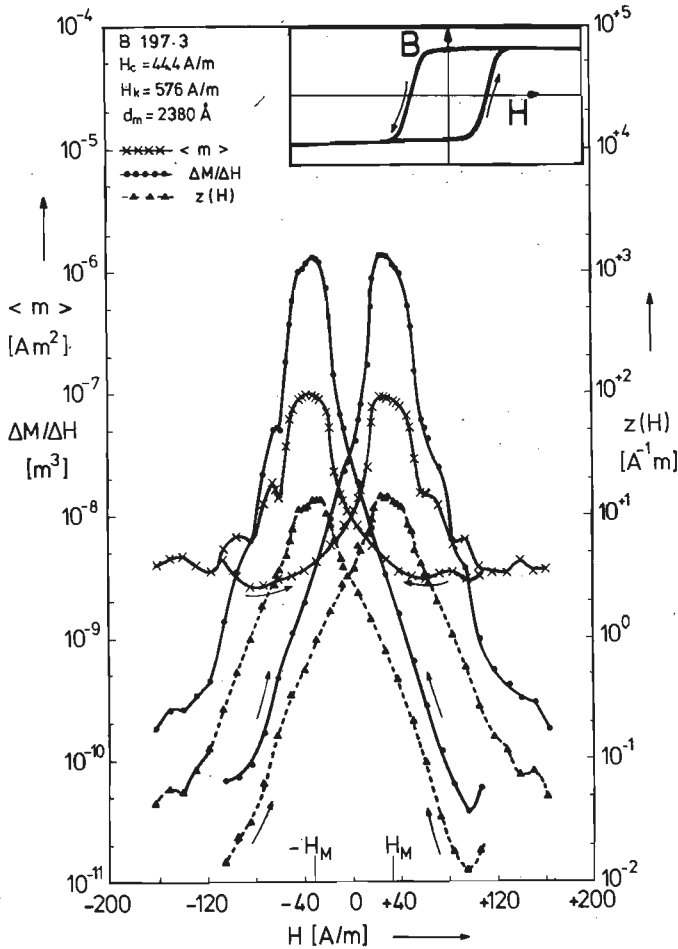
Fig. 4.1. The behaviour of a film with a thickness of 2380Å as a function of the applied field H: z(H), <m> and ΔM/ΔH along the loop; the inset shows the hysteresis loop. The arrows near the curves correspond with the direction along which the hysteresis loop is traversed.

closely that we present here only the results obtained from two samples

In fig. 4.1 (inset) the hysteresis loop (at a field frequency of 50 Hz) has been plotted for a sample of 2380 Å thickness. Fig. 4.1 shows z(H), the frequency-density function of the field H, at which a wall jump starts. From eq. (3.6) it follows that

$$z(H) = \sum_i \sum_j \sum_k z(p_i \tau_{B,j} \Theta_k H) \Delta p_i \Delta \tau_{B,j} \Delta \Theta_k \qquad (4.1a)$$

or $\qquad z(H) = N(H)/\Delta H \qquad \left[A^{-1}m\right] \qquad$ (4.1b)

in which N(H) is the number of wall jumps which start in the interval ΔH around H. Fig. 4.1 shows z(H) during both reversals of the magnetization. The absolute maxima of z(H) during a reversal are reached at a field $\pm H_M$. In this sample the field H_M has a value of about 33 A/m and differs slightly from H_c,

$$H_M < H_c \qquad \left[A/m\right] \qquad (4.2)$$

A difference between H_M and H_c has also been found by other authors [4.10].

We further have considered z(p,H), the frequency-density function of p and H for one particular jump size p as a function of the field H; this was done with the size as parameter. For all jump sizes p we found that z(p,H) as a function of H has the same shape and the absolute maxima of z(p,H) as function of H occur always at $\pm H_M$. Stierstadt and Boeckh [4.11] found a dependence between H_M and the jump size p in their experiments on harddrawn nickel wires.

In our films we found a simple relation between H and z(H) in two parts of a reversal. For the beginning of the reversal and for the last part of the reversal the relation can be approximated by an equation of the form

$$z(H) = C_o \exp\left\{C_1(H - H_o)\right\} \qquad \left[A^{-1}m\right] \qquad (4.3)$$

The values of C_1 and H_o of the sample are given in table 4.1; C_o is about 1 $A^{-1}m$. The influence of temperature, crystallite size and H_c on z(H) has been thoroughly studied, especially by Stierstadt et al. and Deimel et al. [4.1, 4.4, 4.6, 4.12] . The directional dependence of z(H) has also been investigated [4.13]. On single crystals of silicon-iron Salanskii et al. [4.14] found two maxima. The same was found by Deimel et al. [4.2] , which they interpreted as being due to the presence of 180° and 90° walls in different parts of the loop.

Fig. 4.1 also shows the mean value of the change of

Table 4.1

Reversal	section of the curve	C_1 $(A^{-1}m)$	H_0 $(A^{-1}m)$	
$-I_s/\mu_o$ to $+I_s/\mu_o$	nucleation	5.0×10^{-2}	-26	$H < 33\ Am^{-1}$
	appr. to saturation	-5.9×10^{-2}	$+85$	$H > 33\ Am^{-1}$
$+I_s/\mu_o$ to $-I_s/\mu_o$	nucleation	-5.5×10^{-2}	$+21$	$H > -33\ Am^{-1}$
	appr. to saturation	5.8×10^{-2}	-82	$H < -33\ Am^{-1}$

the magnetic moment during the Barkhausen jumps, $<m>$, along the loop (see eq. (3.3)).

$$< m > = \frac{2 I_s}{\mu_o} < V_{jump} > \quad \left[A\ m^2 \right] \qquad (4.4)$$

where I_s is the saturation polarization and V_{jump} the volume reversed in one jump. The minimum detectable value of m in this measurement is $1.3 \times 10^{-9}\ Am^2$, corresponding to a volume of $8 \times 10^{-16}\ m^3$. The absolute maxima of $<m>$ during both reversals are reached at the same fields $\pm H_M$ as the maxima of z(H). The irregularities in the shape of the curves are caused by the motion of wall segments jumping away from a few very strong pinning centres. This has been confirmed by visual observations of the domain wall motion as function of the applied field using the magneto-optic Kerr effect.

The third curve in fig. 4.1 represents the quantity $\Delta M / \Delta H = (2I_s/\mu_o) \Delta V / \Delta H$ as a function of H. V is the volume of the reversed part of the film. Here again the maxima occur at $\pm H_M$. As can be seen from the curve of $\Delta M / \Delta H$ in fig. 4.1 almost the whole reversal of the magnetization takes place in a field interval of about 40 A/m around $\pm H_M$. The jumps which take place in the other part of the reversal are very small and hardly

contribute to the total change of the magnetization. This is true a fortiori for their contribution to the noise spectrum, which is proportional to $\sum_i p_i^2$ (see eq. (6.12)).

Let us consider the steep part of the hysteresis loop where, in this particular sample, about five walls participate in the reversal process. These walls cross the film nearly from one side to the other. If a wall is pinned by a very strong pinning point, no large jumps of this wall can occur. Small sections of the wall corresponding to small jumps can still move (see sec. 1.4). The number of large wall jumps is low compared to that of small jumps, so in the curve of z(H) against H the presence or absence of large wall jumps cannot be detected. In the steep part of the loop the contribution to $<m>$ of large wall jumps is large. Hence, the influence of large wall pinning centra can, in our type of samples, only be detected in the curves of $<m>$ (sometimes a small effect is seen in the curves of $\Delta M/\Delta H$). The irregularities in the shape of these curves are due to this effect. The behaviour along the loop for different films varies only with regard to the position and size of the irregularities in the shape of the curves of $<m>$ and $\Delta M/\Delta H$. Sometimes even two maxima in the curves of $<m>$ are observed [4.15] (fig.4.2).

Two maxima in the curves of z(H) were found by Deimel et al. [4.2]. They attributed those to the presence of 90° walls in their wire-shaped samples. An experimental confirmation of the presence of 180° and 90° walls in their samples was not mentioned.
Most types of magnetic samples show at the beginning of the reversal process usually a rotation of the magnetization which is followed by nucleation of domain walls. The process of domain wall motion is responsible for the largest part of the reversal. The last part of the reversal is completed by rotation again. In the section of the loop where the domain wall displacement takes place often small closure domains (with 90° walls) are present. Their con-
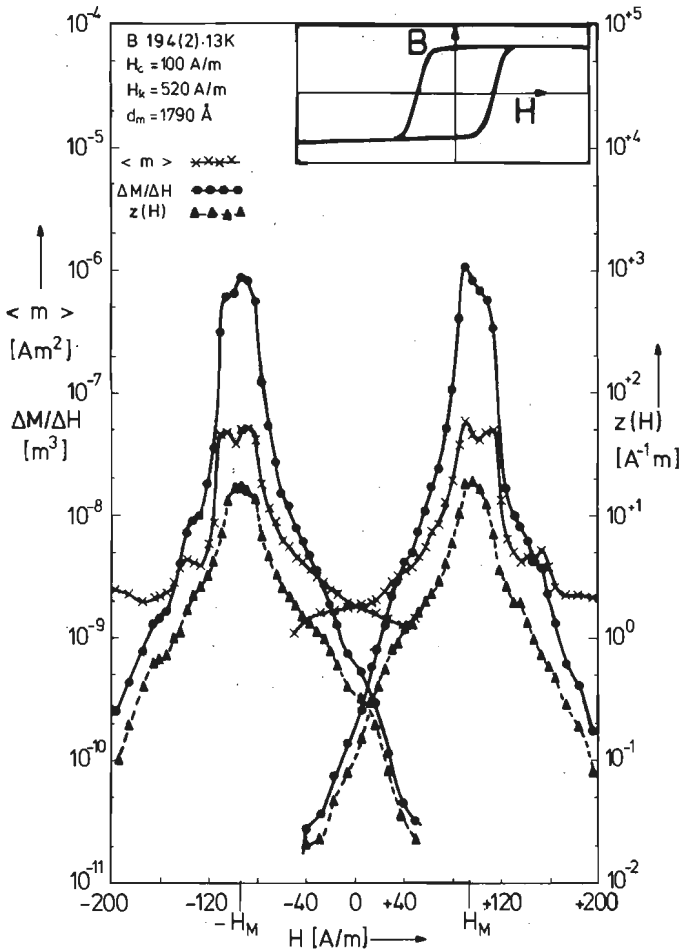
Fig. 4.2. The behaviour of a film with a thickness of 1790Å as a function of the applied field H: z(H), < m > and ΔM/ΔH along the loop; the inset shows the hysteresis loop.

tribution to the remagnetization process, i.e. to $\Delta M/\Delta H$ is small, but they contribute largely to z(H) in those regions where they are nucleated and disappear. This can lead to maxima in the curve of z(H) for the values of H where the nucleation and disappearance of walls takes place. In our samples hardly any 90°-walls are present; yet in a few cases two maxima occur in the curves of <m> and $\Delta M/\Delta H$, as was previously mentioned. This must be due to the presence of strong pinning centres.

4.3. THE STATISTICS OF THE BARKHAUSEN EFFECT ALONG THE "EASY" HYSTERESIS LOOP

The curves of $<m>$ against H (sec. 4.2) show the Barkhausen process to be not a stationary process. However, in all publications dealing with statistical calculations of the Barkhausen spectrum [4.7, 4.8] the authors assume that the process of domain wall jumping is stationary: this means that the probability density functions of the parameters of the Barkhausen process do not vary along the hysteresis loop. This assumption largely simplifies the calculations. Here we shall investigate as to how far the actual behaviour deviates from this assumption [4.15, 4.16] .

For this investigation the reversal time is divided into intervals of constant length of 0.1s, whereas in the steepest part of the loop the intervals are 0.05s. These time intervals corresponds to field intervals ΔH of 11.2 Am^{-1} and 5.6 Am^{-1}, respectively. We measured in the intervals the frequency-density functions $z(H)$, $z(p,H)$ and $z(\tau_B,H)$.

In sec. 4.2 it was shown that $N(H)$, the number of pulses per field interval ΔH around H which is given by

$$N(H) = z(H) \Delta H \qquad (4.5)$$

varies greatly as a function of H. This is a characteristic property of the magnetization process of a ferromagnetic sample [4.4] . Eq. (4.5) can be written as

$$N(H) = \Delta H \sum_i z(p_i, H) \Delta p_i \qquad (4.6a)$$

or
$$N(H) = \Delta H \sum_j z(\tau_{B,j}, H) \Delta \tau_{B,j} \qquad (4.6b)$$

The frequency-density functions $z(p,H)$ and $z(\tau_B,H)$ also vary very much if they are plotted as a function of p, respectively of τ_B with H as parameter. To show clearly how the probability of large wall jumps changes during the reversal as compared to the probability of small

jumps we have determined the conditional probability-density functions pr(p|H) and pr(τ_B|H) as:

$$pr(p \mid H) = \frac{z(p, H)}{z(H)} \qquad \left[V^{-1} s^{-1} \right] \qquad (4.7)$$

and

$$pr(\tau_B \mid H) = \frac{z(\tau_B, H)}{z(H)} \qquad \left[s^{-1} \right] \qquad (4.8)$$

In eqs. (4.7) and (4.8) z(p,H), z(τ_B,H) and z(H) are measured quantities. We have plotted pr(p|H) and pr(τ_B|H) in fig. 4.3 with H as parameter for the different intervals into which the reversal is divided. In each interval,
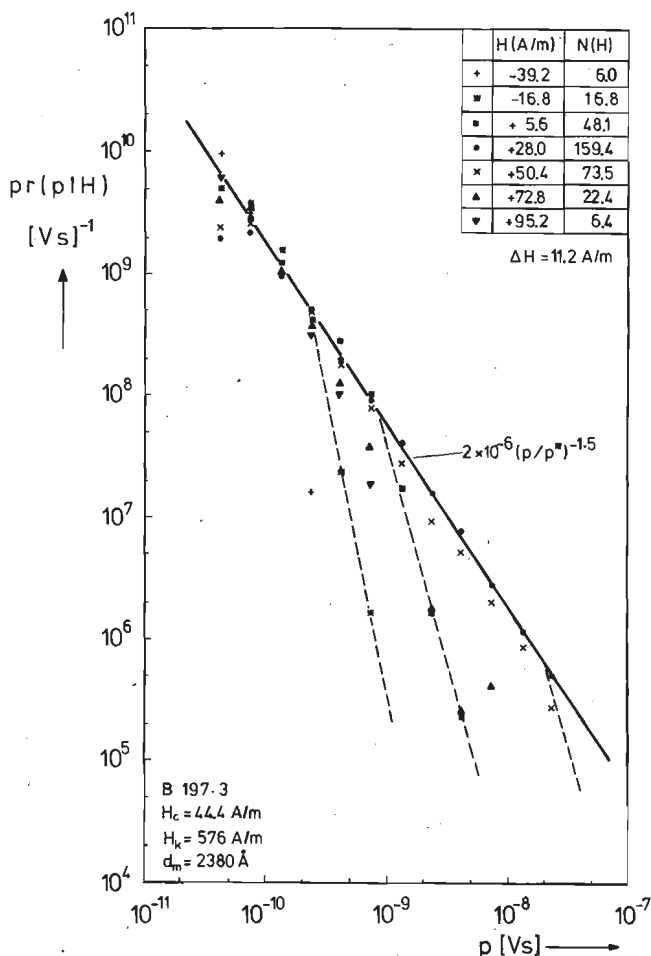
Fig. 4.3.(a) The probability density pr(p|H) during the complete reversal with H as parameter. The broken lines show some curves for p > p_0 (p^* = 1Vs).

77
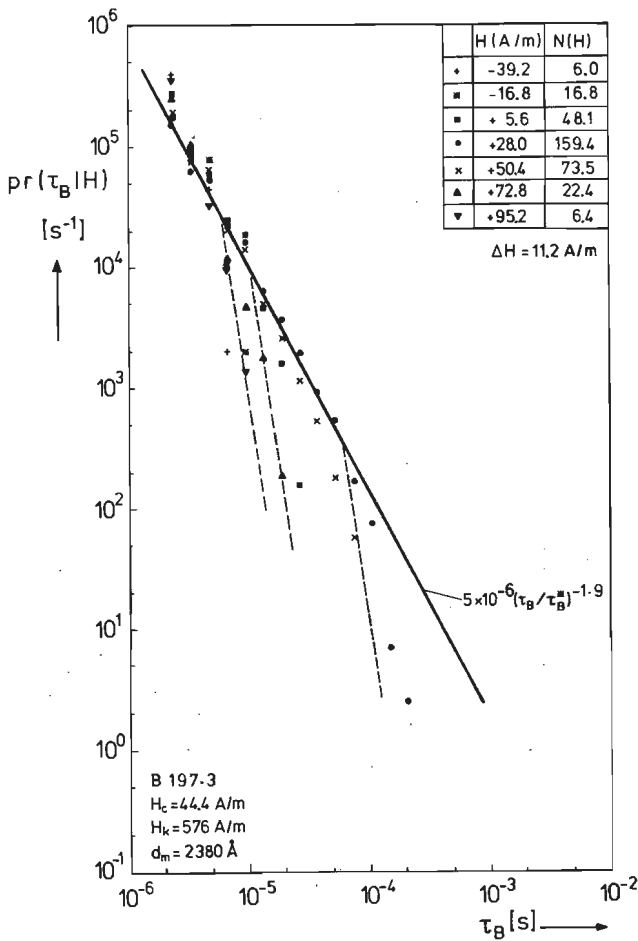
Fig. 4.3.(b) The probability density $pr(\tau_B|H)$ during the complete reversal with H as parameter. The broken lines show some curves for $\tau_B > (\tau_B)_0$ ($\tau_B^* = 1s$).

hence at each value of the parameter $\overset{\backprime}{H}$, the curve fitted to the measured points of $pr(p|H)$ and $pr(\tau_B|H)$ is a function of p and τ_B, respectively. For each H value the measured points follow a curve, which can be described by equations similar to those used in secs. 3.5 and 3.6 (eqs. (3.24) and (3.34)):

$$pr(p|H) = \begin{cases} A_{1H}\left(\dfrac{p}{p^*}\right)^{-\alpha_{1H}} & p_{min} < p \leq p_o \\[3mm] A_{2H}\left(\dfrac{p}{p^*}\right)^{-\alpha_{2H}} & p_o \leq p < p_{max} \end{cases} \tag{4.9}$$

for the pulse size p(with $p^* = 1Vs$) and

$$pr(\tau_B | H) = \begin{cases} D_{1H} \left(\dfrac{\tau_B}{\tau_B^*} \right)^{-\delta_{1H}} & (\tau_B)_{min} < \tau_B \leqslant (\tau_B)_o \\[4mm] D_{2H} \left(\dfrac{\tau_B}{\tau_B^*} \right)^{-\delta_{2H}} & (\tau_B)_o \leqslant \tau_B < (\tau_B)_{max} \end{cases} \qquad (4.10)$$

for the pulse time τ_B (with $\tau_B^* = 1$ s). The solid lines in
fig. 4.3 fit very well to the points measured in the in-
tervals of the steepest part of the hysteresis loop. In
these intervals N(H) has the largest value and thus the
measuring error is minimal here. From the figures it
follows that for all curves of a single sample we find
about the same values of α_{1H}, α_{2H}, δ_{1H}, δ_{2H}, A_{1H} and
D_{1H}. The values of p_o and $(\tau_B)_o$ vary by about a few
orders of magnitude during the reversal, as shown in
fig. 4.3. In the sample of 2380 Å thickness we find about
the following values for the constants:

$$A_{1H} \approx 2 \times 10^{-6} \qquad\qquad D_{1H} \approx 5 \times 10^{-6}$$

$$\alpha_{1H} \approx 1 \cdot 5 \qquad\qquad\qquad \delta_{1H} \approx 1 \cdot 9 \qquad (4.11)$$

$$\alpha_{2H} \geqslant 3 \cdot 5 \qquad\qquad\qquad \delta_{2H} \geqslant 6 \cdot 5$$

The slopes of the functions pr(p|H) for $p < p_o$ and
$pr(\tau_B | H)$ for $\tau_B < (\tau_B)_o$ are smaller by 0.1-0.3 than those
of z(p) and $z(\tau_B)$ of the same sample (see fig. 3.9). This
can be understood from fig. 4.3 if one realizes how z(p)
and $z(\tau_B)$ follow from pr(p|H) and $pr(\tau_B|H)$, respectively.
Using eqs. (4.7) and (4.8) one finds

$$z(p) = \sum_l z(p, H_l) \, \Delta H_l$$

$$z(p) = \sum_l pr(p | H_l) \, z(H_l) \, \Delta H_l$$

$$z(p) = \sum_l pr(p | H_l) \, N(H_l) \qquad (4.12)$$

and
$$z(\tau_B) = \sum_l pr(\tau_B | H_l) \, N(H_l) \qquad (4.13)$$

Summarizing one can say that the probability-density functions pr(p|H) and pr(τ_B|H) are dependent on the applied field, i.e. on the relative position of H in the hysteresis curve. Thus they vary during the reversal of the magnetization. The statistical behaviour is identical in each interval of a pair that lies symmetrical around H_c. At the beginning and the end of the reversal process the statistical behaviour differs from that around H_c. Accordingly, if we consider the total reversal the Barkhausen effect cannot be regarded as a stationary process.

As already indicated in sec. 4.2 the reversal takes place almost completely (>90%) within a field interval around H_M, corresponding to the steep part of the hysteresis curve. In this part of the reversal the susceptibility $\Delta M/\Delta H$ is almost constant (see fig. 4.1). To investigate the stationary behaviour of the signal we must therefore confine ourselves to this region. The functions pr(p|H) and pr(τ_B|H) are examined again for this part of the reversal. For the steep part of the hysteresis loop, pr(p|H) and pr(τ_B|H) are plotted in fig. 4.4 with H as parameter. For all intervals in which the steep part of the loop is divided the curves through the measured points of fig. 4.4 can be described by the same equations as used in fig. 4.3:

$$\text{pr}(p\,|\,H) \approx 2\times 10^{-6} \left(\frac{p}{p^*}\right)^{-1.5} \qquad p_{min} < p \leqslant p_o \qquad (4.14)$$

and

$$\text{pr}(\tau_B|H) \approx 5\times 10^{-6} \left(\frac{\tau_B}{\tau_B^*}\right)^{-1.9} \qquad (\tau_B)_{min} < \tau_B \leqslant (\tau_B)_o \qquad (4.15)$$

From fig. 4.4 it follows that the probability of a jump of a certain size or duration is constant during the steep part of the hysteresis loop. Consequently we may conclude that in the steep part of the loop, i.e. for almost constant value of $\Delta M/\Delta H$, the Barkhausen noise signal is stationary. Only the detected number of jumps varies some-

thing along the steep part of the loop (fig. 4.4). In chapter 6 this important property of the Barkhausen noise in thin magnetic films is used in our calculations.

Combining fig. 4.3, which shows the entire reversal with fig. 4.4 where only the steep part of the hysteresis curve is considered, we observe a strongly decreasing probability of the occurrence of large wall jumps at the beginning and the end of the reversal where the values of $\Delta M/\Delta H$ substantially varies (see fig. 4.1). In our sample the region of constant value of $\Delta M/\Delta H$ covers nearly the whole reversal

	H(A/m)	N(H)
+	+14,0	39
■	+19,6	64
■	+25,2	81
♦	+30,8	81
×	+36,4	73
▲	+42,0	68
▼	+47,6	45

$\Delta H = 5.6$ A/m

$2 \times 10^{-6} (p/p^*)^{-1.5}$

B 197·3
$H_c = 44,4$ A/m
$H_k = 576$ A/m
$d_m = 2380$ Å
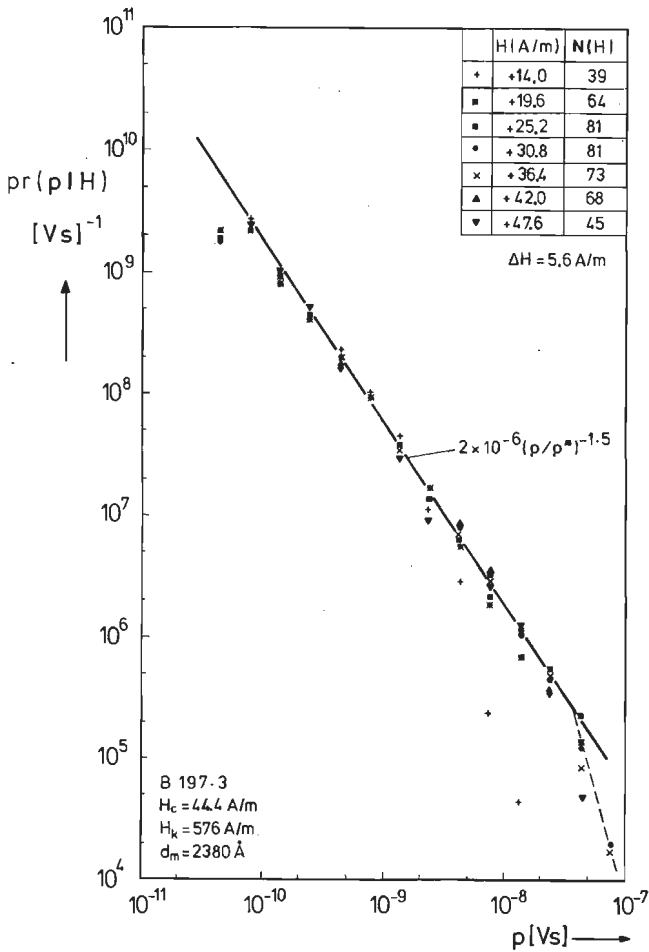
Fig. 4.4.(a)   The probability density function pr(p|H) during the steep part of the loop $(p^* = 1 Vs)$.
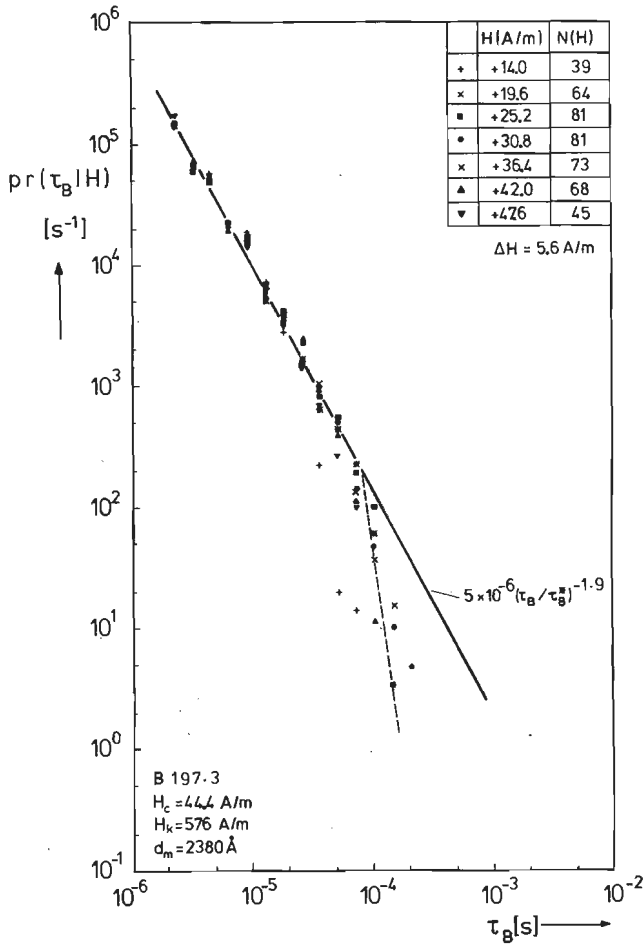
Fig. 4.4.(b)   The probability density function $pr(\tau_B|H)$ during the steep part of the loop $(\tau_B^* = 1s)$.

($>90\%$). In most bulk samples, however, the section of the hysteresis loop with an almost constant susceptibility covers   only a small part of the magnetization reversal by domain wall motion. In those samples the condition of a stationary statistical Barkhausen process is therefore not expected to be fulfilled completely.

4.4. THE BEHAVIOUR OF THE WALL JUMPS PER REVERSAL OF THE MAGNETIZATION

Several authors [4.2, 4.3, 4.12] have investigated the influence of Hc and d_m (in thin films) on the detected mean pulse size, $<p>$, or the measured total number of pulses per loop, N_{tot}. The measured mean pulse size per loop, as a function of the film thickness d_m is shown in fig. 4.5(a). In fig. 4.5(b) $<p>$ is shown as a function of H_c. From fig. 4.5 a slight dependence of $<p>$ on the thick-
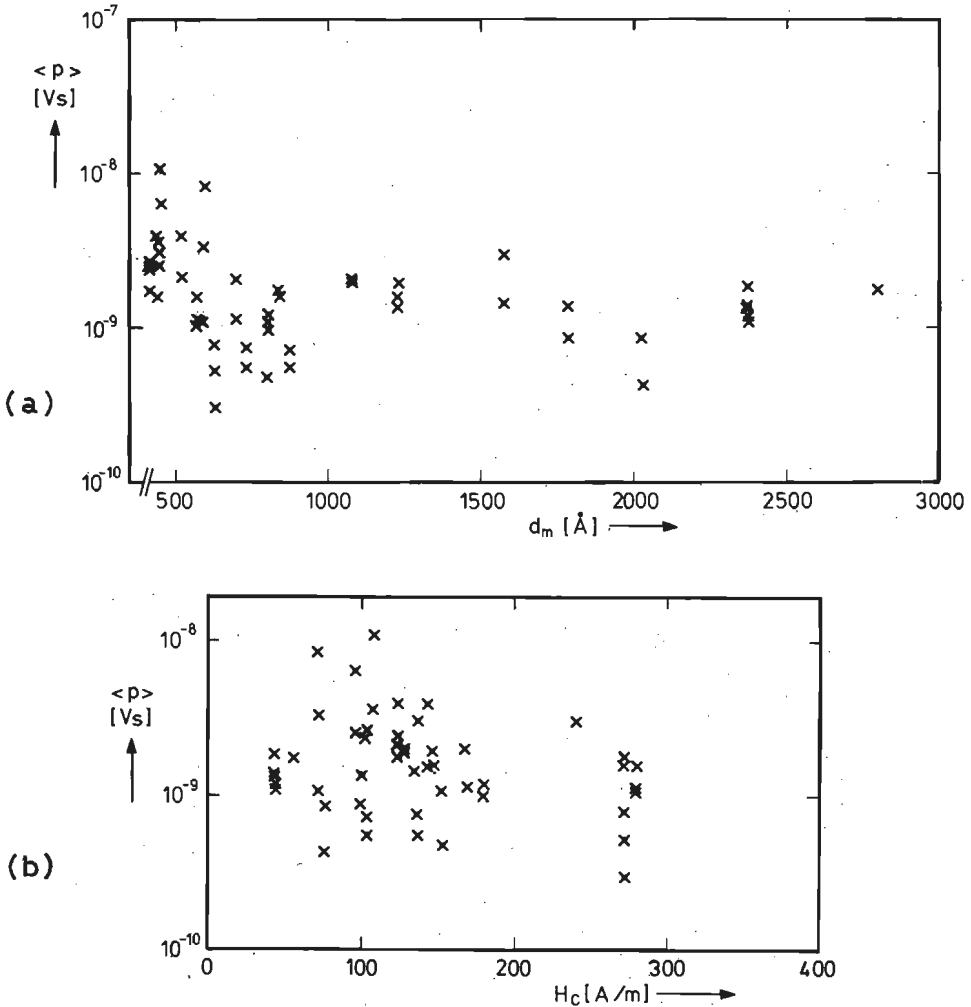
Fig. 4.5.   The detected mean pulse size, $<p>$, as a function of d_m (a) and H_c (b).
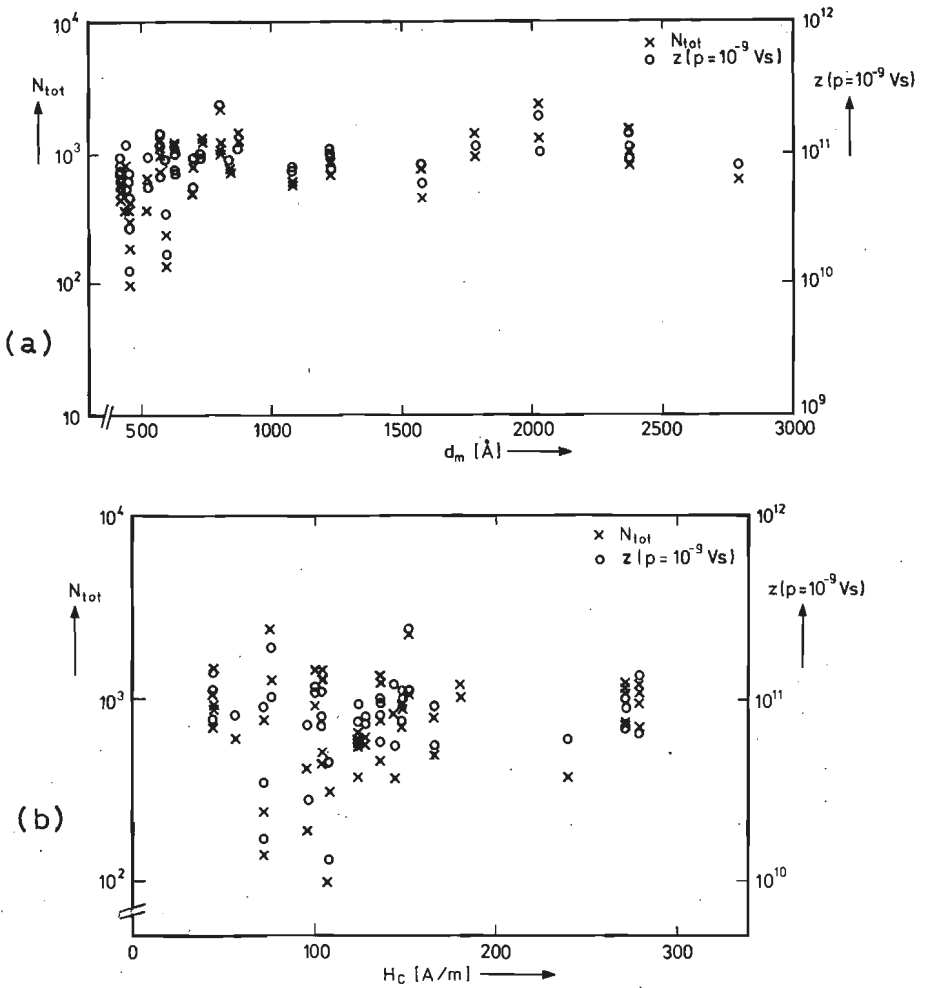
Fig. 4.6. The total number of detected pulses, N_{tot}, and $z(p = 10^{-9} Vs)$, the density of pulses of size $p = 10^{-9} Vs$, as a function of d_m (a) and H_c (b).

ness and on H_c seems to be present in our films. This agrees with some decrease of the total number of detected pulses per loop with decreasing d_m and H_c (see fig. 4.6). As explained in sec. 3.2, the density functions are unknown for small values of p and τ_B. It is not possible to determine the actual total number of pulses per loop and the actual value of the mean pulse size per loop [4.17]. Only the pulses with p and τ_B values that lie within the measuring range are considered in the measurements of $<p>$ and N_{tot}. The minimum detectable level varies for the dif-

ferent samples and so does the inaccuracy in$<p>$ and N_{tot} (compare sec. 3.5). Therefore it is difficult to draw conclusions from our measurements shown in figs. 4.5 and 4.6, because they show scarcely any indication about a relationship between $<p>$ or N_{tot} and d_m and H_c in our samples. In similar investigations by different authors the ranges of p and τ_B values, which can be detected, vary as well as the measured frequency-density functions of these quantities. For the different types of samples investigated, the ranges of p and τ_B values vary also from sample to sample. Hence one must be very careful in comparing the experimental results of measurements concerning $<p>$ and N_{tot} of different authors [4.3, 4.16, 4.18, 4.19]. An improvement in the measuring procedure of a variation of the number of pulses with H_c and d_m is to plot the number of pulses of a certain size as a function of H_c and d_m, as was done by Parzefall and Stierstadt [4.1]. Fig. 4.6 shows a plot of z(p) for p=10^{-9}Vs and N_{tot}. We infer from that figure that the total number of pulses and z(p) per loop are independent of H_c and d_m.
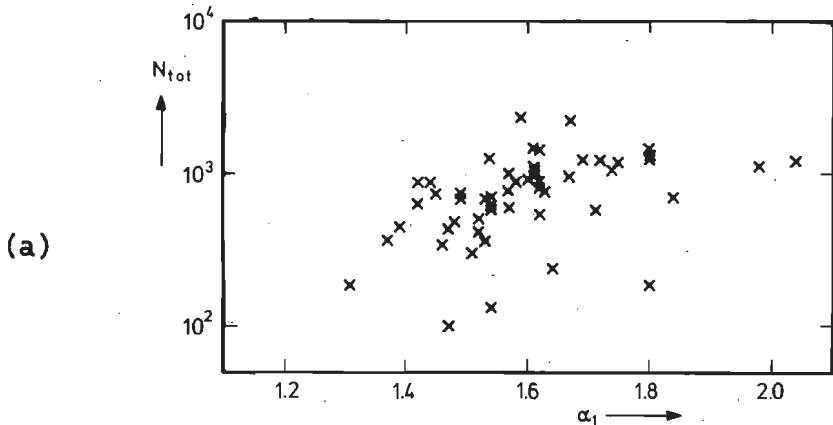
In their investigation of polycrystalline nickel wires Parzefall and Stierstadt [4.1] found that the density function z(μ_0m) for μ_0m = 5×10^{-15}Vsm depends on H_c, i.e. a decrease for z(p) with increasing H_c. In the contrary to this Deimel et al. [4.2] found an increase in the total number of jumps per reversal with increasing H_c in annealed polycrystalline iron wires. The temperature treatment of the samples was different. Deimel et al. observed in their limited measuring range an increase in the number of jumps of "all" sizes with increasing Hc. This may be attributed to the limited measuring range. Another cause can be the variation of the reversible part of the magnetization in their different measurements.

The quantity $<p>$ is normalized to thickness of 1000 Å; thus proportional to the jump area A_{jump}. Hence the figs. 4.5 and 4.6 show that the area reversed by a jump is independent of d_m, while m, which is proportional

85

to d_m (eq. (3.3)), increases with film thicness. The lat-
ter result agrees with the experimental result found by
Salanskii et al. [4.3] . Any information about a possible
transition to the single domain state of a thin mag-
netic film must follow from an extrapolation to zero p of
the curve of $<p>$ versus d_m, instead of an extrapolation
of the curve of m against d_m, as was done by Salanskii.
In our experiments down to 420 Å we found no indication
of any transition to the single domain state. This agrees
with Middelhoeks observations on very thin films of Ni-Fe
$(d_m > 100$ Å) [4.20] .

The very small number of jumps (of the order of 100)
detected in some films is due to difficulties in the do-
main growth from the spikes. When the domain growth starts
the jumps at the beginning of the reversal process will be
very large (see sec. 2.2.2). The total region which must
be reversed is constant, so that the total number of jumps
will be appreciably reduced.

Fig. 4.7a shows the total number of detected jumps,
N_{tot}, as a function of the exponent α_1 of the density
function z(p). In fig. 4.7b some samples of the same films
are considered. No relation between N_{tot} and α_1 can be
detected. The same holds for z(p) for $p=10^{-9}$Vs and α_1. Ac-
cording to Bleil et al. [4.9] α_1 is dependent on the count-

(a)

(b)

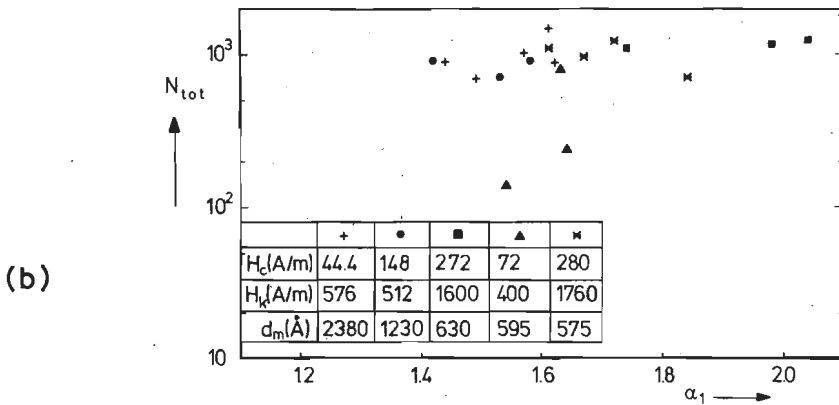|	+	•	■	▲	×
H_c(A/m)	44.4	148	272	72	280
H_k(A/m)	576	512	1600	400	1760
d_m(Å)	2380	1230	630	595	575

Fig. 4.7. N_{tot} as a function of the exponent α, of z(p): (a) for all our measured films; (b) for five films of different thicknesses.

ing rate of the jumps; the blocking mechanism of the de-magnetizing field [4.21] generates this effect. In our films the demagnetizing factor is negligible and so α_1 must be independent of the counting rate and the frequency of the driving field. This is confirmed by the curve of α_1 against f_{FIELD} in fig. 4.8. The blocking mechanism is indeed absent in our samples, in accordance with the in-fluence of the demagnetizing field calculated in sec. 2.2. The influence of the field frequency on the Barkhausen effect is observed in the density functions and the noise spectrum [4.22] (see sec. 1.2(b)). Fig. 4.8 shows the in-fluence on α_1 and δ_1 (of z(p) and z(τ_B) respectively) and on the exponent $\varkappa$, which describes the relation be-tween p and τ_B (see sec. 3.4). These measurements are performed with a digital equipment [4.5]. By the method of noise elimination (see sec. 2.5) used in this equip-ment, the influence of f_{FIELD} can be measured to much lower frequencies than in the analog measurements of the noise spectrum (curve of n against f_{FIELD} in fig. 4.8, where n is the slope of the noise spectrum, see eq.(1.4)). Fig. 4.8 shows that a value of $f_{FIELD} \leqslant 5 \times 10^{-2}$ Hz is low enough to give reliable measurements. The high mobility of the domain walls in the films enables such a high field frequency to be used in the experiments.
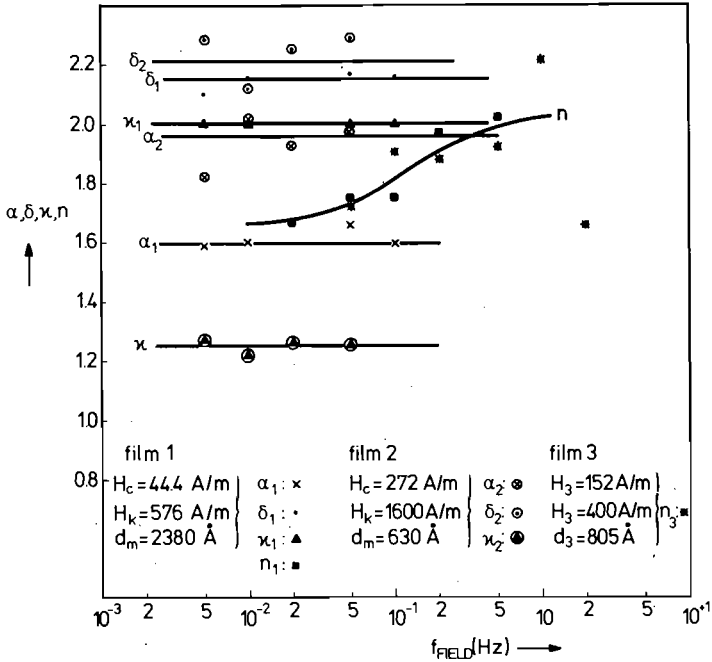
Fig. 4.8. The influence of the frequency f_{FIELD} of the applied magnetic field on the Barkhausen effect: the exponents of the frequency-density functions (α_1, δ_1 and κ) and the slope n of the noise spectrum as a function of f_{FIELD}.

4.5 CONCLUSIONS

In this chapter we have examined the behaviour of the Barkhausen effect in thin NiFe films. The behaviour of the Barkhausen effect in our samples is in general the same as found by others in bulk samples. However in the films the reversal of the magnetization takes place entirely by domain wall motion. The time domain analysis has been used to investigate for the first time the stationarity of the noise signal along the loop. In previous calculations a statistically stationary behaviour has always been assumed. Our results indicate that this is only correct if the susceptibility has about a constant value in the region considered. In our samples the measured quantities $<p>$ and

88

N_{tot} show no dependence on H_c and d_m. The actual values of the mean pulse size and the total number of pulses per reversal cannot be determined. No dependence is found between the surface area reversed by a wall jump and d_m. The density functions do not change when the driving field frequency is varied, which agrees with the absence of demagnetizing effects. The high mobility of the domain walls in the films enables field frequencies up to 5×10^{-2} Hz (dH/dt = 112 A/sm) to be used in the experiments.

REFERENCES

4. 1   F. Parzefall, K. Stierstadt, Z. Physik, **224**, 1969, p. 126 - 134.
4. 2   P. Deimel, B. Röde, R. Wislaug, Z. Naturforsch. **31a**, 1976, p. 163 - 168.
4. 3   N.M. Salanskii, A.M. Rodichev, M.K. Savchenko, Bull. Ac. Sc. USSR. Ser. Phys. **25**, 1961, p. 612 - 615.
4. 4   K. Stierstadt, "Der Magnetische Barkhausen-Effect", Springer Tracts in Modern Physics, **40**, 1966, p. 1 - 106.
4. 5   R. ter Stege, N.J. Wiegman, J. Phys. E: Sc. Instr. **11**, 1978, p. 791 - 794.
4. 6   J.C. McClure Jr, K. Schröder, CRC. Crit. Rev. Sol. St. Sc. **6**(1), 1976, p. 45 - 83.
4. 7   U. Lieneweg, W. Grosse-Nobis, Int. J. Magn. **3**, 1972, p. 11 - 16.
4. 8   M. Celasco, F. Fiorillo, P. Mazzetti, Il. Nuovo Cimento, **23B**, 1974, p. 376 - 383.
4. 9   U. Bleil, A. Loichinger, K. Stierstadt, Z. Physik, **241**, 1971, p. 291 - 294.
4.10   K. Stierstadt, 1966, see ref. 4.4, p. 18.
4.11   K. Stierstadt, W. Boechk, Z. Physik, **186**, 1965, p. 154 - 167.
4.12   P. Deimel, B. Röde, G. von Trentini, J. Magn. Magn. Mat., **6**, 1977, p. 256 - 259.
4.13   A. Gründl, P. Deimel, B. Röde, H. Daniel, J. Magn. Magn. Mat., **6**, 1977, p. 249 - 251.
4.14   N.M. Salanskii, A.M. Rodichev, V.A. Buravikhin, Phys. Met. Metall. USSR, **11**, 1961, p. 843 - 850.
4.15   N.J. Wiegman, R. ter Stege, A.H. de Kuyper, Proc. 5th, Int. Conf. on Noise in Phys. Systems, 1978, Bad-Nauheim, Western Germany.
4.16.   N.J. Wiegman, R. ter Stege, Appl. Phys. **16**, 1978, p. 167 - 174.
4.17   K. Stierstadt, 1966 see ref. 4.4, p. 15.
4.18   K. Stierstadt, E. Preuss, Z. Physik, **199**, 1967, p. 456 - 464.
4.19   P. Deimel, A. Waas, H. Daniel, Z. Naturforsch. **29a**, 1974, p. 524 - 526.
4.20   S. Middelhoek, D. Wild, IBM J. Res. & Dev. **11**, 1967, p. 93 - 105.
4.21   H. Bittel, Forschungsbericht Nr. 251 des Landes Nordrhein-Westfalen, Westd. Verlag, Köln + Opladen, 1956.
4.22   N.J. Wiegman, Appl. Phys. **12**, 1977, p. 157 - 161.

5. THE RELATION BETWEEN THE PULSE SIZE AND THE PULSE DURATION.

5.1. INTRODUCTION

The reversal of the magnetization in our films has been investigated and described at length by Middelhoek [5.1-5.6] . A brief review has been given in sec. 2.2.

Magnetic hysteresis and the Barkhausen effect are attributed to random perturbations of the properties of the magnetic material. The character of the perturbations is usually not known. The perturbations can be regarded either as varying more or less smoothly across the material or as highly localized variations in the properties of the sample. In the latter case the disturbances are called "pinning centres" or "defects". Most experimental results can be interpreted equally well from either point of view [5.7, 5.8] . In sec. 1.1 the character of the Barkhausen process has been explained using a potential energy model which is a smoothly varying function of the wall position. In this chapter (see also fig. 1.4) we shall use the model in which the perturbations take the form of highly local-ized pinning centres.

A model for the Barkhausen effect with which one can deduce the measured relationship between the pulse size p and the pulse duration τ_B (see sec. 3.4) has as yet not been published. The subject is very difficult because of the poor knowledge available on the interaction between domain walls and inclusions. In this chapter, in the secs. 5.2.2. to 5.4, we will make an attempt to present in simple terms a description of the Barkhausen effect which en-

ables us to outline the relationship between p and τ_B in
the secs. 5.4 to 5.7. This relation has the functional
form $p_w(\tau_B) \propto \tau_B^{\varkappa}$.

In sec. 5.2 we discuss a wall jumping process governed
by wall pinning. The length of a wall segment between two
pinning points can easily be derived in this case. In sec.
5.3 some general comments are made on the relation between
p and τ_B. In sec. 3.4 the measured two-dimensional fre-
quency-density functions of p and τ_B have been discussed.
In secs. 5.4 to 5.7 three wall jumping models are present
ed for which we can derive the values of $\varkappa$. In sec. 5.7
the results of the calculations are compared with the meas-
ured relations. The results of the theory agree with the
experimental findings.

5.2. DOMAIN WALL PINNING PROCESS

In this chapter we will use the term inclusions for
all localized disturbances that interact with the wall. A
localized disturbance that actually pins a wall is called
a pinning point.

In the first subsection 5.2.1 we will start with a
simple description of the inclusions that play a part in
the Barkhausen effect. Then, in sec. 5.2.2., we will dis-
cuss the wall jumping process and some assumptions which
enable us to derive (sec. 5.2.3) the distance d between two
pinning points.

5.2.1. The types of inclusion

Considering the interaction between an inclusion and
a domain wall, the inclusions can be divided into three
groups [5.9] :
(a) Inclusions having dimensions that are much smaller
    than the domain wall width δ_w. These inclusions can
    not pin the wall. The wall passes them reversibly.

(b) Inclusions with dimensions much larger than the domain
    wall width. They are passed via an interaction of the
    wall with the secondary magnetic domain structure sur-
    rounding the inclusions (see fig. 5.1) [5.10] . When
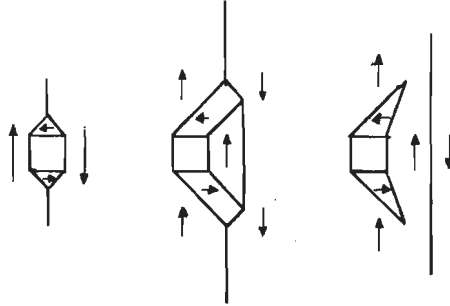   the wall comes within the acquisition distance of the

Fig. 5.1. General form of the secondary domain structure arising from the interaction
between a domain wall and an inclusion.

inclusion, the wall attaches itself to the pinning
point, and at a certain value of the increasing applied
field the wall snaps free from the Néel spikes. This
can readily occur for cross-tie walls (see fig. 2.7),
because these walls can adjust their structure [5.10]
by the displacement of the cross-ties over some dis-
tance in the wall. In this way the energy of the wall
structure surrounding the pinning point can be mini-
mized.

(c) Inclusions with dimensions of the same order of mag-
    nitude as the domain wall width. Only these inclusions
    can directly pin the wall. As calculated by Middelhoek
    [5.3] , the domain wall width δ_w in our samples is of
    the order of 400 Å.

In the Barkhausen process only those inclusions are import-
ant that impede the domain wall motion, resulting in wall
jumps. Hence we neglect the inclusions of type (a) in the
following sections of this chapter.

5.2.2. The wall jumping process

In all our experiments a sample is placed in a magnetic field which increases linearly in time and under these conditions we measure the Barkhausen effect which occurs during a reversal of the magnetization. In this experiment we define the strength H_p of an inclusion or pinning point as the field H_{cp} necessary to start the movement of the wall pinned by the disturbance minus the field $H_{c,min}$ at which the domain wall motion in the film begins (see sec. 2.2.2.):

$$H_p = H_{cp} - H_{c,min} \qquad \left[Am^{-1} \right] \qquad (5.1)$$

We use this definition for all samples except the few macroscopically inhomogeneous samples (sec. 2.2.2).

After the wall has overcome a pinning point i with strength $H_{p,i}$ any following point j which can pin the wall will satisfy

$$H_{p,j} > H_{p,i} \quad \text{and hence} \quad H_{cp,j} > H_{cp,i} \qquad (5.2)$$

At a value H of the applied field with

$$H = H_{cp,i} \qquad (5.3)$$

all inclusions of strength H_p for which:

$$H_p \leqslant H_{p,i} \quad \text{and hence} \quad H_{cp} \leqslant H_{cp,i} \qquad (5.4)$$

cannot pin the wall any more. As mentioned in sec. 2.2.2 H_{cp} varies between $H_{c,min}$ and $H_{c,max}$.

In general the wall does not move as a whole but only a part of the wall is displaced as shown in fig. 1.4. An area of the film which has not yet been reversed, can be remagnetized in two ways:
(a) The area can be reversed by the motion of each of the two adjacent walls (fig. 5.2a). The strongest pinned wall will make the smallest contribution to the remagnetization of this part of the film.
(b) Another possibility is the growth of a new domain in the non-reversed area from a spike at one of the edges
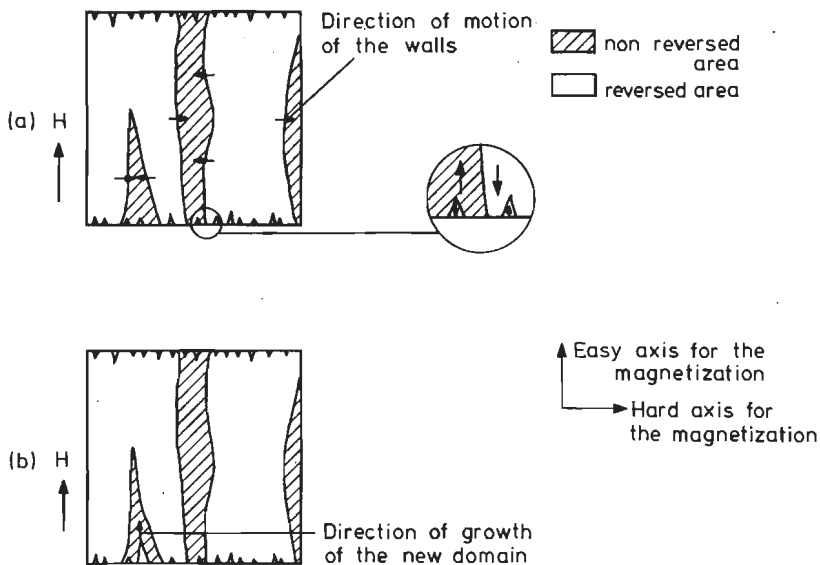
Fig. 5.2. The remagnetization behaviour after the reversal of most of the film: (a) by motion of the adjacent walls, (b) by new domain growth from a spike domain at the edge of the film.

of the film (fig. 5.2b).

Both these cases were observed during the reversal.

Baldwin et al. [5.11] found in toroids of perminvar and in cores of 50-50 Ni-Fe that weak inclusions are very numerous, whereas very strong inclusions are scarcely present. We assume that his results also hold for our thin films. Therefore at first sight one might think that the number of weak pinning points far exceeds the number of strong pinning points. However, this is not true as we will explain below.

If the applied field exceeds $H_{c,min}$ very small spikes are present at the edges of the film (see sec. 2.2.2). Since our films with a surface area of 1 cm^2 had been cut from large 25 cm^2 slices, the film edges are disturbed regions so that most of the spikes are strongly pinned. Let us assume for example that one spike grows if the value H of the applied field just exceeds $H_{c,min}$. In this case inclusions of nearly all values of H_p can pin the wall. By the first inclusion with $H_{cp} > H_1$ that is encountered, one

94

wall of the spike is pinned. The growth of the spike continuous (fig. 5.3) until also the second wall of the spike is pinned at H_2. These pinning points are characterized by $H_{cp,1}$ and $H_{cp,2}$ respectively, which satisfy for example $H_{cp,1} > H_{cp,2}$. If the applied field increases then the spike begins to grow again at $H_3 = H_{cp,2}$. All other inclusions in the film with $H_{cp} \leqslant H_{cp,2}$ cannot pin the wall any more. Thus only one of the inclusions with $H_{cp} \leqslant H_{cp,2}$ has pinned a wall. Now if the spike is pinned by an inclusion $H_{cp,3}$ with $H_{cp,3} > H_{cp,1}$, the spike growth stops for the
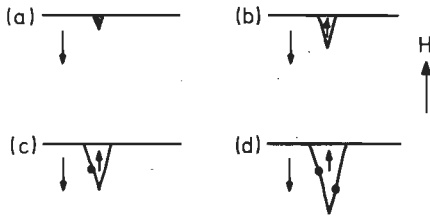

Fig. 5.3. The growth and pinning of a spike domain.

second time (at H_4) and starts again at an applied field $H_5 = H_{cp,1}$, etc. We thus see that in spite of the enormous number of weak inclusions only a very small fraction of them can indeed pin a wall.

In the last part of the reversal the situation is as follows. The strong inclusions, which can pin the wall in this part of the reversal lie in the non reversed domains in the films. There number is small. The total wall length also decreases substantially (sec. 2.2.2) in this part of the reversal. Therefore the walls are pinned by most of these inclusions.

Usually a few spikes grow simultaneously. The total wall length in the film increases rapidly at the beginning of the reversal. The wall length is nearly constant during the steep part of the hysteresis loop $(H_{RB} \leqslant H \leqslant H_{RE}$, see fig. 2.5) and then, at the end of the reversal it decreases sharply to zero as discussed in sec. 2.2.2. Let us first consider the case that the film is reversed by one rigid domain wall which is pinned by one pinning point. If at

a field H_a the wall jumps and is pinned again by a pinning point $H_{cp,i}$ with $H_{cp,i} >> H_a$ then none of the other inclusions with $H_a < H_{cp,j} < H_{cp,i}$ can pin the wall at following jumps. If, however, different walls are present in the film, then a number of the inclusions which satisfy $H_a < H_{cp,j} < H_{cp,i}$ can still pin domain walls. Therefore in the central part of the reversal of our samples the number of pinning points per constant field interval ΔH which were passed by all walls together is larger than for a single domain wall. It is possible that two different wall segments can be pinned by pinning points with the same H_{cp} values; so two wall jumps can occur at the same value of the applied field. However, this occurs scarcely (see sec. 3.7).

We have presented above a description of the wall pinning process. For the wall jumps with a size and duration that can be measured by our Barkhausen Computer Interface (sec. 2.5), the frequency-density function of H_{cp} can be measured. The reversal is divided into field intervals ΔH of constant length. The number of Barkhausen jumps measured in a field interval equals the number of pinning points which are overcome in this interval. By measuring this throughout the entire reversal we can find the frequency-density function of the values of H_{cp} of the pinning points. In chapter 4 [5.12] we presented results of an investigation of the features of the Barkhausen effect along the hysteresis loop. In sec. 4.2, in figs. 4.1 and 4.2 we have also plotted results of this type of measurement. The curves of $z(H)$ in these figures present in principle the distribution of H_{cp} values of two samples throughout the entire reversal. At the beginning the values of $z(H)$ increase and at the end of the reversal they decrease rapidly with increasing field H. Fig. 5.4 shows that in the steep part of the loop ($H_{RB} \lesssim H \lesssim H_{RE}$, fig. 2.5) $z(H)$ varies only by a factor of about 2. Almost the whole reversal of the magnetization takes place in the steep part of the loop. Thus in first order approximation

we can take the values of H_{cp} to be uniformly distributed between H_{RB} and H_{RE}.

We have considered rigid wall motion which starts when a pinning point is overcome and which is finished by encountering another pinning point again. The influence of a finite value of the wall stiffness was ignored. When the domain wall is rigid then after overcoming a pinning point i a wall segment will only move if large wall segments are

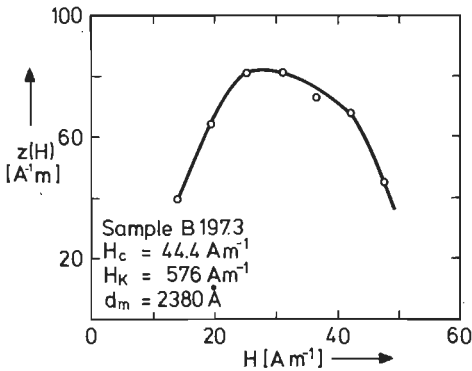
Fig. 5.4. The variation of the number of wall jumps z(H) (averaged over different reversals) along the steep part of the hysteresis loop.

detached from all inclusions which pin the wall at both sides of pinning point i. Thus at most "pinning points" which are overcome no wall displacement occurs. A flexible wall, on the contrary, will move as follows. When a pinning point is overcome then the small wall segment, which is now free, moves. It keeps moving until the energy increase (increase in wall energy, stray field energy and anisotropy energy) caused by bending the wall between the neighbouring pinning centres counterbalances the increase of the energy supplied by the field. In this case the wall motion is mostly stopped before this wall segment encounters again a pinning centre (compare fig. 5.5a and 5.5b). Whereas in the first case where a straight wall is moving in general wall pinning will stop the displacement.

The term with which we indicate the wall jumping process will be derived from the mechanism that mostly stops
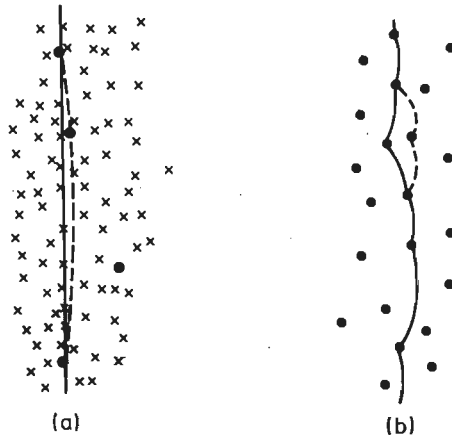
Fig. 5.5. (a) Wall jump of a rigid domain wall at $H_{p,i}$ ($\bullet$: pinning points with $H_p > H_{p,i}$ and . x : pinning points with $H_p < H_{p,i}$); (b) Wall jump of a flexible wall. The wall before (—) and after (– – –) the jumps.
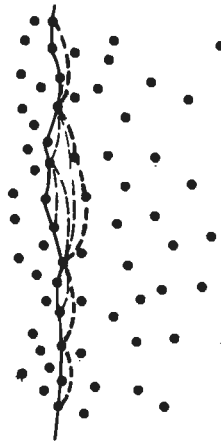

Fig. 5.6. Wall position before (—) and after (– – –) a large number of small wall jumps (– – –) which form an avalanche of snapping free wall segments.

the wall. When in general pinning stops the wall displacement we call this a pinning-dominated wall motion, when the movement is ended by wall-stiffness we call this a stiffness-dominated process.

In a stiffness-dominated process the area of a wall jump, which occurs after the wall snaps free from a pinning centre, is very small. Often during the movement of the wall segment neighbouring wall sections also begin to move so that

98

an avalanche effect can occur. The resulting wall jump consists of a large number of small single wall jumps which occur simultaneously and consecutively. This is sketched in fig. 5.6.

5.2.3. The distance between two inclusions

We shall deduce here the distance between two inclusions of strength $H_p > H_{p,i}$. Therefore we consider two cases: (a) the simplified case of a very flexible wall; (b) the case of a rigid wall. We shall calculate the length of a moving wall segment. In this calculation we assume that the wall motion is stopped by pinning of the wall.

(a) *Flexible wall*

A domain wall is pinned by three pinning points (fig. 5.7). If the applied field H equals $H_{cp,i}$, then the wall snaps free from pinning point i (with strength $H_{p,i}$) and the i-th jump takes place. Pinning point j pins the wall again.
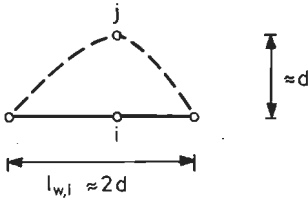

Fig. 5.7. The wall before (—) and after (– – –) the i-th jump.

In the i-th jump an area $A_i(H_{p,i})$ of the film is reversed. We can experimentally determine the mean value $A(H_{p,i})$ from measurements of a large number of reversals. We take the mean distance $d(H_{p,i})$ between two adjacent inclusions of strength $H_p > H_{p,i}$ to be:

$$d(H_{p,i}) \approx \sqrt{A(H_{p,i})} \qquad [m] \tag{5.5}$$

We can relate $d(H_{p,i})$ to the pulse size $p(H_{p,i})$ by using eqs. (3.3) and (3.4)

$$(2I_s/\mu_0) V_{jump} = (2I_s/\mu_0) 10^{-10} d_m A_{jump}$$

$$= (d_m / 1000) p / \{ (N/l) \times 0.5 \times 0.75 \ \mu_0 \}$$

or $\qquad p = 0.75 \times 10^{-2} \, A_{jump} \qquad \left[V s \right] \qquad (5.6)$

where V_{jump} is the jump volume, A_{jump} the jump area, I_s the saturation polarization (1 Wb m^{-2}), $N/1 = 10^5$ the number of turns per unit length of the pick-up coil and 0.5x0.75 the transfer factor of the pick-up coil system (sec. 2.3). The use of eq. (5.6) in eq. (5.5) gives

$$d(H_{p,i}) \approx \sqrt{p(H_{p,i}) / (0.75 \times 10^{-2})} \qquad \left[m \right] \qquad (5.7)$$

where $p(H_{p,i})$ represents the mean jump size of a wall jumping away from a pinning point of strength $H_{p,i}$. The mean length $l_w(H_{p,i})$ of the moving wall segment, just after the wall has snapped free from a pinning point of strength $H_{p,i}$ is (fig. 5.7)

$$l_w(H_{p,i}) \approx 2d(H_{p,i}) \approx 2\sqrt{p(H_{p,i}) / (0.75 \times 10^{-2})} \qquad \left[m \right] (5.8)$$

(b) *Rigid wall*

Domain walls have a certain stiffness, which strongly depends on the wall type. For example a Bloch wall has a much larger stiffness than a cross-tie wall. The Bloch wall behaves as a rigid wall while the cross-tie wall can easily be bent at low values of H_K. In sec. 5.5 we shall further discuss this wall bending. Here we discuss the jump of a rigid wall. In the case of a rigid wall the displacement will be small compared with the length of the moving wall segment. At a certain moment the wall is pinned by a number of pinning points. On increasing the applied field much pinning points are overcome by the wall but this hardly gives rise to wall jumps, until a large
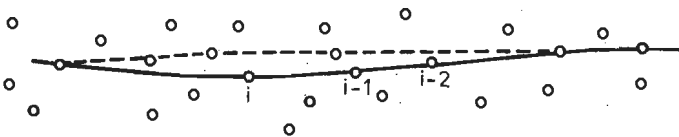

Fig. 5.8. The wall before (——) and after (— — —) the i-th jump if the rigid wall snaps free from pinning point i, as the pinning points i — 1 and i — 2 were already overcome.

wall segment is detached from all the pinning centres
(fig. 5.8). Let us assume that this happens if a pinning
centre of strength $H_{p,i}$ is overcome. When the wall jump is
stopped by wall pinning, an area $A(H_{p,i})$ (eq. (5.5)) has
been reversed during this jump. Let us assume that the
wall will be displaced through a distance $x_w(H_{p,i})$ of

$$x_w(H_{p,i}) \approx (2/\hat{n}_{w,i}) \, d(H_{p,i}) \qquad [m] \qquad (5.9)$$

where $d(H_{p,i})$ is given by eq. (5.7) and $n_{w,i}$ is a number.
The length $l_w(H_{p,i})$ of the whole moving wall segment is
then

$$l_w(H_{p,i}) \approx n_{w,i} \, d(H_{p,i}) \approx \frac{n_{w,i}^2}{2} \, x_{w,i}$$

$$(5.10)$$

$$l_w(H_{p,i}) \approx n_{w,i} \sqrt{p(H_{p,i}) / (0.75 \times 10^{-2})}$$

with $n_{w,i} \geqslant 2$. For a pinning determined Barkhausen pro-
cess we shall use eq. (5.10) in sec. 5.6 in the deriva-
tion of a relationship between p and τ_B.

5.3. SOME GENERAL COMMENTS ON THE RELATION
     BETWEEN p AND τ_B

The size p of the wall jump is given by

$$p = 0.75 \times 10^{-2} \, A_{jump} \qquad [Vs] \qquad (5.6)$$

With $l_{w,i} = l_w(H_{p,i})$ the length of the moving wall seg-
ment and $x_{w,i} = x_w(H_{p,i})$, the displacement of the wall
(fig. 5.9) at the i-th jump, we find for $p_i = p(H_{p,i})$

$$p_i \approx 0.75 \times 10^{-2} \, l_{w,i} \, x_{w,i} \qquad [Vs] \qquad (5.14)$$

For the wall velocity we use the viscous flow approx-
imation of the equation of motion of a domain wall [5.6].
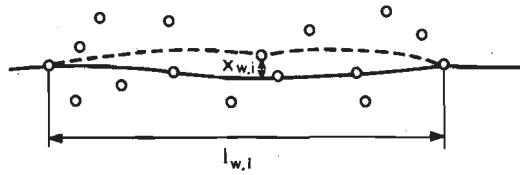The wall velocity v is then given by

Fig. 5.9. The length $l_{w,i}$ and displacement $x_{w,i}$ of the i-th Barkhausen jump.

$$v = \mu(H - H_{cl}) \qquad [ms^{-1}] \qquad (5.15)$$

in which μ is the wall mobility and H the applied field. The wall motion is impeded by the local coercive field H_{cl} during the jump. When the wall snaps free from pinning point i(with $H_{cp,i}$) then the wall velocity v_i given by

$$v_i = \mu(H_{cp,i} - H_{cl,i}) \qquad (5.16)$$

represents the velocity at the beginning of the motion.

Now we must consider two cases: (a) a uniform motion of the wall during the jump and (b) a non-uniform wall motion:

(a) If we may assume a uniform motion of the wall during the jump, then the wall displacement is at the i-th jump

$$x_{w,i} = v_i \tau_{B,i} \qquad (5.17)$$

where v_i is the wall velocity and $\tau_{B,i}$ the time duration of the i-th jump. With eqs. (5.16) and (5.17) we find for the pulse size p_i (eq. (5.14)) in this case

$$p_i \approx 0.75 \times 10^{-2} l_{w,i} \mu(H_{cp,i} - H_{cl,i}) \tau_{B,i} \qquad (5.18)$$

(b) For a non-uniform wall motion the wall displacement is

$$x_{w,i} = \int_0^\infty v_i(t) \, dt \qquad (5.19)$$

The pulse shape of $v_i(t)$ of the Barkhausen process eq. (5.19) can often be described by (see sec. 5.5.2)

$$x_{w,i} = c \, v_{o,i} \, \tau_{B,i} \qquad\qquad (5.20)$$

where $v_{o,i}$ represents the velocity just after the wall
motion is started and is given by eq. (5.16). The time
duration of the pulse is given by $\tau_{B,i}$ and c depends
on the shape of $v_i(t)$. According to eq. (5.18) we find
thus for the pulse size

$$p_i \approx 0.75 \times 10^{-2} \, l_{w,i} \, c \, \mu \, (H_{cp,i} - H_{cl,i}) \, \tau_{B,i} \qquad (5.18a)$$

For pinning-dominated processes we will use case (a)
(eq. (5.18)), for the stiffness-dominated processes case
(b) (eq. (5.18a)) can be used as discussed in secs. 5.4
to 5.6.

We shall now proceed to discuss the variation of the
driving field $H_d = (H_{cp} - H_{cl})$ during the reversal of the
magnetization. The value of the local coercive field
$H_{cl,i}$ during the i-th jump depends on the number and
strength of the disturbances, that are reversibly passed,
in the area reversed in this jump. This value will vary
from jump to jump. The number and strength of the inclu-
sions which can be passed reversibly, increases with the
applied field H (see sec. 5.2.2.). Therefore the value
of H_{cl} shows a tendency to increase with H. Since it is
likely that the surface-frequency-density function of in-
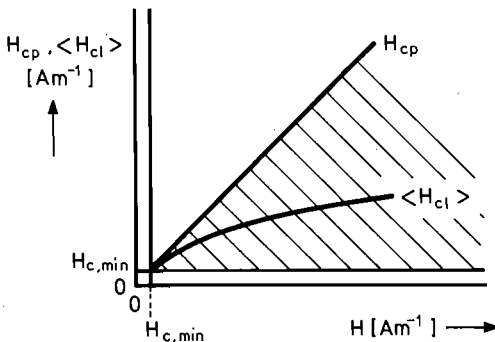clusions of strength H_p decreases with increasing H_p, thus

Fig. 5.10. The average value of H_{cl} as a function of H. The value of H_{cl} varies within the
shaded area.

with increasing H(see sec. 5.2.2.), it is plausible that
with increasing H the averaged growth of H_{cl} decreases and
the absolute value of the scattering of the H_{cl} values of
successive jumps will increase ($H_{c,min} \lesssim H_{cl,i} \lesssim H_{cp,i}$).
This is shown in fig. 5.10.

The frequency-density function of $H_{d,i} = H_{cp,i} - H_{cl,i}$
cannot be measured. We assume the frequency-density func-
tions of H_{cp} to be uniform. In sec. 5.2.2 we have given
arguments and experimental results that support this assump-
tion. In the case described above we assume that $H_{d,i}$ is
also uniformly distributed. Wall motion takes place if
$H_d > 0$. For the maximum driving field $H_{d,max}$ we can choose
two different values based on the following observed re-
versal processes. In principle we can distinguish two
forms of reversing the films.

(a) In some films the reversal takes place as follows:
    at the moment at which the bulk of the reversal pro-
    cess begins, one or more spikes grow rapidly until
    they form narrow reversed domains, which cross the
    film from one side to the other, parallel to the easy
    axis (fig. 2.3b). The walls of these domains are re-
    sponsible for almost the whole reversal. In this case
    the maximum value of the driving field can be approx-
    imated by

$$H_{d,max} \approx H_{c,max} - H_{c,min} = H_{m,1} \tag{5.21}$$

(b) In other films the behaviour is different. A larger
    number of spike-domains is growing during the increase
    of the applied field; at the moment when these domains
    reach the other side, about one half of the film is
    reversed; for this process we have the property that
    $(H_{d,max})_1 \approx H_c - H_{c,min}$ (fig. 5.11). Then the reversal
    is completed by domain walls crossing the whole film
    which move as indicated in fig. 2.3b, resulting in
    $(H_{d,max})_2 \approx H_{c,max} - H_c$. In this case $H_{d,max}$ equals

$$H_{d,max} \approx H_c - H_{c,min} \approx H_{c,max} - H_c = H_{m,2} \tag{5.22}$$

Our microscopic observations of the reversal process showed that in thinner films ($d_m \leqslant 900$ Å) mostly the first process is found, while in thicker films the second magnetization reversal processes usually dominate. Both cases are used in sec. 5.7, where the theory and experimental results are compared. For the value of $H_{c,min}$ we choose the
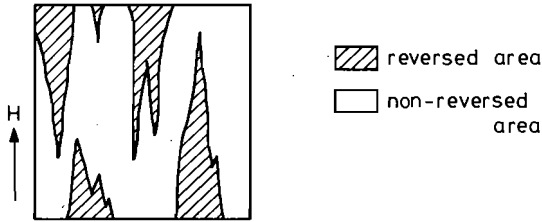

Fig. 5.11. Growth of reversed domains from different spikes.

field H_{RB} just before the spikes start to grow; for $H_{c,max}$ we use the field H_{RE} at which the film is nearly saturated (see fig. 2.5).

In the following sections 5.4 to 5.7 we shall consider 3 different wall jumping models.
(A) A wall, crossing the film along the easy axis from one side to the other, moves as a whole through the film. (fig. 5.12a). Thus $l_{w,i}$ = constant = 10^{-2}m. The wall movement is stopped by wall pinning and $x_{w,i}$ varies in the different wall jumps.

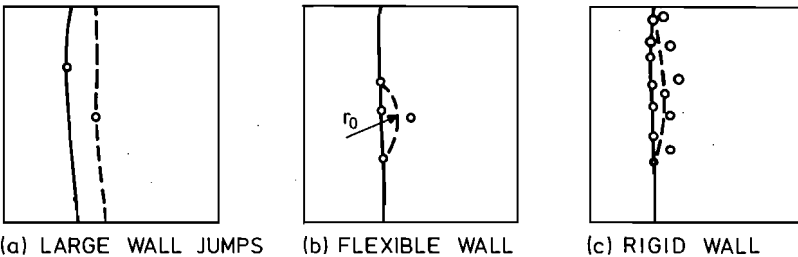(a) LARGE WALL JUMPS   (b) FLEXIBLE WALL   (c) RIGID WALL

Fig. 5.12. The three models of wall motion (schematically): —— wall position before the jump and − − − − wall position after the jump.

(B) The size of the wall jump is determined by the wall stiffness: the wall segment is displaced until the radius of curvature of the wall segment equals the minimum radius of wall curvature in the film. This leads to a relationship between $l_{w,i}$ and $x_{w,i}$ (see fig. 5.12b).

(C) We consider a pinning-dominated wall motion: the wall motion is finished by the pinning of the moving wall segment (fig. 5.12c). In this process the length $l_{w,i}$ of the moving wall segment varies just as the wall displacement $x_{w,i}$.

To derive the relation between p and τ_B we start from eq. (5.18) or eq. (5.18a). In all models we assume that the driving field $H_{d,i} = (H_{cp,i} - H_{cl,i})$ is uniformly distributed between the values $H_{d,min}$ and $H_{d,max}$, while $H_{d,min} \ll H_{d,max}$. As previously discussed this can be considered as a first order approximation of the frequency density function of H_d.

5.4. LARGE WALL JUMPS

In this model the wall moves as a whole. There are no wall segments. The length of the moving wall segment equals the length of the film

$$l_{w,i} = 10^{-2} \text{ m} \qquad (5.23)$$

In this case the wall motion is finished by wall pinning. The pinning points can be considered as highly localized disturbances of the magnetic properties of the thin film (sec. 5.1). Hence the wall motion is abruptly stopped. This occurs in general after a small wall displacement. Therefore the driving field H_d can be considered to be constant during the wall jump and thus the wall motion may be regarded as uniform. We neglect variations of $H_{cl,i}$ during the jump, the influence of which is diminished by the stiffness of the domain wall. We can then

use the results of sec. 5.3. Substituting eq. (5.23) in
eq. (5.18), we obtain:

$$p_i(\tau_B) \approx 0.75 \times 10^{-4} \; \mu \; H_{d,i} \; \tau_{B,i} \qquad (5.24)$$

The value of the driving field $H_{d,i} = H_{cp,i} - H_{cl,i}$ is
determined by the value of $H_{cp,i}$ of the pinning point i,
which has been overcome by the wall at the i-th jump, and
the value of $H_{cl,i}$ around pinning point i (see sec. 5.3).
The value of $\tau_{B,i}$ is determined by the distance to the
next pinning point which stops the wall motion, i.e. the
first pinning point encountered by the wall with $H_p > H_{p,i}$.
So we can take the driving field $H_{d,i}$ independent of $\tau_{B,i}$.
Averaging eq. (5.2) over all jumps with a given value of
τ_B therefore gives for the most probable pulse size

$$p_w(\tau_B) \approx 0.75 \times 10^{-4} \; \mu \; < H_{d,i} > \; \tau_B \qquad (5.25)$$

In table 5.1 (sec. 5.7) a comparison is made between the
results of relation (5.25) and the results of the meas-
urements.

5.5. STIFFNESS-DOMINATED WALL MOTION: THE DISPLACEMENT OF A FLEXIBLE WALL

We consider here the case of a flexible wall the mo-
tion of which is stopped by wall stiffness instead of by
wall pinning (compare the figs. 5.5a and 5.5b of sec.
5.2.2). Stiffness-dominated wall motion is partially re-
versible when the applied field is reduced again. By fur-
ther increasing the applied field the wall can move revers-
ibly until pinning follows. The length of the wall seg-
ment l_w (before the wall jump takes place) is of course
determined by wall pinning. So we can characterize this
wall jumping process as follows: stiffness-dominated in
the direction of motion and pinning-dominated along the
wall, i.e. normal to the direction of motion.

The wall stiffness determines a minimum radius of curvature r_o of the wall at a particular jump. The minimum radius of curvature together with the distance between two adjacent pinning points (l_w) determines the jump size. The
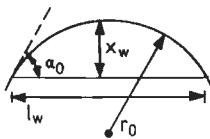

Fig. 5.13. A wall segment with radius of curvature r_0.

relation between the length of the wall segment and the wall displacement is derived using fig. 5.13. For the wall displacement one finds

$$x_w = r_o - \sqrt{r_o^2 - \left(\frac{l_w}{2}\right)^2} = r_o\left\{1 - \left(1 - \frac{l_w^2}{4r_o^2}\right)^{0.5}\right\} \qquad (5.26)$$

Our microscopic observations showed that we can assume that the maximum jump size always occurs for $l_w < 1.5\ r_o$. Thus we can use the following approximation

$$\sqrt{1 - \left(\frac{l_w}{2r_o}\right)^2} \approx 1 - \frac{l_w^2}{8r_o^2} \qquad (5.27)$$

with an error smaller than 20%. Hence for x_w one finds

$$x_w \approx l_w^2 / 8r_o \qquad (5.28)$$

or

$$l_w \approx \sqrt{8r_o x_w} \qquad (5.28a)$$

The jump area A_{jump} and the angle α_o can also be deduced from fig. 5.13. After some calculations one finds

$$A_{jump} \approx \frac{2}{3} x_w l_w \qquad (5.29)$$

and

$$\alpha_o \approx \frac{4 x_w}{l_w} \qquad (5.30)$$

Substituting eq. (5.29) in eq. (5.6) we obtain the following relation

108

$$p_i \approx 5 \times 10^{-3} \; x_w \; l_w \tag{5.31}$$

With eq. (5.28) this becomes

$$p_i \approx \frac{5}{8} \times 10^{-3} \; \frac{l_w^3}{r_o} \tag{5.31a}$$

or with eq. (5.28a)

$$p_i \approx 10^{-2} \sqrt{2 r_o} \; x_w^{1.5} \tag{5.31b}$$

In a process in which a jump is ended by pinning, the wall motion is abruptly stopped when the wall is catched by a stronger pinning point. Then we can consider the wall motion to be uniform (see sec. 5.4), which gives $x_{w,i} = v_i \; \tau_{B,i}$. We consider in this section a stiffness-dominated wall motion. Owing to wall bending the energy of the wall, the anisotropy energy and the stray field energy increase during the jump. The applied field must supply the increase of the energy. This energy balance determines the new equilibrium position of the wall when a pinning point has been overcome. Therefore one might wonder if we still may consider $x_{w,i} \propto \tau_{B,i}$. We will discuss this in the subsecs. 5.5.1 and 5.5.2.

First in subsection 5.5.1 we calculate the different energies which are important in the stiffness-dominated wall jumping process: the field energy (e_H), the increase in wall energy (e_w), and the increase in stray field (e_s) and anisotropy energy (e_A) at bending the wall. Then we determine the minimum radius of wall curvature. In subsection 5.5.2 the equation of motion is considered. The wall displacement is calculated and the pulse size of a single wall jump derived. In subsection 5.5.3 the clustering of single wall jumps is considered.

5.5.1. The energy balance

(a) *The increase in field energy* e_H.

The field energy increases during a jump with (fig. 5.14)

$$e_H = -2 I_s H_d A_{jump} d_m \qquad [J] \qquad (5.32)$$

using eq. (5.29) this becomes

$$e_H = -\frac{4}{3} I_s H_d x_w l_w d_m \qquad (5.32a)$$

(b) *The increase in wall energy* e_w.

If during a wall jump the domain wall is bent then the length of the domain wall segment will grow. If we represent the wall bending by a cylinder (fig. 5.13 and 5.14)
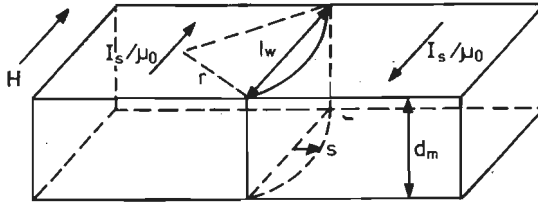

Fig. 5.14. A bulged 180° wall under the action of an applied field H.

we can easily calculate the wall length increment Δl_w as a function of the wall displacement x_w:

$$\Delta l_w \approx \frac{8}{3} \frac{x_w^2}{l_w} \qquad [m] \qquad (5.33)$$

so that the increase in wall energy is

$$e_w \approx \frac{8}{3} \frac{x_w^2}{l_w} \gamma_w d_m \qquad [J] \qquad (5.34)$$

where the surface energy of the wall is given by γ_w ($\approx 5 \times 10^{-3}$ Jm^{-2}). We assume that γ_w is constant during the wall motion.

(c) *The increase in stray field and anisotropy energies:* e_s *and* e_A.

When the wall is bent, strong magnetic poles are induced at the bent portion of the wall [5.13]. They give a very large demagnetizing field at the bulged portion of the domain and thus a large stray field energy (fig. 5.15a).

(a)

I_S/μ_0

H_D

I_S/μ_0

domain wall

H_D

I_S/μ_0 H

(b)

I_S/μ_0

H_D

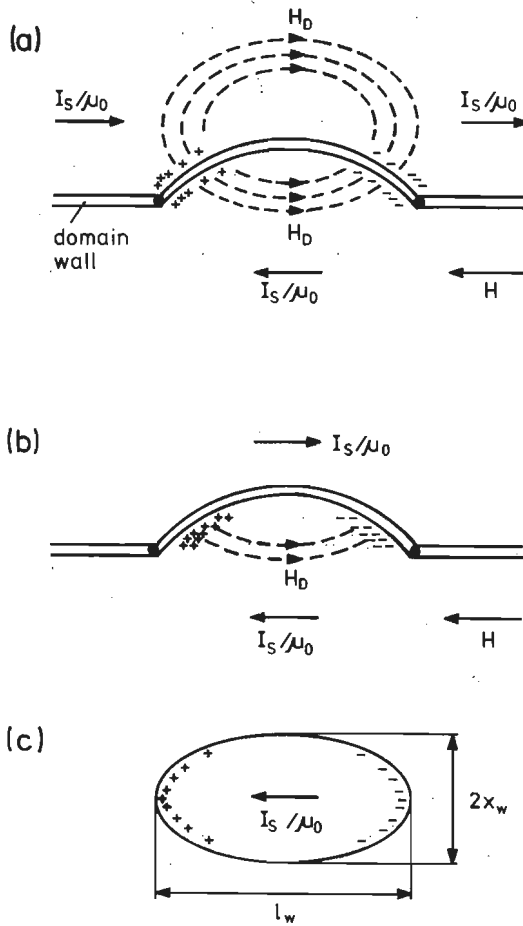I_S/μ_0 H

(c)

I_S/μ_0

$2x_w$

l_w

Fig. 5.15 (a) The free pole distribution at the surfaces of a bent wall without compensating free poles of the wall; (b) curved wall which has a wall structure with compensating free poles on it; (c) free pole distribution on an ellipsoid magnetized along the long axis. The dashed lines show the direction of the demagnetizing field.

The stray field energy is difficult to calculate except for the case that there are no free poles at the outside of the wall (fig. 5.15b). Then the stray field energy can be approximated by a half of that of a very flat ellipsoid with axes l_w, $2x_w$ and d_m ($l_w > 2x_w \gg d_m$), which is magnetized parallel to the long axis (fig. 5.15c) and has the double free pole intensity at the inside of the wall. The increase in stray field energy during the wall jump is estimated to be

$$e_s \approx \left(-\frac{1}{2} H_D I_s \right) \times \left(0.75\, l_w\, x_w\, d_m \right) \qquad \left[J \right] \qquad (5.35)$$

where H_D is the demagnetizing field and is given by

$$H_D = -N_D \frac{2 I_s}{\mu_o} \qquad \left[A\, m^{-1} \right] \qquad (5.36)$$

The demagnetizing factor N_D is given by (see Osborn [5.14])

$$N_D \approx \frac{2\, x_w\, d_m}{l_w^2} \left\{ K(m) - E(m) \right\} \qquad (5.37)$$

where $K(m)$ and $E(m)$ are complete elliptic integrals [5.15] Their argument m is

$$m = \left| 1 - \left(\frac{2\, x_w}{l_w} \right)^2 \right|^{0.5} \qquad (5.38)$$

We find for e_s the formula

$$e_s \approx 1.5 \cdot \frac{I_s^2}{\mu_o} \frac{x_w^2\, d_m^2}{l_w} \left\{ K(m) - E(m) \right\} \qquad (5.39)$$

For $2x_w/l_w = 0.1$ we find $K(m) - E(m) \approx 3$ and for $2x_w/l_w = 0.01$ the value of $K(m) - E(m)$ is about 5. To present an order of magnitude we calculate e_s and e_w for $d_m = 7 \times 10^{-8}$ m:

$$e_s \approx 5.8 \times 10^{-9} \frac{x_w^2}{l_w} \left\{ K(m) - E(m) \right\} \qquad (5.40a)$$

and

$$e_w \approx 9.3 \times 10^{-10} \frac{x_w^2}{l_w} \qquad (5.40b)$$

and find for $x_w = 10^{-5}$ m and $l_w = 2 \times 10^{-4}$ m the values

$$e_s \approx 9 \times 10^{-15}\ J \qquad (5.40aa)$$

and

$$e_w \approx 5 \times 10^{-16}\ J \qquad (5.40bb)$$

Thus the stray field energy strongly exceeds e_w.

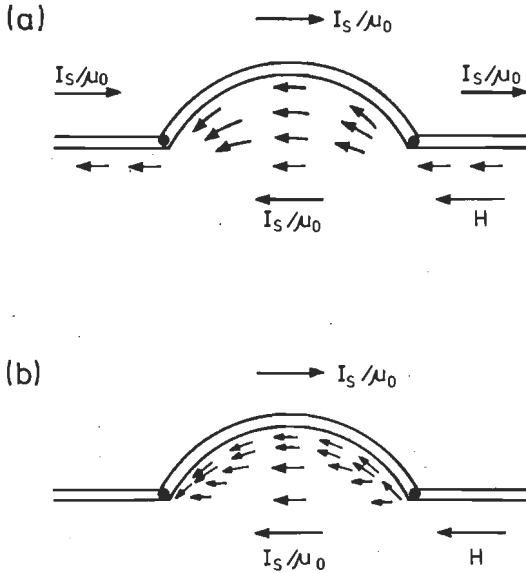To reduce the stray field energy the direction of the

Fig. 5.16. (a) and (b) The magnetization distributions around a curved wall without free poles on the outside of the bulged domain wall.

magnetization around the bent wall will follow the wall curvature (fig. 5.16) which gives rise to an increase of the anisotropy energy. The free pole intensity is now diluted over a surface area with width w (fig. 5.17) inside the wall (compare the Néel spikes [5.16]). With a lattice constant a the free pole intensity is diluted over M atoms with

$$M \doteq \frac{w}{a} \tag{5.41}$$

We estimate the stray field energy to be in this case

$$e_s \approx \frac{1.5}{M} \frac{I_s^2}{\mu_o} \frac{x_w^2 d_m^2}{l_w} \left\{ K(m) - E(m) \right\} \tag{5.42}$$

Let us calculate the anisotropy energy. Here we assume that the wall is bent into a cylindrical form (fig. 5.17). The angle $\alpha(r, \varphi)$ between the magnetization and the easy axis is assumed to be

$$\alpha(r, \varphi) = \frac{-\varphi}{w} |r - r_o| + \varphi \tag{5.43}$$
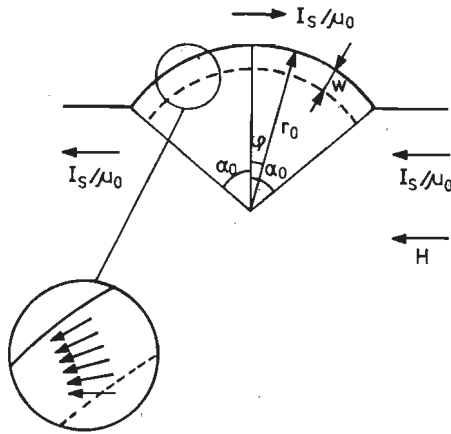
Fig. 5.17. The dilution of free poles.

The increase in anisotropy energy e_A is now

$$e_A \approx \iint\limits_{G} K\, d_m \sin^2\{\alpha(r,\varphi)\}\, r\, dr\, d\varphi \qquad [J] \qquad (5.44)$$

with G the area where the magnetization deviates from the easy axis and K the uniaxial anisotropy constant of the film. The angle $\alpha(r,\varphi)$ is small thus

$$e_A \approx 2 \int\limits_{\varphi=0}^{\alpha_0} \int\limits_{r=r_0-w}^{0} K\, d_m\, \alpha^2(r,\varphi)\, r\, dr\, d\varphi \qquad (5.44a)$$

$$e_A \approx \frac{2}{9} K\, \alpha_0^3 \left(-\frac{1}{4} w^2 + r_0 w\right) d_m$$

Using $w \ll r_0$ we find

$$e_A \approx \frac{2}{9} K\, \alpha_0^3\, r_0\, w\, d_m \qquad (5.44b)$$

Using the property that $\alpha_0 = 4x_w/l_w$ (eq. 5.30) in eq.(5.40b) and substituting r_0 from eq. (5.28) gives for e_A

$$e_A \approx \frac{16}{9} K\, \frac{x_w^2}{l_w} M\, \sigma\, d_m \qquad (5.45)$$

The width w of the resulting magnetization distribution

114

around the wall is such that the sum of the anisotropy energy and the stray field energy is a minimum. Thus M follows from

$$\frac{d}{dM} (e_s + e_A) = 0 \tag{5.46}$$

which results in

$$M = \frac{3}{4} I_s \sqrt{\frac{1.5 \, d_m \, \{K(m) - E(m)\}}{\mu_o \, K \, a}} \tag{5.47}$$

The sum of the stray field and anisotropy energy is hence $(e_s = e_A)$

$$e_s + e_A = \frac{8}{3} I_s \sqrt{\frac{1.5 d_m^3 \, K \, a \, \{K(m) - E(m)\}}{\mu_o}} \quad \frac{x_w^2}{l_w} \tag{5.48}$$

With $d_m = 7 \times 10^{-8}$ m, $K = 200$ Jm^{-3} and $a \approx 3 \times 10^{-10}$m we find for M and $e_s + e_A$

$$M \approx 8.9 \times 10^2 \sqrt{K(m) - E(m)} \tag{5.49}$$

and

$$e_s + e_A \approx 1.3 \times 10^{-11} \sqrt{K(m) - E(m)} \quad \frac{x_w^2}{l_w} \tag{5.50}$$

choosing $x_w = 10^{-5}$m and $l_w = 2 \times 10^{-4}$m this becomes

$$M \approx 1500 \tag{5.51a}$$

and

$$e_s + e_A \approx 1.1 \times 10^{-17} \text{ J} \tag{5.51b}$$

which is a reduction with a factor of about 10^3 compared with e_s of eq. (5.40). We thus see that by dilution of the free pole intensity over M atoms the energy increase caused by the presence of the free poles can be neglected with respect to the increase in wall energy e_w at bending the wall. In the case considered the increase in wall energy e_w thus dominates the process of wall jumping.
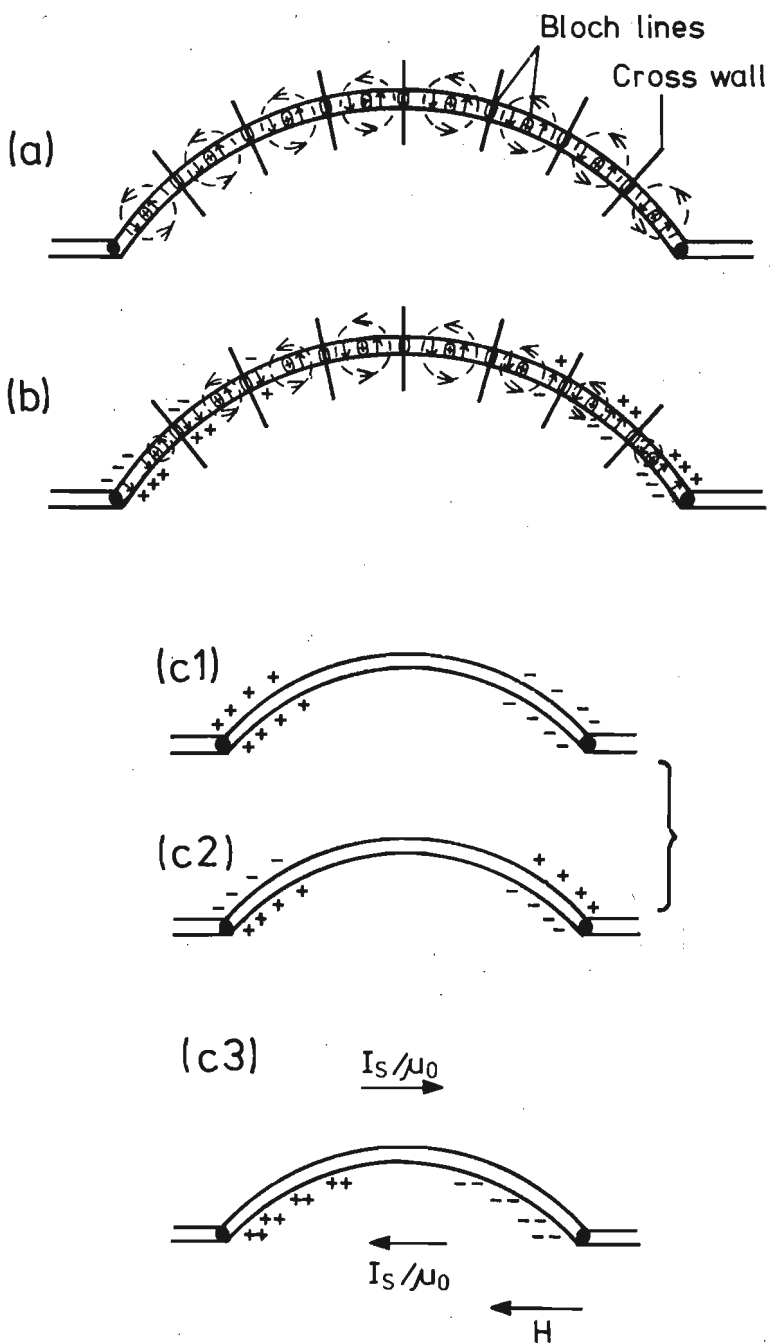
Fig. 5.18. (a) The symmetrical cross-tie wall; (b) the asymmetrical cross-tie wall with free poles on its surface; (c) macroscopic free pole distributions caused by wall curvature (c1), of a symmetrical cross-tie wall (c2) and of a bulged asymmetrical cross-tie wall (c3).

As described at the beginning of sec. 5.5.1c the re-
sults can be applied to a domain wall where the free poles,
which are caused by the curved shape of the wall are pre-
sent only at the inside of the bulged wall (see fig. 5.15b).
This can be realized if the wall itself can generate compen-
sating free poles on its surfaces. Of the three wall types
occurring in thin films only the cross-tie wall (see sec.
2.2.3, fig. 2.7) with legs of Néel walls can do this.
Fig. 5.18a shows a cross-tie wall in which all Néel wall
segments have equal length. On macroscopic scale no free
poles are present, while by shifting the Bloch lines free
poles occur at the surfaces of the wall as shown in fig.
5.18b. The macroscopic free pole distribution on the cross-
tie wall can compensate the free poles caused by the wall
bending. This is explained in fig. 5.18c. A bulged wall
with a Bloch wall structure has stray fields as shown in
fig. 5.15a. Fig. 5.19 shows the resulting magnetization
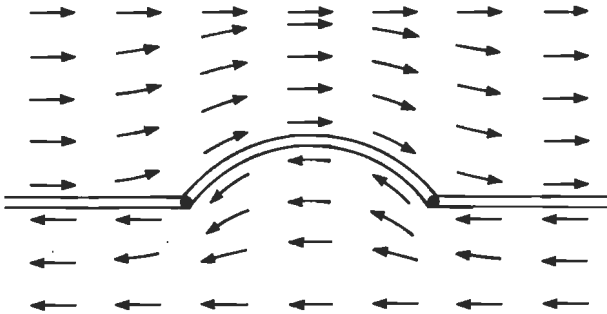
Fig. 5.19. Magnetization distribution round a bulged Bloch wall.

distribution which has a stray field and anisotropy energy
which is extremely large compared with that of the pre-
vious case (see also sec. 5.6). So the energy increase by
bending the wall is much larger for a Bloch wall than for
a cross-tie wall. By this proporty the large flexability
of the cross-tie wall compared with that of the Bloch wall
can be explained: the cross-tie wall behaves as a flexible
wall, the Bloch wall as a rigid wall.

(d) *The energy balance for a flexible (cross-tie) wall at wall bending* . The energy terms which are important at wall bending of a flexible wall are thus the energy supplied by the field

$$e_H = - \frac{4}{3} I_s H_d x_w l_w d_m \qquad (5.32a)$$

and the wall energy increase

$$e_w \approx \frac{8}{3} \frac{x_w^2}{l_w} \gamma_w d_m \qquad (5.34)$$

The minimum radius r_o of wall curvature for a particular jump follows from the following equation

$$\frac{d}{dx}(e_{tot}) = 0 \qquad or \qquad \frac{d}{dx}(e_H + e_w) = 0 \qquad (5.52)$$

which gives

$$x_w = \frac{I_s H_d l_w^2}{4 \gamma_w} \qquad (5.53)$$

Using now eq. (5.28) we find for r_o

$$r_o = \frac{\gamma_w}{2 I_s H_d} \qquad [m] \qquad (5.54)$$

With $\gamma_w \approx 5 \times 10^{-3}$ Jm^{-2} and $I_s \approx 1$ Wbm^{-2} we find

$$r_o \approx \frac{2.5 \times 10^{-3}}{H_d} \qquad (5.54a)$$

The minimum radius of wall curvature for a particular jump decreases for increasing H_d until at $2r_o = l_o$ an irreversible expansion of the wall occurs [5.17] . When the field exceeds the critical field H_{do}

$$H_{do} = \frac{\gamma_w}{I_s l_w} \qquad [Am^{-1}] \qquad (5.55)$$

than the wall will expand discontinuously. In the previous calculations of the model of flexible wall motion only small values of x_w with respect to l_w occur. We have used there the property that $l_w < 2r_o$. Thus we have not

considered there the irreversible wall jumps of a flexible
wall. As explained in sec. 5.2.2. when a pinning point of
a rigid wall is overcome mostly no wall jump occurs. Only
if nearly the whole wall is free of pinning centres then
wall motion can follow. At a flexible wall a small wall
jump follows everytime that the wall overcomes a pinning
centre. Therefore l_w of a flexible wall is much smaller
than l_w of a rigid wall. So with our range of driving
fields the irreversible wall jumping of a flexible wall
will scarcely occur.

5.5.2. The equation of motion and the pulse size of a single wall jump

Let us now consider the wall motion during a jump. The
equation of motion (viscous flow approximation [5.6]) for a
domain wall jump is

$$\frac{2\, l_w\, d_m\, I_s}{\mu}\, \frac{dx}{dt}\, +\, \frac{d}{dx}\left(e_{tot}\right)\, =\, 0 \qquad (5.56)$$

with μ the domain wall mobility. Substituting the eqs.
(5.32a) and (5.34) in eq. (5.56) results in

$$\frac{dx}{dt}\, +\, \frac{8}{3}\, \frac{\mu\, \gamma_w}{I_s\, l_w^2}\, x\, -\, \frac{2}{3}\, \mu\, H_d\, =\, 0 \qquad (5.57)$$

which has the simple solution

$$v(t)\, =\, \frac{2}{3}\, \mu\, H_d\, \exp(-t/\tau)\, =\, v_o\, \exp(-t/\tau)\quad \left[m\,s^{-1}\right]\quad (5.58)$$

where the time constant τ is given by

$$\tau\, =\, \frac{3}{8}\, \frac{I_s\, l_w^2}{\mu\, \gamma_w} \qquad \left[s\right] \qquad (5.59)$$

In our films

$$\tau\, \approx\, 7.5\, \times\, 10\, \frac{l_w^2}{\mu} \qquad (5.59a)$$

The total wall displacement in a single jump is

119

$$x_w = \frac{2}{3} \mu H_d \tau \qquad (5.60)$$

Let us now consider the relation between the measured pulse duration τ_B and the measured wall displacement $x_B = x(t = \tau_B)$. In our equipment the pulse duration τ_B is measured as the time that the pulse amplitude $h(t)$ exceeds the reference voltage of the Barkhausen Computer Interface (see sec. 2.5), which corresponds to a pulse amplitude h_{min}. The pulse amplitude $h(t)$ is

$$h(t) \propto l_w v(t) \qquad (5.61)$$

The pulse duration τ_B is defined as the time interval from the beginning of the pulse until the moment that the pulse amplitude has decreased to h_{min}. Then the relation between x_B and τ_B can be deduced from eq. (5.58):

$$x_B = v_o \tau_B \left| \frac{(h_{min}/l_w v_o) - 1}{\ln(h_{min}/l_w v_o)} \right| \qquad (5.62)$$

with $v_o = \frac{2}{3} \mu H_d$ (see eq. (5.58))

or $\quad x_B = c v_o \tau_B \quad$ with $\quad c = \dfrac{(h_{min}/l_w v_o) - 1}{\ln(h_{min}/l_w v_o)} \qquad (5.63)$

In fig. 5.20 the factor c is plotted as a function of $h_{min}/l_w v_o$. Thus in this non-uniform wall motion the measured wall displacement is still proportional to the measured pulse duration, only $c < 1$.

Using the eqs. (5.31b) and (5.63) we find for the relation between the pulse size p_i and the time duration $\tau_{B,i}$ for the case that the wall snaps free from <u>one</u> pinning centre i:

$$p_i = \left(\frac{2}{3}\right)^{1.5} 10^{-2} c^{1.5} \sqrt{\frac{\gamma_w}{I_s}} H_{d,i}^{1.5} \mu^{1.5} \tau_{B,i}^{1.5} \qquad (5.64)$$

or $\quad p_i = 3.8 \times 10^{-4} c^{1.5} H_{d,i}^{1.5} \mu^{1.5} \tau_{B,i}^{1.5} \qquad (5.64a)$

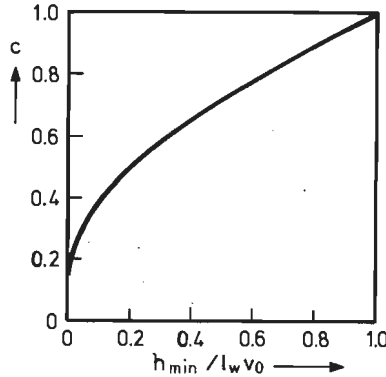The maximum variation of the factor $h_{min}/l_w v_o$ ranges be-

Fig. 5.20. The factor $c = \{ (h_{min}/l_w v_0) - 1 \} / \ln(h_{min}/l_w v_0)$ as a function of $h_{min}/l_w v_0$.

tween about 0.05 and 0.86 in the samples in which we find $p \propto \tau_B^{1.5}$. This corresponds to a variation of c between 0.32 and 0.92, i.e. c varies a factor 3. In our calculation we use $c \approx 0.62$ which gives for eq. (5.64a).

$$p_i \approx 2 \cdot 4 \times 10^{-4} \; H_{d,i} \; \mu^{1.5} \tau_{B,i}^{1.5} \qquad (5.64b)$$

The driving field of the motion of a flexible wall segment equals that of the pinning-dominated wall motion and is discussed in sec. 5.3. The time duration of a wall jump is independent of H_d as shown in eq. (5.59). Therefore at a given value of τ_B we find for the most probable pulse size of a single wall jump

$$p_w(\tau_B) \approx 2 \cdot 4 \times 10^{-4} < H_{d,i} > \mu^{1.5} \tau_B^{1.5} \qquad (5.65)$$

With the assumption made in sec. 5.3 of a uniform frequency density function of the driving field, one finds

$$< H_{d,i} > = 0 \cdot 5 \; H_{d,max} \qquad (5.66)$$

which gives for the most probable pulse size $p_w(\tau_B)$ of a single wall jump:

$$p_w(\tau_B) \approx 1 \cdot 2 \times 10^{-4} \; H_{d,max} \; \mu^{1.5} \tau_B^{1.5} \qquad (5.67)$$

For the stiffness dominated wall jumps of a flexible wall

we find thus for the relation between p and τ_B an equation
of the form

$$p_w(\tau_B) = K \tau_B^{1.5} \qquad\qquad (5.67a)$$

Table 5.2 (sec. 5.7) shows a number of measured K values
which are compared with the K values calculated with eq.
(5.67). A deviation of a factor ranging between 5 and 35
is found between the measured and calculated K values.
Mostly the deviation is a factor of about 10. The measured
K values always exceed the K values calculated from eq.
(5.67) for single wall jumps. This indicates that at the
motion of a flexible wall complicated wall jumps occur as
already discussed in sec. 5.2.2 (see also fig. 5.6). In
subsection 5.5.3 we shall explain with the help of an
illustrative example that the K value of a wall jump com-
posed of many single wall jumps can be much larger than
that of a single wall jump.

5.5.3. The clustering of single wall jumps

When during the movement of the wall segment neigh-
bouring wall sections also begin to move an avalanche ef-
fect can occur. The resulting wall jump consists of a
large number of smaller single wall jumps each satisfying
relation (5.67). We assume that the measured Barkhausen
pulses of the cross-tie wall consist of such complicated
large wall jumps.

With the aid of a simple example we shall illustrate
that the constant K of such a complicated wall jump can be
much larger than that of a single wall jump. We use in
this example a single pulse with shape as shown in fig.
5.21a: pulse amplitude h_e, pulse duration τ_e and pulse
size p_e. We assume that a complicated pulse consists of a
series of n_τ pulse each of which consists of n_h single
pulses which occur simultaneously (fig. 5.21b). Further
we assume that the single pulses are independent of each
other.

The pulse size p of the large pulse is given by
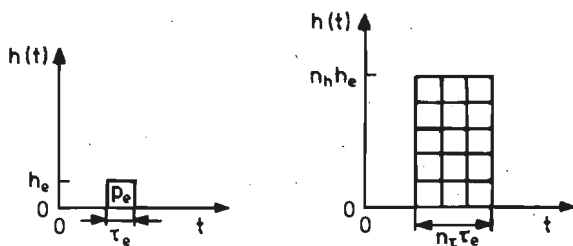
Fig. 5.21. A single pulse (a) and a complicated pulse composed of many single pulses (b).

$$p = n_h n_\tau p_e \qquad (5.68)$$

while the duration of this pulse is

$$\tau = n_\tau \tau_e \qquad (5.69)$$

If for a single pulse holds

$$p_e = K_e \tau_e^\varkappa \qquad (5.70)$$

then we can deduce from

$$p = n_h n_\tau K_e \tau_e^\varkappa \qquad (5.71)$$

that
$$p = \frac{n_h}{n_\tau^{\varkappa-1}} K_e \tau^\varkappa = K \tau^\varkappa \qquad (5.72)$$
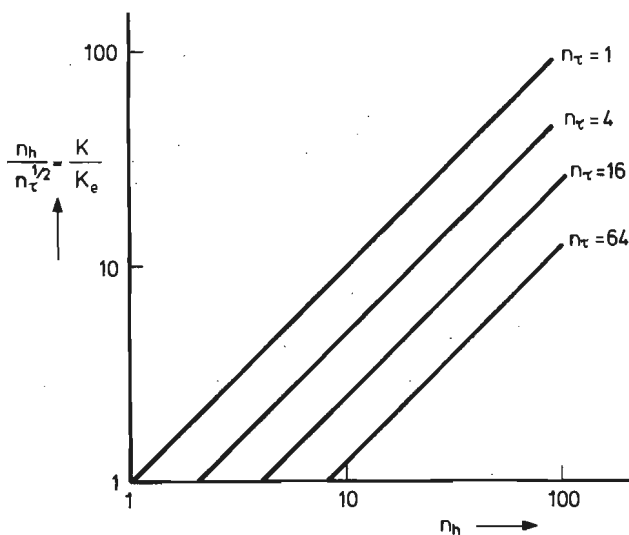
Fig. 5.22. The factor K/K_e as a function of n_k with n_τ as parameter, when $\kappa = 1.5$.

123

Fig. 5.22 shows the factor $K/K_e = n_h/n_\tau^{\varkappa-1}$ for $\varkappa = 1.5$ as function of n_h with n_τ as parameter. A value of 10 for K/K_e can be easily obtained.

With the presented simple example we have illustrated that a complicated pulse can have a much larger K value than the single pulse if $n_h >> n_\tau^{\varkappa-1}$.

5.6. PINNING-DOMINATED WALL MOTION: THE DISPLACEMENT OF A RIGID WALL

In this model a rigid wall is considered the motion of which is stopped by pinning of the domain wall (see fig. 5.8). We can characterize this jumping model as follows: pinning dominated in the direction of motion and stiffness dominated along the wall.

After overcoming a pinning point i (with strength $H_{p,i}$), a wall segment with length $l_{w,i}$ moves through the film. As discussed in sec. 5.2.3 $l_{w,i}$ depends on the number of adjacent pinning points of about the same strength as $H_{p,i}$ which were passed before the wall jump takes place. The wall motion is finished by wall pinning and the time duration of the wall jump is given by $\tau_{B,i}$. In a pinning-dominated wall jumping process we may consider the wall motion as uniform (see sec. 5.4). Thus we can apply here the results of sec. 5.3. Substitution of eqs. (5.10), (5.16) and (5.17) in eq. (5.18) results in

$$ p_i \approx \frac{0.75 \times 10^{-2}}{2} \; n_{w,i}^2 \; \mu^2 \, H_{d,i}^2 \; \tau_{B,i}^2 \qquad (5.73) $$

Just as discussed in sec. 5.4 the driving field and time duration of the i-th jump are independent of each other. The value of $n_{w,i}$ depends on the ratio between the length of the moving wall segment and the mean distance between the pinning points of strength $H_p > H_{p,i}$, as discussed in sec. 5.2.3. So we can also take $n_{w,i}$ to be independent of $\tau_{B,i}$ and the driving field $H_{d,i}$. Averaging over all jumps

gives for a given value τ_B a most probable pulse size

$$p_w(\tau_B) \approx \frac{0.75 \times 10^{-2}}{6} \; n_w^2 \, \mu^2 \, H_{d,max}^2 \, \tau_B^2 \qquad (5.74)$$

for $\qquad\qquad <H_{d,i}^2> \; \approx \; \frac{1}{3} \, H_{d,max}^2 \qquad\qquad (5.75)$

and $\qquad\qquad <n_{w,i}^2> \; \approx \; n_w^2 \qquad\qquad\qquad (5.76)$

If we insert $n_w = 5$, $\mu = 1 \; m^2 A^{-1} s^{-1}$ and $H_{d,max} \approx 20 Am^{-1}$ in eq. (5.45) we obtain

$$p_w(\tau_B) \approx 12.5 \; \tau_B^2 \qquad (5.74a)$$

Eq. (5.45) is calculated for some films and the results are listed in table 5.3 in sec. 5.7.

5.7. COMPARISON BETWEEN THEORY AND EXPERIMENT

The different quantities which were presented in the model calculations of secs. 5.4 to 5.7, are estimated as follows. For the wall mobility μ we use the mean value at the given film thickness d_m as found by Middelhoek [5.6] (see fig. 2.9). The maximum deviation is of the order of 25%. The value of the constant n_w, varies from film to film. An averaged value of about 5 is experimentally estimated and is used for all samples. The range of the driving field H_d was already discussed in sec. 5.3.

The inaccuracy in the experimentally determined value of K (see sec. 3.4) in the expression

$$p_w(\tau_B) = K \; \tau_B^{\varkappa} \qquad (3.19)$$

was estimated to be about ±25%, partially caused by an inaccuracy in the amplifier gain.

Now the three models developed in the secs. 5.4 to 5.7 are compared with the experimental results.

$$p_w(\tau_B)' = K\,\tau_B \qquad (5.77)$$

This form of the two-dimensional frequency-density function was observed in about one third of our samples but only for large values of p. It corresponds to the model of large wall jumps derived in sec.5.4 (eq. 5.25). In table 5.1 the results are presented for $<H_{d,i}>=H_{d,max}/2$. The results calculated with eq. (5.25) can be higher or lower than the experimental results by at most a factor of about 2. In spite of the inaccuracy in the estimation of μ and $<H_{d,i}>$

TABLE 5.1. The relation between p and τ_B for large wall jumps

DATA OF SAMPLES					K-values		
sample number	d_m $[\text{Å}]$	μ $[\text{m}^2\text{A}^{-1}\text{s}^{-1}]$	$H_{m,1}/2$ $[\text{Am}^{-1}]$	$H_{m,2}/2$ $[\text{Am}^{-1}]$	measured	calculated, eq. (5.25) with $H_{m,1}$	with $H_{m,2}$
B199.21	2030	1.35	13	8	8.4×10^{-4}	1.3×10^{-3}	8.1×10^{-4}
B198.29K	1580	1.1	16	11	2.4×10^{-3}	1.3×10^{-3}	9.1×10^{-4}
B194(1).46	1230	1.1	12	10	1.6×10^{-3}	9.9×10^{-4}	8.3×10^{-4}
B194(1).54	1230	1.1	12	8	1.6×10^{-3}	9.9×10^{-4}	6.6×10^{-4}
S941.47	875	0.78	8	6	4.1×10^{-4}	4.7×10^{-4}	3.5×10^{-4}
B192.9K	840	0.75	18	11	1.4×10^{-3}	1.0×10^{-3}	6.2×10^{-4}
B190.50	805	0.71	8	5	6.1×10^{-4}	4.3×10^{-4}	2.7×10^{-4}
S782.14	700	0.42	26	12	3.9×10^{-4}	8.2×10^{-4}	3.8×10^{-4}
S842.41*	575	0.17	26	17	7.4×10^{-4}	3.3×10^{-4}	2.2×10^{-4}
S724.38	525	0.3	13	8	6.6×10^{-4}	2.9×10^{-4}	1.8×10^{-4}
S724.51*	525	0.3	31	22	6.6×10^{-4}	7.0×10^{-4}	5.0×10^{-4}
S725.36	455	0.5	9	6	1.2×10^{-3}	3.4×10^{-4}	2.3×10^{-4}
S725.42	455	0.5	9	6	9.5×10^{-4}	3.4×10^{-4}	2.3×10^{-4}
B340.52	455	0.5	11	8	1.1×10^{-3}	4.1×10^{-4}	3.0×10^{-4}
B193.31	450	0.5	13	8	1.1×10^{-3}	4.9×10^{-4}	3.0×10^{-4}
B289.34	437	0.58	11	6	8.8×10^{-4}	4.8×10^{-4}	2.6×10^{-4}
S723.32	420	0.66	14	9	8.2×10^{-4}	6.9×10^{-4}	4.5×10^{-4}
S723.53	420	0.66	16	11	9.2×10^{-4}	7.9×10^{-4}	5.4×10^{-4}

x sample with irregularities in the hysteresis loop

there is a reasonable agreement between theory and
experiment.

(B) The model based on the wall stiffness (sec. 5.5, eq.
(5.67)) gives the relation

$$p_w(\tau_B) = K \tau_B^{1.5} \qquad (5.67a)$$

Just as in the previous case the measured values of
agree within $\pm 5\%$ with the derived value of $\varkappa = 1.5$.
Here we deal with films thinner than about 900Å,
where the reversal begins with the growth of a few
spikes. In this case the value of $H_{d,max}$ is equal to
$H_{m,1}$ in eq. (5.21). In table 5.2 all resulting K
values of the measurements for $\varkappa = 1,5$ are compared with
the calculated results. The experimentally determined
K values are always larger than those calculated with
eq. (5.67). A deviation of a factor ranging between 5
and 35 is found, mostly the deviation is a factor 10.
In table 5.2 we compare the measured K values with the
K values calculated for a process of single wall
jumps, whereas the actual wall jumps in films with
$d_m < 900Å$ will be composed of many individual single
wall jumps which are generated simultaneously and con-
secutively. In table 5.2 two different processes are
thus compared. In sec. 5.5.3 we have illustrated with
a very simple example that for a process consisting
of large pulses each of which is composed of many sin-
gle pulses occurring simultaneously and consecutively,
the K value can be much larger than the K value of a
process consisting of the single pulses. We think that
the deviation between the measured and calculated K
values in table 5.2 is caused by the fact that at the
motion of a flexible wall such complicated wall jumps
occur.

(C) The quadratic dependence of $p_w(\tau_B)$ on τ_B is mostly
found in thick films $(d_m \geqslant 900Å)$

$$p_w(\tau_B) = K \tau_B^2 \qquad (5.78)$$

TABLE 5.2. The relation between p and τ_B for a flexible wall

DATA OF SAMPLES				K-values	
sample number	d_m $[\text{Å}]$	μ $[m^2 A^{-1} s^{-1}]$	$H_{m,2}$ $[Am^{-1}]$	measured	calculated eq. (5.67)
B380.24	1080	0.92	18	2.9×10^{-2}	1.9×10^{-3}
S941.47	875	0.78	16	1.3×10^{-2}	1.3×10^{-3}
S941.48	875	0.78	11	1.2×10^{-2}	9.1×10^{-4}
S954.1	805	0.71	21	1.4×10^{-2}	1.5×10^{-3}
S954.49	805	0.71	46	1.4×10^{-2}	3.3×10^{-3}
B190.5	805	0.71	29	1.6×10^{-2}	2.1×10^{-3}
B190.50	805	0.71	16	2.1×10^{-2}	1.1×10^{-3}
S782.14	700	0.42	51	1.8×10^{-2}	1.7×10^{-3}
S782.43	700	0.42	43	1.3×10^{-2}	1.4×10^{-3}
S951.10	595	0.18	10	1.3×10^{-2}	9.2×10^{-5}
S951.22[x]	595	0.18	54	1.7×10^{-2}	4.9×10^{-4}
S951.23	595	0.18	107	1.6×10^{-2}	9.8×10^{-4}
S724.38	525	0.3	26	1.5×10^{-2}	5.1×10^{-4}
S724.51[x]	525	0.3	62	1.5×10^{-2}	1.2×10^{-3}
S725.36	455	0.5	19	1.9×10^{-2}	8.1×10^{-4}
S725.42	455	0.5	19	1.9×10^{-2}	8.1×10^{-4}
B340.37[x]	455	0.5	88	2.0×10^{-2}	3.7×10^{-3}
B340.52	455	0.5	22	2.3×10^{-2}	9.3×10^{-4}
B193.31	450	0.5	27	2.4×10^{-2}	1.1×10^{-3}
B289.34	437	0.58	22	1.7×10^{-2}	1.2×10^{-3}
B289.35	437	0.58	27	1.6×10^{-2}	1.4×10^{-3}
S781.20	420	0.66	19	1.8×10^{-2}	1.2×10^{-3}
S781.33[x]	420	0.66	53	1.8×10^{-2}	3.4×10^{-3}
S723.32	420	0.66	29	2.4×10^{-2}	1.9×10^{-3}
S723.53	420	0.66	32	2.4×10^{-2}	2.1×10^{-3}

x sample with irregularities in the hysteresis loop

The pinning-dominated model of wall motion of section
5.6 (eq. (5.74)) gives this relation. Because in
these films the reversal process begins with the
growth of different spikes (see sec. 5.3) we only
tabulate $H_{d,max}=H_{m,2}$ (eq. (5.22)). In table 5.3 the
calculated results of this model are presented for
$n_w=5$ and the measured results are given too. All meas-
ured slopes are exactly equal to two. Macroscopical-
ly inhomogeneous samples (see sec. 2.2.2) give calcu-
lated values of K which are extremely large. The fre-
quency-density function of the driving field H_d of
the jumps is not uniform in this case as was assumed
in the derivation (see sec. 5.6). This effect can also
be seen in the other tables. Regarding the rough esti-

TABLE 5.3. The relation between p and τ_B for a rigid wall

DATA OF SAMPLES				K-values	
sample number	d_m [$\overset{\circ}{A}$]	μ [$m^2A^{-1}s^{-1}$]	$H_{m,2}$ [Am^{-1}]	measured	calculated eq. (5.74)
636.45[+]	2800	1.5	35	1.4	86
B197.2	2380	1.5	15	8.1	16
B197.3	2380	1.5	13	6	12
B197.8K	2380	1.5	17	6.5	20
B197.27K	2380	1.5	17	9.7	20
B197.28K	2380	1.5	17	6.5	20
B199.19[x]	2030	1.35	69	4.7	272
B199.21	2030	1.35	16	4.5	14
B198.18K	1580	1.1	19	7.3	14
B194(1).11K[x]	1230	1.1	35	5.9	46
B194(1).46	1230	1.1	10	7.5	4
B194(1).54	1230	1.1	17	9.4	10
B192.6	840	0.75	14	4.6	4

+ $H_d \approx 1120$ Am^{-1}

x sample with irregularities in the hysteresis loop

mation of the unknown parameter n_w, which is choosen
the same for all samples, and the inaccuracy in the
value of μ a good agreement between theory and experi-
ment is found . for the samples with a smooth hystere-
sis curve.

Before discussing the samples with $\varkappa$ values which are
at variance with the previous models, we will first com-
pare the structure of the domain walls in those thin films
where $\varkappa$ agrees with one of the models.

The different types of wall in thin Ni-Fe films were
extensively described in sec. 2.2.3. The Bloch walls are
present in the thicker films ($d_m \gtrsim 900\text{Å}$) used in our inves-
tigation and the cross-tie walls in our thinner films with
$d_m \lesssim 900\text{Å}$ as can be seen from fig. 2.8. We conclude now
that in general a value $\varkappa = 2$ is found for Bloch walls and
$\varkappa = 1.5$ for cross-tie walls in this type of sample. In other
words: we were the first to show experimentally that the
Barkhausen process in films with Bloch walls is in general
pinning dominated in the direction of motion and in films
with cross-tie walls it is stiffness dominated in the di-
rection of motion.

(D) In sec. 3.4 (fig. 3.7) we showed that some samples
    have a value of $\varkappa$ between 1.5 and 2. This exponent
    cannot be accounted for directly by one of our models,
    but it can be attributed to the fact that pinning- and
    stiffness-dominated wall motion are about equally im-
    portant in these samples. The measured frequency-den-
    sity function is then composed of the frequency-den-
    sity functions of both processes and can be obtained
    by adding the frequency-density functions of both pro-
    cesses together. This can give values of $\varkappa$ ranging be-
    tween 1.5 and 2. For the two cases which can be dis-
    tinguished we shall illustrate this using a simple
    example.

(D1) At the same value of p both processes are about
     equally important. Let us now consider in the $p\,\tau_B$-
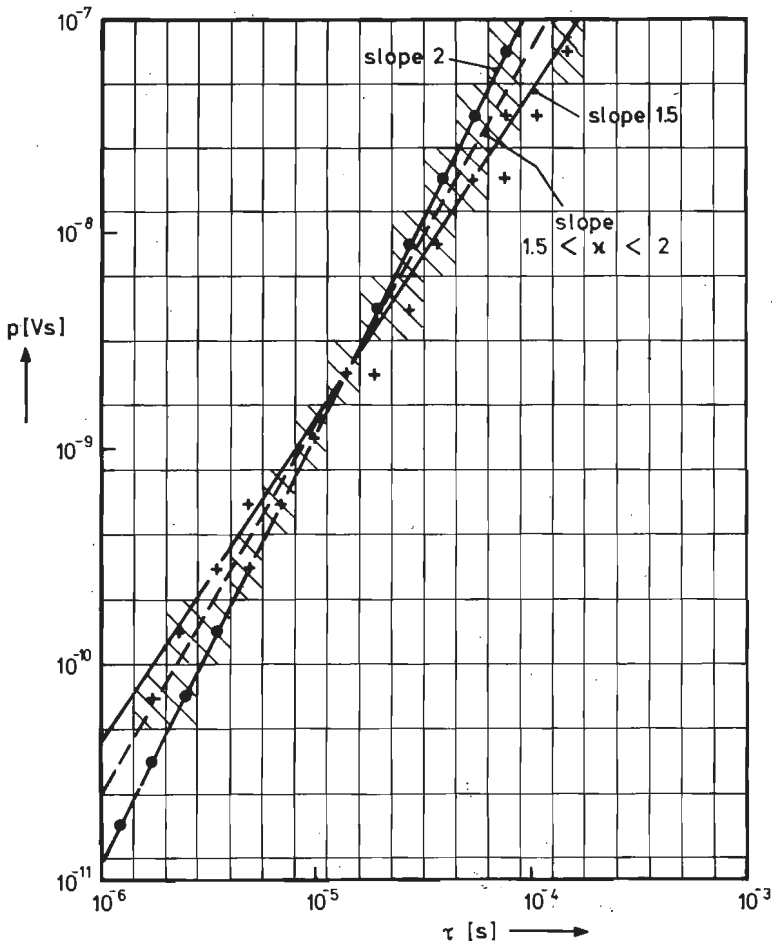   plane the number of pulses measured in the intervals.

Fig. 5.23. The maximum number of detected pulses for a process with $\kappa = 2$ (•), for a process with $\kappa = 1.5$ (+) and for a mixed process (shaded intervals).

In fig. 5.23 the interval in which for a given value of τ_B the number of pulses is maximum for the process with $\kappa = 2$ is indicated with • , for the process with $\kappa = 1.5$ is indicated with +. We assume that the number of the pulses measured in the adjacent intervals at the same τ_B is about a half of the maximum number. In fig. 5.23 the shaded intervals are the intervals where the resulting total number of pulses is maximum. The slope of the line through these points has a value κ with $1.5 < \kappa < 2$. The same result can be found for the frequency-density function.

(D2) For low p values one process dominates, e.g. the pro-
cess with $\varkappa=2$, while for higher p values the other
process dominates, so in this example the process with
$\varkappa=1.5$. Just as in (1), this also gives a slope $\varkappa$ be-
tween 1.5 and 2.

In both cases (1) and (2) the value of $\varkappa$ of the sam-
ple can vary between 1.5 and 2. We found such a behav-
iour in 4 films; of each film two specimens were mea-
ured. Five samples showed a $\varkappa$ value between 1.5 and
2, the remaining specimens of these films had $\varkappa$ values
of either 1.5 or 2.

(E) In fig. 3.7 we see that three films possess values of
$\varkappa$ around 1.3. All ten specimens of these three films
which were measured show $\varkappa$ values around 1.3. An ex-
ponent $\varkappa \approx 1.3$ can be obtained in two ways:

(E1) As explained in (D) this can be caused by the fact
that during the reversal jumping processes with $\varkappa=1.5$
and $\varkappa=1$ both are important in these films. However,
the model of sec. 5.4, which gives $\varkappa=1$, can not be
applied for a jumping process with $\varkappa=1$ in a large
range of p and τ_B values.

(E2) Another possibility is that apart from the relation-
ships between p and τ_B, which are treated in secs.
5.4 to 5.7, a relationship between p and τ_B can be
present in the films, which gives $\varkappa \approx 1^1/3$.

Until now we found no theoretical model which
can account for a $\varkappa$ value of about 1.3 in either way.

We now pay some attention to the three samples
(d_m=575Å, 630Å and 735Å) in which values of $\varkappa$ around 1.3
are found. The film with d_m=735Å has values of the coer-
cive field Hc(≈ 130Am^{-1}) and the anisotropy field
H_K(≈ 360Am^{-1}) which are often found in our films. The
two films with d_m=630Å and 575Å are the only ones in our
investigation which contained an additional amount of
10% Co (see sec. 2.2.1). The uniaxial anisotropy of the
films is therefore very large ($\geqslant 1600$Am^{-1}), resulting in
walls with a very large cross-tie density [5.3] (see fig.
2.7). The cross-tie length c_t is, however, small ($\approx 2\,\mu$m

[5.3]) and equals the distance between adjacent cross-
ties. Hence the walls can be pinned by the inclusions
over a larger area than with walls in a low (uniaxial)
anisotropy film (with a smaller number of cross-tie of
larger c_t). In this case the wall will contain about all
pinning centres within an area of width c_t around the
wall. Furthermore a high density cross-tie wall has a
larger stiffness than a low density cross-tie wall. It
is striking that we have found these values of $\varkappa$ in the
films with a high anisotropy which show a characteristic
magnetization behaviour. Of all 23 films with different
specifications 21 films have a uniaxial anisotropy field
H_K between 300 and 600Am^{-1}. In only one film (735Å thick,
$H_K \approx 360Am^{-1}$) did we measure a $\varkappa$ value of 1.35 (two spe-
cimens of this film were measured).

From the previous part of this section it is evident
that the three models of the secs. 5.4 to 5.7 present a
description of the Barkhausen process during quasi-static
reversal of the magnetization in thin Ni-Fe films. Perhaps
it is also possible to describe the relationship between
jump size and duration with similar models in samples with
a three-dimensional growth of the domains. Such a relation
between p and τ_B has already been measured by some authors
in those samples [5.18] .

5.8. CONCLUSIONS

In this chapter we have presented some models for the
Barkhausen effect in thin Ni-Fe films. The comparison be-
tween our theory and the experiments shows that it is pos-
sible to describe the wall jumps and the relationship be-
tween p and τ_B with simple models. In samples of all
thicknesses large wall jumps can take place, which follow
the relation $p \propto \tau_B$ for large p values. In general in
thick films, $d_m \gtrsim 900$Å, the process is completely deter-

mined by wall pinning in the direction of motion and by stiffness along the wall ($p \propto \tau_B{}^2$), while in thinner samples the process is mostly stiffness dominated in the direction of motion and pinning dominated along the wall ($p \propto \tau_B{}^{1.5}$). In some samples these two processes are both equally important. Comparison of our wall jumping models with the experimental results shows that in general the measured value of $\varkappa$ gives information on the wall structure present in the sample: $\varkappa = 2$ corresponds to a Bloch-wall and $\varkappa = 1.5$ to a cross-tie wall.

REFERENCES
5. 1   S. Middelhoek, in J. Smit (ed.), "Magnetic Properties of materials", McGraw-Hill, New York, 1971, p. 263 - 339.
5. 2   S. Middelhoek, IBM J. Res. & Dev. **6**, 1962, p. 394 - 406.
5. 3   S. Middelhoek, J. Appl. Phys. **34**, 1963, p. 1054 - 1059.
5. 4   S. Middelhoek, D. Wild, IBM J. Res. & Dev. **11**, 1967, p. 93 - 105.
5. 5   S. Middelhoek, "Ferromagnetic domains in thin Ni-Fe films", Thesis, University of Amsterdam, 1961.
5. 6   S. Middelhoek, IBM J. Res. & Dev. **10**, 1966, p. 351 - 354.
5. 7   J.A. Baldwin Jr, J. Appl. Phys., **38**, 1967, p. 501 - 506.
5. 8   J.A. Baldwin Jr, J. Appl. Phys., **39**, 1968, p. 5982 - 5986.
5. 9   R.S. Tebble, Proc. Phys. Soc. B68, 1955, p. 1017 - 1032.
5.10   see 5.5, p. 38.
5.11   J.A. Baldwin Jr., F. Milstein, N. Duc Vinh, J. Appl. Phys. **44**, 1973, p. 5100 - 5105; J.A. Baldwin Jr., F. Milstein, J. Appl. Phys. **44**, 1973, p. 1798 - 1800.
5.12   N.J. Wiegman, R. ter Stege, Appl. Phys. **16**, 1978, p. 167 - 174.
5.13   S. Chikazumi, "Physics of Magnetism", Wiley, New York, 1964, p. 193.
5.14   J.A. Osborn, Phys. Rev. **67**, 1945, p. 351 - 352.
5.15   M. Abramowitz, I.A. Stegun, "Handbook of Mathematical functions", Dover, New York, 1965.
5.16   see ref. 5.13, p. 212.
5.17   see ref. 5.13, p. 188.
5.18   U. Lieneweg, W. Grosse-Nobis, Int. J. Magn. **3**, 1972, p. 11 - 16.

6. BARKHAUSEN NOISE SPECTRA.

6.1. INTRODUCTION

A commonly used method for investigating the statistical properties of a physical process of a more or less random nature is the measurement of their power spectrum. In many cases, the process can be represented by a sequence of random pulses.

Often one considers a pulse sequence with an average number of v pulses per unit time. All pulses have the same shape $g(t)$ and amplitude h; the pulse size p is defined by

$$p = h \int_{-\infty}^{\infty} g(t)\, dt \qquad (6.1)$$

The occurrence of any pulse is assumed to be independent of the occurrence of other pulses. The shot noise in a vacuum tube is a physical process which behaves as described above. The resulting power spectrum $S(f)$ has the form [6.1]

$$S(f) = v\, S_0(f) + v^2 p^2 \delta(f) \qquad (6.2)$$

where $S_0(f)$ is determined by the Fourier transform $G_0(f)$ of the individual pulse

$$S_0(f) = \left| \int_{-\infty}^{\infty} h\, g(t)\, \exp(-2\pi i f t)\, dt \right|^2 = h^2 G_0(f)\, G_0^*(f) \qquad (6.3)$$

The second term of equation (6.2) represents the contribution of the dc-component of the pulse sequence; $\delta(f)$ is

the Dirac δ-function. The dc-term will be omitted in the
following treatment.

General expressions for the power spectrum and the
correlation function of random pulse sequences have been
derived by different authors [6.2-6.7]. Arbitrary fre-
quency-density functions of θ (i.e. the time period pre-
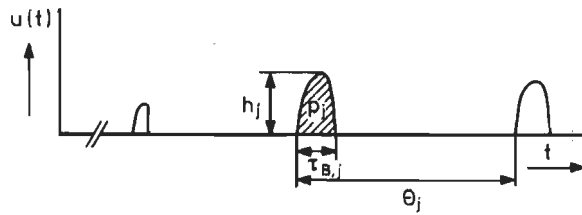ceding or following a pulse (fig. 6.1)) and h, and randomly

Fig. 6.1. Definition of the pulse parameters.

varying pulse shapes g(t) were taken into account.
Mazzetti et al. [6.3, 6.4] have calculated the power
spectrum in the case of a complete correlation between
the amplitude h_j and the time θ_j of the form $h_j = h(\theta_j)$.
Heiden [6.7] has extended the theory further by consider-
ing the general case of a combined probability density
function $\gamma(\theta, \tau_B, h)$ which permitted a coupling between
the pulse parameters, amplitude h, time duration τ_B and
the time period θ preceding or following a pulse; he
assumed that the shape function $g(t/\tau_B)$ was the same
for all pulses.

In sec. 6.2 we shall derive the form of the power
spectrum for pulse sequences with a relation between the
pulse size p and the pulse duration τ_B [6.7]. In our
derivation we assume that the pulses occur independently
of one another which is a simplification of the actual
behaviour (see sec. 3.7). The same case is also discussed
by Lieneweg [6.8]. In sec. 6.3 we apply the results of
sec. 6.2 to the Barkhausen effect in thin films. The meas-
ured frequency-density functions are substituted into

the equations found in sec. 6.2 and we investigate the
influence of the different parameters on the slope of
the noise spectrum. In sec. 6.4 the calculated and meas-
ured noise spectra of three samples are discussed. Further-
more we compare in this section the measured and calcu-
lated slopes of the frequency spectra of a large number of
films [6.9 [x]]. The measured slopes and cut-off frequen-
cies are also shown as functions of the film thickness.

6.2. THE FORM OF THE POWER SPECTRUM FOR PULSES WITH A RELATION BETWEEN p AND τ_B

We will derive here the power spectrum of a sequence
of pulses with the following properties [6.7, 6.8]:
(a) the pulse sequences are stationary and ergodic;
(b) the parameter values of the successive pulses are
    independent of one another;
(c) the shape of the j-th pulse is shown in fig. 6.1 and
    can be described by

$$u_j(t) = \begin{cases} h \, g \, (t - \sum_{i=1}^{j-1} \theta_i) & \text{for} \quad \sum_{i=1}^{j-1} \theta_i < t < \tau_{B,j} + \sum_{i=1}^{j-1} \theta_i \\ 0 & \text{elsewhere} \end{cases} \quad (6.4)$$

with
$$\int_0^\infty g(x) \, dx = \tau_B \quad (6.5)$$

(d) we only consider the fluctuating part, $u(t) - <u(t)>$,
    of the signal;
(e) the pulses occur independently of one another, we con-
    sider thus a Poisson process.

---

[x] *Preliminary results of measured noise spectra have been published*
    in: N.J. Wiegman, "Barkhausen effect in magnetic thin films:
    Experimental noise spectra", Appl. Phys. 12, 1977, p. 157-161.

A sequence of N pulses in a time period T can be described by

$$u(t) = \sum_j u_j(t) = \sum_j h_j\, g_j(t - \Theta_j) \qquad [v] \qquad (6.6)$$

with
$$\Theta_j = \sum_{i=1}^{j-1} \Theta_i \qquad\qquad (6.7)$$

With the properties (b) to (e) we find for the power spectrum S(f) of the sequence of independent pulses [6.10, 6.11]

$$S(f) = \frac{2}{T} U(f) U^*(f) = \frac{2}{T} \sum_i h_i^2 G_i(f)\, G_i^*(f) \qquad (6.8)$$

where U(f) is the Fourier transform of u(t) and G(f) the Fourier transform of g(t). A large variety of pulse shapes g(t) all give a spectrum $S_g(f)$ which can be approximated by [6.11]

$$S_g(f) = 2\, G(f)\, G^*(f) \;\approx\; \frac{2\, \tau_B^2}{1 + (2\pi f\, \tau_B)^2} \qquad (6.9)$$

Eq. (6.9) is exact for a pulse shape $g(t) = \exp(-t/\tau_B)$. So the power spectrum S(f) of the pulse sequence becomes

$$S(f) = \frac{2}{T} \sum_i \frac{h_i^2\, \tau_{B,i}^2}{1 + (2\pi f\, \tau_{B,i})^2} \qquad [v^2 s] \qquad (6.10)$$

or, using the pulse size p_i, expressed by the formula:

$$p_i = \int_o^\infty h_j\, g_i(t)\, dt \qquad [vs] \qquad (6.11)$$

one finds

$$S(f) = \frac{2}{T} \sum_i \frac{p_i^2}{1 + (2\pi f\, \tau_{B,i})^2} \qquad (6.12)$$

The number of pulses per second is given by N/T=ν. Using the probability density function pr(p, τ_B, θ) of the

pulse parameters p, τ_B and θ eq. (6.12) can be written as

$$S(f) = 2v \iiint\limits_{0}^{\infty} pr(p,\tau_B,\theta) \frac{p^2}{1 + (2\pi f \tau_B)^2} \, dp \, d\tau_B \, d\theta \qquad (6.13)$$

We consider the case that p and τ_B do not depend on θ. Eq. (6.13) then becomes

$$S(f) = 2v \iint\limits_{0}^{\infty} pr(p,\tau_B) \frac{p^2}{1 + (2\pi f \tau_B)^2} \, dp \, d\tau_B \; . \qquad (6.14)$$

$$= 2v \int\limits_{\tau_B = 0}^{\infty} \frac{1}{1 + (2\pi f \tau_B)^2} \int\limits_{p = 0}^{\infty} p^2 \, pr(p,\tau_B) \, dp \, d\tau_B \qquad (6.14a)$$

The mean value of p^2 for a given value of τ_B is given by

$$< p^2(\tau_B) > = \frac{\int\limits_{0}^{\infty} p^2 \, pr(p,\tau_B) \, dp}{\int\limits_{0}^{\infty} pr(p,\tau_B) \, dp} \qquad \left[v^2 s^2 \right] \qquad (6.15)$$

Substitution of eq. (6.15) in eq. (6.14) gives

$$S(f) = 2v \int\limits_{0}^{\infty} \frac{< p^2(\tau_B) >}{1 + (2\pi f \tau_B)^2} \, pr(\tau_B) \, d\tau_B \qquad \left[v^2 s \right] \qquad (6.16)$$

The low frequency limit $S(0)$ of $S(f)$ for this case becomes

$$S(0) = 2v \int\limits_{0}^{\infty} < p^2(\tau_B) > \, pr(\tau_B) \, d\tau_B \qquad \left[v^2 s \right] \qquad (6.16a)$$

Equation (6.16) represents the power spectrum $S(f)$ of a sequence of v pulses per second; the pulses are independent of one another but there is a relation between the pulse size p and the pulse duration τ_B.

6.3. THE BARKHAUSEN NOISE SPECTRA OF MAGNETIC THIN FILMS

First we will show that eq. (6.16) can be applied to the Barkhausen effect of thin magnetic films. In sec. 4.3 [6.12] we showed that the Barkhausen effect in thin films is a stationary process. Furthermore we take the process to be ergodic. Using the Barkhausen Computer Interface we also looked for a possible correlation between the parameters of two successive wall jumps; no relation has been found. Since only a relation has been found between p and τ_B of a jump the combined probability-density function $pr (\theta, \tau_B, p)$ can be written as (secs. 3.4 and 3.7):

$$pr(p, \tau_B, \theta) = pr(p, \tau_B)\, pr(\theta) \qquad (6.17)$$

Fig. 6.2 shows a computer plot of pulses measured with the Barkhausen Computer Interface. The pulses have an irregular shape as explained in sec. 1.4 (see also fig. 1.4). A large variety of pulse shapes $g(t)$ all give a spectrum $S_g(f)$
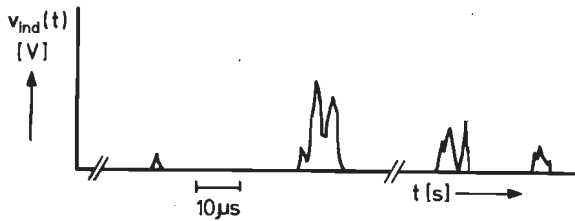

Fig. 6.2. Computer plot of pulses measured with the Barkhausen Computer Interface.

which can be approximated very well by eq. (6.9): the spectrum $S_g(f)$ is only slightly dependent on the pulse shape. Therefore we can use for the power spectrum of a Barkhausen pulse with amplitude h_i and time duration $\tau_{B,i}$ the equation

$$S_{u_i} \approx \frac{h_i^2\, \tau_{B,i}^2}{1 + (2\pi f \tau_{B,i})^2} = \frac{p_i^2}{1 + (2\pi f \tau_{B,i})^2} \qquad (6.18)$$

with (see fig. 6.1)

$$p_i = \int_0^\infty u_i(t)\, dt \qquad (6.18a)$$

The shape of the frequency-density function of θ shows that the Barkhausen jumps are not independent of one another. In our samples we have that:

$$v < \tau_B > \quad \ll 1 \qquad (6.19)$$

The measured values of $v < \tau_B >$ range between 1/30 and 1/1000; for most samples this value is about 1/300, so overlapping of pulses can be neglected. In the calcula-tions we take, therefore, the pulses to be indepen-dently of one another. Thus the Barkhausen process sat-isfies the properties used in sec. 6.2 for the derivation of the power spectrum (eq. 6.16).

In our case we are interested in the noise spectral density per hysteresis loop. The time duration of a hys-teresis loop is denoted by T_{loop}; multiplying eq. (6.16) with T_{loop} gives the noise per hysteresis loop. Using then

$$T_{loop}\, v\, pr(\tau_B) = z(\tau_B) \qquad (6.20)$$

in which $z(\tau_B)$ represents the frequency-density function per hysteresis loop of the pulse duration τ_B, gives for the noise spectral density of the Barkhausen noise per hys-teresis loop the following formula:

$$E(f) = 2 \int_0^\infty \frac{< p^2(\tau_B) >}{1 + (2\pi f \tau_B)^2}\, z(\tau_B)\, d\tau_B \quad \left[v^2 s^2 \right] \qquad (6.21)$$

For the mean value of $p^2(\tau_B)$ at a given value of τ_B we take (see sec. 3.4)

$$< p^2(\tau_B) > \approx p_w^2(\tau_B) \qquad (6.22)$$

The measured frequency-density function of τ_B has been discussed in sec. 3.6 and is given by the empirical rela-tion [6.13] of eq. (3.34). So for the noise spectrum of

the Barkhausen effect we find with $\eta = f\tau_B$

$$E(f) \approx 2K^2 \left[\frac{D_1}{f^{2\varkappa-\delta_1+1}} \int_{f(\tau_B)_{min}}^{f(\tau_B)_o} \frac{\eta^{2\varkappa-\delta_1}}{1+4\pi^2\eta^2} d\eta \right.$$

$$\left. + \frac{D_2}{f^{2\varkappa-\delta_2+1}} \int_{f(\tau_B)_o}^{f(\tau_B)_{max}} \frac{\eta^{2\varkappa-\delta_2}}{1+4\pi^2\eta^2} d\eta \right]$$

(6.23)

In most cases $z(\tau_B)$ can be accurately measured for large values of τ_B and we may write

$$D_2 = D_1 (\tau_B)_o^{\delta_2-\delta_1}$$

(6.24)

We assume that in all other cases eq. (6.24) is also valid. Hence eq. (6.23) becomes

$$E(f) \approx 2D_1 K^2 \left[\frac{1}{f^{2\varkappa-\delta_1+1}} \int_{f(\tau_B)_{min}}^{f(\tau_B)_o} \frac{\eta^{2\varkappa-\delta_1}}{1+4\pi^2\eta^2} d\eta \right.$$

(6.25)

$$\left. + \frac{(\tau_B)_o^{\delta_2-\delta_1}}{f^{2\varkappa-\delta_2+1}} \int_{f(\tau_B)_o}^{f(\tau_B)_{max}} \frac{\eta^{2\varkappa-\delta_2}}{1+4\pi^2\eta^2} d\eta \right]$$

or written in a convenient form:

$$E(f) \approx 2D_1 K^2 \{ I_1(f) + I_2(f) \}$$

(6.25a)

The integrals of eq. (6.25) must be calculated using a numerical integration method. First we shall discuss the function

$$I = \frac{1}{f^{2\varkappa-\delta+1}} \int_{\eta_1}^{\eta_2} \frac{\eta^{2\varkappa-\delta}}{1+4\pi^2\eta^2} d\eta \quad \text{where} \quad \eta = f\tau_B \quad (6.26)$$

which appeared in eq. (6.25). If the integration boundaries are $\eta_1 = 0$ and $\eta_2 = \infty$ the frequency dependence of

I is fully determined by the values of δ and $\varkappa$:

$$I \; \propto \; \frac{1}{f^{2\varkappa - \delta + 1}} \tag{6.27}$$

The calculated slope $(2\varkappa - \delta_1 + 1)$ varies between 1 and 3 for the measured values of $\varkappa$ and δ_1.

If $\eta_1 = f\,\tau_{B,1}$ and $\eta_2 = f\,\tau_{B,2}$, then the value of the integral

$$\int\limits_{f(\tau_B)_1}^{f(\tau_B)_2} \frac{\eta^{2\varkappa - \delta}}{1 + 4\pi^2 \eta^2} \, d\eta \tag{6.28}$$

depends on the frequency f and I is no longer proportional to

$$\frac{1}{f^{2\varkappa - \delta + 1}}$$

If $\tau_{B,2} \gg \tau_{B,1}$, then I is almost independent of the lower integration boundary. We have numerically calculated the dependence of I on f for $\tau_{B,1} = 10^{-8}$ s, $\tau_{B,2} = 2 \times 10^{-4}$ s and f ranging between 1 Hz and 1 MHz with $2\varkappa - \delta + 1$ as parameter. We can represent I as a function of f by the following equation:

$$I \; \propto \; \frac{1}{1 + (f/f_o)^{n_c}} \tag{6.29}$$

where n_c depends on $2\varkappa - \delta + 1$ as is shown in fig. 6.3. In this case f_o does not equal $(2\pi \tau_{B,2})^{-1}$ but f_o exceeds $(2\pi \tau_{B,2})^{-1}$ and depends on n_c.
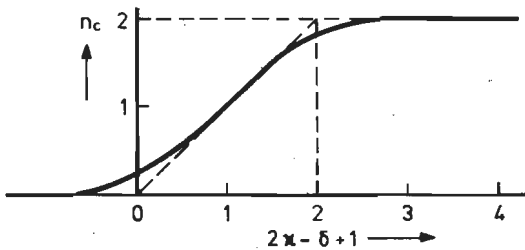

Fig. 6.3. Slope n_c as function of $2\kappa - \delta + 1$.

Let us now pay attention to the Barkhausen noise spectrum given by eq. (6.25). The first term $I_1(f)$ represents a summation of spectra over a wide range of τ_B values. We can apply the previous discussion to $I_1(f)$: the slope in the higher frequency range $(f \gg \{2\pi\,(\tau_B)_o\}^{-1})$ can be found from fig. 6.3. The contribution of the second term $I_2(f)$ of eq. (6.25) represents a summation of spectra over a small range of τ_B values. This gives a spectrum with a slope 2 in the higher frequency range, $f > \{2\pi\,(\tau_B)_o\}^{-1}$. The influence of the integral $I_2(f)$ on the spectrum given by $I_1(f)$ is determined by the slope of the quantity $I_1(f)$ for $f \gg \{2\pi\,(\tau_B)_o\}^{-1}$ and by the ratio I_2/I_1 for $f \ll \{2\pi\,(\tau_B)_o\}^{-1}$ i.e. $I_2(o)/I_1(0)$ with

$$\frac{I_2(0)}{I_1(0)} \approx \frac{2\varkappa - \delta_1 + 1}{2\varkappa - \delta_2 + 1}\left[\;\left|\frac{(\tau_B)_{max}}{(\tau_B)_o}\right|^{2\varkappa - \delta_2 + 1} - 1\right] \qquad (6.30)$$

For the range of our measured $\varkappa$, δ_1 and δ_2 values, the calculated noise spectra can be represented accurately by an equation of the form

$$E(f) = \frac{E(0)}{1 + (f/f_o)^{n_c}} \qquad \left[V^2 s^2\right] \qquad (6.31)$$

where f_o is the cut-off frequency of the noise spectrum. In fig. 6.4 we have plotted the calculated value n_c as a function of δ_1 with $\varkappa$ as parameter choosing $\delta_2 = 2.5 \times \delta_1$, $(\tau_B)_{min} = 10^{-8}$ s, $(\tau_B)_o = 2 \times 10^{-4}$ s and $(\tau_B)_{max} = 2 \times (\tau_B)_o$. All
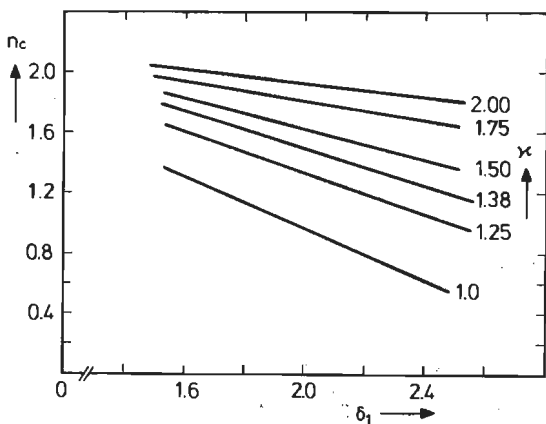

Fig. 6.4.

Calculated slope n_c as a function of δ_1 with $\varkappa$ as parameter.

spectra are calculated for frequencies ranging between
10 Hz and 1 MHz. From fig. 6.4 it follows that dependent
on the value of the parameter $\varkappa$ the variation in the value
of n_c is about 0.7 to 0.2 for a variation of δ_1 between
1.6 and 2.4. The calculations show that the influence of
the slope δ_1 on the slope n_c of the noise spectral density
$(f \gg f_o)$ decreases with increasing $\varkappa$.
Furthermore we see from fig. 6.4 that in our case (for
$1.6 < \delta_1 < 2.4$) low values of $n_c (\leqslant 1.3)$ can only be ob-
tained with low values of $\varkappa$ $(\leqslant 1.25)$. High $\varkappa$ values (≈ 2)
always give rise to high values of n_c $(1.8 \leqslant n_c \leqslant 2.0)$.

6.4. COMPARISON BETWEEN CALCULATED AND MEASURED NOISE
SPECTRA

We have plotted $E(f)$, the noise spectral densities
averaged over 40 to 60 hysteresis loops. Furthermore the
noise spectrum is normalized to a film thickness of
1000 $\overset{o}{A}$ (sec. 2.4, eq. (2.5)). The experimental fre-
quency-density functions to be used in the calculation of
the noise spectra were obtained by measuring 10 to 30 hys-
teresis loops (see sec. 2.5).

The measured noise spectra can be described by an
equation of the form

$$E(f) = \frac{e(f)}{1 + (f/f_o)^n} \qquad \left[V^2 s^2 \right] \qquad (6.32)$$

with f_o the cut-off frequency, n the measured slope in the
high-frequency range $(f \gg f_o)$ and $e(f)$ the level of the
spectrum in the low-frequency range $(f \ll f_o)$. In the measured
ured spectra of some samples $e(f)$ is a slowly decreasing
function of f. The measured spectra of other samples have
a constant density $e(f) = E(0)$ for $f \ll f_o$. In the calculated
spectra (see eq. (6.25)), however, the noise spectral density
always has a constant value for $f \ll f_o$.

After these general remarks we will compare the measured and calculated spectra of three samples. In the figs. 6.5 upto 6.7 we present the measured and calculated noise spectra of samples which are 2380 Å, 630 Å and 420 Å thick.
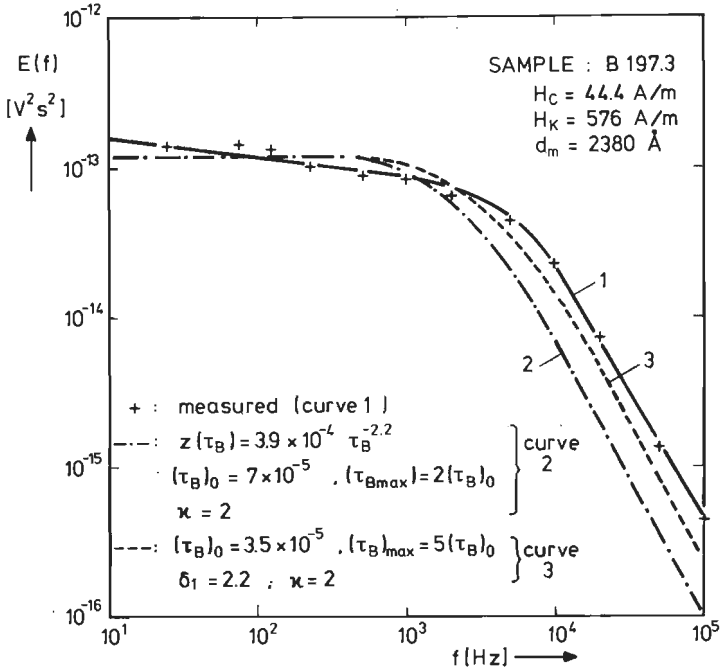

Fig. 6.5.   Measured (1) and calculated (2 and 3) spectra of a 2380Å thick sample.

Fig. 6.5 shows the calculated and measured noise spectra of a sample which is 2380 Å thick. Using the measured values of $\varkappa$, δ_1 and $(\tau_B)_0$ which are $\varkappa = 2$, $\delta_1 = 2.2$ and $(\tau_B)_0 = 7 \times 10^{-5}$s and taking $\delta_2 = 2.5$ δ_1 and $(\tau_B)_{max} = 2(\tau_B)_0$, the shape of the measured (curve 1) and calculated (curve 2) spectra agree very well. For the value $K^2 D_1 = 3.6 \times 10^{-2}$ the levels of the calculated and measured spectra are in good agreement in the low-frequency range. In the high-frequency range $(f > f_0)$, however, a deviation by a factor of about 3.5 is found, as is shown in fig. 6.5. The value of f_0 of the calculated spectrum is lower by a factor of about two than the value of f_0 in the measured spectrum. The frequency-density function of

τ_B is inaccurate for small values of τ_B (see section 3.2).
In this sample the range of τ_B values is very small (about
one and a half decade). Therefore the inaccuracy in the
frequency-density function of τ_B can give rise to a rather
large error in the measured values of D_1 and δ_1. The in-
fluence of the error in δ_1 on the noise spectrum is very
small because $\varkappa = 2$ (see fig. 6.4). The number of jumps with
$\tau_B \gtrsim 0.5\ (\tau_B)_0$ is so small that the density function
comes inaccurate. This causes an error in the calculated
value of f_0. Comparison between the calculated and measured
values showed a factor two difference. The calculated value
of f_0 in this sample can be fitted to the measured value by
taking the value of $(\tau_B)_0$ to be smaller. In order to pre-
serve the agreement with the measured function of $z(\tau_B)$
one must also increase the value of $(\tau_B)_{max}$. For the third
spectrum, we use $(\tau_B)_0 = 3.5 \times 10^{-5}$ s, $(\tau_B)_{max} = 5(\tau_B)_0$ and
$K^2 D_1 = 1.7 \times 10^{-1}$. This calculated spectrum (curve 3 in fig.
6.5) agrees better with the measured spectrum (curve 1)
than does the calculated spectrum represented by curve 2.

Fig. 6.6 presents the calculated and measured (curve 1)
noise spectra of a 630 Å thick sample. Using the results of
the measurements of the frequency-density functions of the
pulse parameters we calculate the noise spectral density
shown by curve 2 in fig. 6.6. Here we used $K^2 D_1 = 1.3 \times 10^{-11}$
to fit the calculated to the measured (curve 1) noise spec-
tra in the high-frequency range. Good agreement between
measured and calculated slopes is found, as can be seen in
fig. 6.6. The calculated cut-off frequency f_0 is larger by
a factor of about 6 than the measured value of f_0. Increas-
ing $(\tau_B)_0$ with a factor 6 and decreasing δ_1 with 0.1
results in a calculated (curve 3) spectrum which shows an
excellent agreement with the measured one. In this case we
use $K^2 D_1 = 8 \times 10^{-11}$. The adjustment of δ_1 is within the
accuracy of the measurement of $z(\tau_B)$ (see sec. 3.6). Be-
cause wall jumps with a large time duration $(\tau_B \approx (\tau_B)_0)$
are scarcely present, the statistics for large values of
$\tau_B(\approx (\tau_B)_0)$ can show large errors. For two other samples
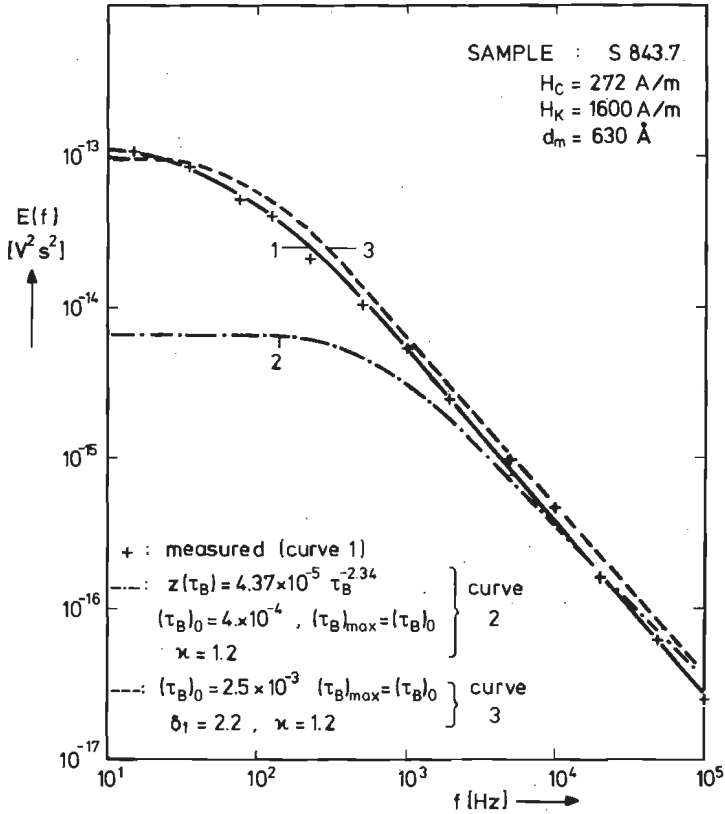of the same film (630 Å) the measured value of $(\tau_B)_0$ is

Fig. 6.6. Measured (1) and calculated (2 and 3) spectra of a 630Å thick sample.

10^{-3}s. In the sample presented in fig. 6.6 at the (digital) measurements of the frequency-density functions only 24% of the remagnetized volume is measured: $(P_{tot})_m \approx 0.24\ P_{tot}$ (see sec. 4.2). Therefore it is not surprising that a large discrepancy is found between the curves 1 and 2 in fig. 6.6.

Fig. 6.7 presents the noise spectra of a 420 Å thick sample being a wall stiffness dominated one so that $\varkappa = 1.5$. When the calculated spectrum fits the measured spectrum in the high frequency range, the calculated noise spectral density in the low frequency range (at about 10 Hz) is about a factor of 2 too large using the measured frequency-density functions. By taking $(\tau_B)_{max} = 2(\tau_B)_o$ instead of the measured value $(\tau_B)_{max} \approx 5(\tau_B)_o$ a good agreement between measured and calculated spectra is found in the investiga-
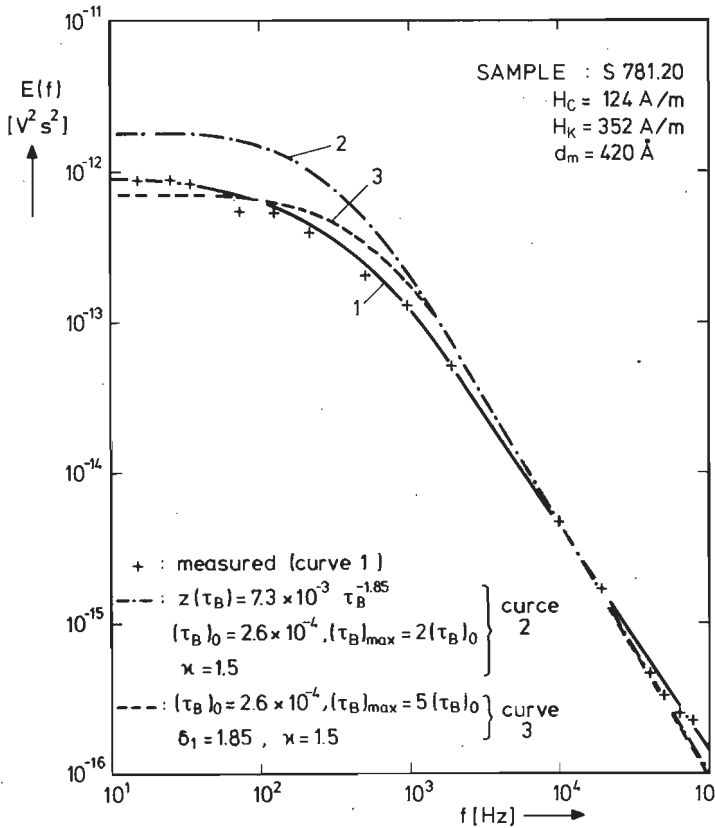
Fig. 6.7. Measured (1) and calculated (2 and 3) noise spectra of a sample with a thickness of 420Å.

ted frequency range of 10 Hz to 100 kHz.

In general the agreement between measured spectra and spectra calculated with the measured density function, is very good, as is shown in figs. 6.5 and 6.7.

We have shown that it is possible to obtain agreement between calculated and measured spectra by adjusting the measured frequency-density functions within the limits of accuracy of the experimental procedure. We will now make some general remarks about this point and therefore we shall distinguish the samples in two groups with regard to the spectra: (a) samples with e(f) = constant and (b) samples for which e(f) varies slowly with frequency.

149

(a) This concerns samples where the measured noise spectrum in the low-frequency range ($f \ll f_o$) has a constant value. Here the agreement of the calculated spectrum with the measured spectrum can be obtained by adjusting $(\tau_B)_o$. In this way we can ensure that the measured and calculated cut-off frequencies are equal. The level can be fitted by choosing a proper value of K^2D_1 (see figs. 6.5 and 6.6).

(b) Samples, in which some frequency dependence of the noise spectral density is found in the low-frequency range. In these samples we can adjust the measured and calculated spectra by varying $(\tau_B)_{max}$ and by changing the value of $(\tau_B)_o$.

Fig. 6.8 shows the measured slope n of all samples as a function of the film thickness d_m [6.9]. A comparison between the calculated slope n_c and the measured slope n is shown in fig. 6.9 for all our samples. The calculated slopes n_c were determined with the aid of the curves of fig. 6.4, thus all for the same $(\tau_B)_o$, and $(\tau_B)_{max}$. The variations of $(\tau_B)_o$ and $(\tau_B)_{max}$ between the different samples were neglected. In spite of the errors thus incurred and of
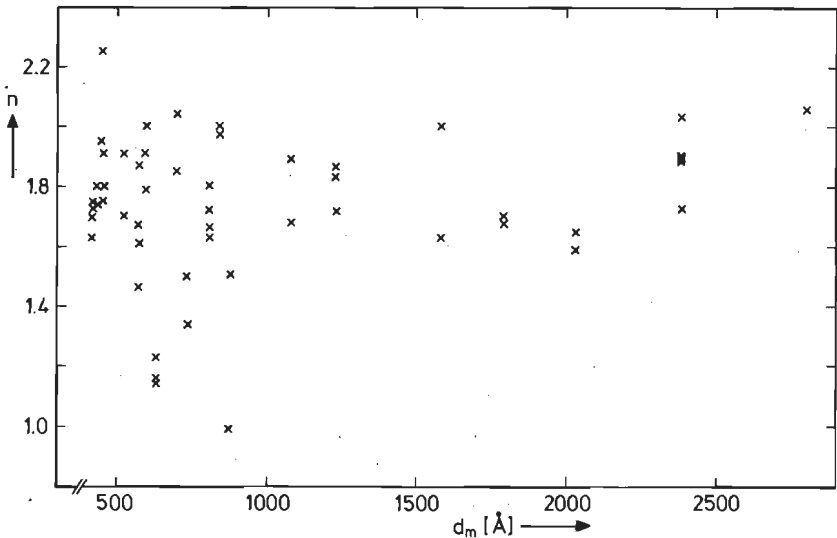

Fig. 6.8. Measured slope n of the noise spectra as a function of the film thickness.

the error in the measured value of δ_1 and δ_2 the value of n_c and n agree very well. In three samples the deviation between n_c and n is larger than 0.3. These samples are macroscopically inhomogeneous samples (sec. 2.2.2) or they show large irregularities in the magnetization process.

The measured slopes of the largest part of our samples varies between 1.6 and 2.0 (fig. 6.9). Only a small number of samples show a slope n ranging between 1 and 1.5.
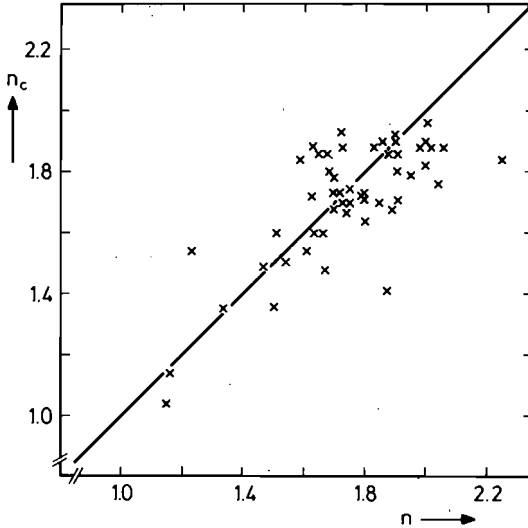

Fig. 6.9. Comparison between the measured and calculated slopes of the spectra.

The value of δ_1 is not the same for the different samples and therefore the measured value of the slope n does not decrease with decreasing $\varkappa$ (see fig. 6.4). Thus the value of n is not an unequivocal measure for the value of $\varkappa$ [6.12]. This corresponds with the experimental fact that in most samples in which the value of $\varkappa$ becomes smaller the value of δ_1 decreases also. For most samples with $\varkappa \leqslant 1.5$ we find n > 1.6 (figs. 3.7, 3.14 and 6.4).

Fig. 6.10 shows the measured cut-off frequency f_o as a function of the film thickness d_m. We will show that f_o is strongly dependent on the domain wall mobility μ of the films. For this purpose we will consider the value of
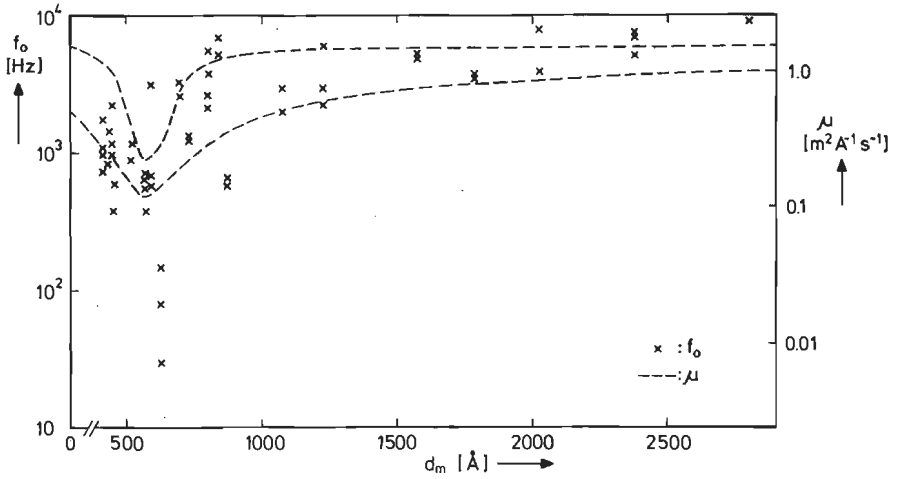
Fig. 6.10. Cut-off frequency f_0 and mobility μ as a function of d_m.

f_0 of all our samples: in different samples of one film and in different films in which μ varies by a factor of about 10. We were not able to measure the mobility in our samples. We assume that the samples of one film have about the same mobility and that in our films the mobilities vary as a function of the film thickness as found by Middelhoek [6.14].

From eqs. (5.17) and (5.20) it follows that

$$\tau_B \propto \frac{x_w}{\mu (H_{cp} - H_{cl})} \qquad (6.33)$$

where μ is the wall mobility, $(H_{cp} - H_{cl})$ the driving field and x_w the wall displacement. For f_0 we have the relation

$$f_0 \propto \frac{1}{2\pi (\tau_B)_0} \qquad [Hz] \qquad (6.34)$$

In general the measured values of f_0 varies by a factor of two at the most in samples of the same film, as can be seen in fig. 6.10. Thus we may conclude that in different samples of the same film the range of values of $(H_{cp} - H_{cl})/x_w$ varies only slightly. Let us now assume that this is also true for different films. Then from eqs. (6.33) and (6.34) it follows that, if μ shows a certain dependence

152

on the thickness, then nearly the same dependence must be found for f_o. In fig. 6.10 the domain wall mobility μ is also shown as a function of d_m, as measured by Middelhoek [6.14](compare fig. 2.9). In fig. 6.10 we see that the band containing the wall mobilities closely resembles the band containing our measured cut-off frequencies.

6.5. DISCUSSION

In the calculations we assumed that the pulses occur independently of one another, which is not in agreement with experiment. In spite of this simplification of the Barkhausen effect we find in the calculations a good agreement with the experimental results when we use the other results of the statistical analysis in the time domain.

The measured one- and two-dimensional frequency-density functions give values of $\varkappa$ and δ_1, which were used in the calculation of n_c. For small values of $\varkappa$ and large values of δ_1 the influence of the inaccuracy of $\varkappa$ and δ_1 on the value of n_c is strongest, as follows from fig. 6.4. Furthermore a deviation in $\varkappa$ has a larger influence on n_c than has a deviation in δ_1. For a large range of $\varkappa$ and δ_1 values the measured and calculated slopes, agree within 0.2. Hence we conclude that δ_1 and $\varkappa$ were determined accurately from $z(\tau_B)$ and $z(p, \tau_B)$.

In general a simple relation between n and $\varkappa$ has not been found. The values of n is almost completely determined by $\varkappa$ and δ_1, whereas in our samples δ_1 varies between 1.6 and 2.4. However large values of $\varkappa$ (≈ 2) are always related to values of n around 2. A decrease of $\varkappa$ at a fixed value of δ_1 gives a decreasing n. From the relation between n, $\varkappa$ and δ_1 we conclude that the value of $\varkappa$ can be estimated from a measurement of n and δ_1. In chapter 5 it has been shown that $\varkappa$ is determined by the mechanism of domain wall motion. Thus from the measurement of n and δ_1 we can find the mechanism of domain wall motion.

In the noise spectra the calculated and measured cut-off frequencies differ by a factor of about two. The cut-off frequency f_o is proportional to μ and also depends on the range of values of $(H_{cp}-H_{cl})/x_w$. In different samples differences are found in the strength and number of pinning points, the number of walls, the wall structure, the wall stopping mechanism, etc. They all have an influence on $(H_{cp}-H_{cl})/x_w$. Experiments performed on a large number of samples show that a plot of the measured values of f_o against the film thickness closely resembles the plot of μ against d_m. Thus the differences mentioned above only slightly affect f_o.

REFERENCES

6. 1   D.K.C. Mac Donald, "Noise and Fluctuations: an introduction", Wiley, New York, 1962.
6. 2   T. Lukes, Proc. Phys. Soc., 78, 1961, p. 153 - 168.
6. 3   P. Mazzetti, Nuovo Cimento, 31, 1964, p. 88 - 97.
6. 4   G. Biorci, P. Mazzetti, P. Soardo, A.E.U. 19, 1965, p. 91 - 94.
6. 5   G. Bonnet, Compt. Rend., 261, 1965, p. 5307 - 5310.
6. 6   G. Bonnet, P.-Y. Arques, Compt. Rend., 263, 1966, p. 798 - 801.
6. 7   Chr. Heiden, Phys. Rev. 188, 1969, p. 319 - 326.
6. 8   U. Lieneweg, W. Grosse-Nobis, Int. J. Magn. 3, 1972, p. 11 - 16.
6. 9   N.J. Wiegman, Appl. Phys. 12, 1977, p. 157 - 161.
6.10   J.J. Freeman, "Principles of Noise", Wiley, New York, 1958.
6.11   H. Bittel, L. Storm, "Rauschen", Springer, Berlin, 1971.
6.12   N.J. Wiegman, R. ter Stege, Appl. Phys. 16, 1978, p. 167 - 174.
6.13   N.J. Wiegman, to be published.
6.14   S. Middelhoek, IBM J. Res. & Dev. 10, 1966, p. 351 - 354.

APPENDIX 1: DATA OF THE INVESTIGATED SAMPLES.

film thick-ness d_m (Å)	sample number	coercive field H_c (Am^{-1})	anisotropy field H_k (Am^{-1})
2800	636.45	56	624
2380	B197.2 B197.3 B197.8K B197.27K B197.28K	44.4	576
2030	B199.19 B199.21	76	560
1790	B194(2).4 B194(2).13K	100	520
1580	B198.18K B198.29K	136	560
1230	B194(1).11K B194(1).46 B194(1).54	148	512
1080	B380.24 B380.30	128	400
875	S941.47 S941.48	104	368

$d_m(\text{Å})$	sample number	$H_c(\text{Am}^{-1})$	$H_k(\text{Am}^{-1})$
840	B192.6 B192.9K	272	560
805	S954.1 S954.49	152	400
805	B190.5 B190.50	180	544
735	S952.12 S952.44K	136	360
700	S782.14 S782.43	168	376
630	S843.7 S843.16 S843.17	272	1600
595	S951.10 S951.22 S951.23	72	400
575	S842.15 S842.39 S842.40 S842.41	280	1760
525	S724.38 S724.51K	124	416
455	S725.36 S725.42	108	448

$d_m(Å)$	sample number	$H_c(Am^{-1})$	$H_k(Am^{-1})$
455	B340.37 B340.52K	96	448
450	B193.31	240	640
437	B289.34 B289.35	144	448
420	S781.20 S781.33	124	352
420	S723.32 S723.53K	104	448

The assumed actual frequency-density function of p, z'(p) and the measured frequency-density function z(p) given by eqs. (3.30) and (3.24), respectively determine the relative error of P_{tot}:

$$\frac{P'_{tot} - P_{tot}}{P'_{tot}} \qquad (A2.1)$$

On substituting eq. (3.24) in eq. (3.28) for $\alpha_1 \neq 2$ and $\alpha_2 > 2$, we find

$$P_{tot} = \frac{A_1}{2 - \alpha_1} \left| p_o^{2-\alpha_1} - p_{min}^{2-\alpha_1} \right| + \frac{A_2}{2 - \alpha_2} \left| p_{max}^{2-\alpha_2} - p_o^{2-\alpha_2} \right| \quad (A2.2a)$$

and by the use of eq. (3.28) for $\alpha_1 = 2$, we can calculate:

$$P_{tot} = A_1 \ln\left(\frac{p_o}{p_{min}}\right) + \frac{A_2}{2 - \alpha_2} \left| p_{max}^{2-\alpha_2} - p_o^{2-\alpha_2} \right| \quad (A2.2b)$$

Correspondingly for $\alpha'_1 \neq 2$ we find for P'_{tot}:

$$P'_{tot} = \frac{A'_1}{2 - \alpha'_1} \left| p_o^{2-\alpha'_1} - (p'_{min})^{2-\alpha'_1} \right| + \frac{A_2}{2 - \alpha_2} \left| p_{max}^{2-\alpha_2} - p_o^{2-\alpha_2} \right| \quad (A2.3a)$$

and for $\alpha'_1 = 2$:

$$P'_{tot} = A'_1 \ln\left(\frac{p_o}{p'_{min}}\right) + \frac{A_2}{2 - \alpha_2} \left| p_{max}^{2-\alpha_2} - p_o^{2-\alpha_2} \right| \quad (A2.3b)$$

The relative error of P_{tot} for $\alpha_1 \neq 2$ and $\alpha'_1 \neq 2$ is given by

$$\frac{P'_{tot} - P_{tot}}{P'_{tot}} = \frac{\dfrac{A'_1}{2-\alpha'_1}\left\{P_o^{2-\alpha'_1} - (p'_{min})^{2-\alpha'_1}\right\} - \dfrac{A_1}{2-\alpha_1}\left\{P_o^{2-\alpha_1} - P_{min}^{2-\alpha_1}\right\}}{\dfrac{A'_1}{2-\alpha'_1}\left\{P_o^{2-\alpha'_1} - (p'_{min})^{2-\alpha'_1}\right\} + \dfrac{A_2}{2-\alpha_2}\left\{P_{max}^{2-\alpha_2} - P_o^{2-\alpha_2}\right\}}$$

$$(A2.4a)$$

and for $\alpha_1' = 2$ and $\Delta\alpha \neq 0$ one finds

$$\frac{P'_{tot} - P_{tot}}{P'_{tot}} = \frac{A'_1 \ln\left(\dfrac{P_o}{P'_{min}}\right) - \dfrac{A_1}{2-\alpha_1}\left\{P_o^{2-\alpha_1} - P_{min}^{2-\alpha_1}\right\}}{A'_1 \ln\left(\dfrac{P_o}{P'_{min}}\right) + \dfrac{A_2}{2-\alpha_2}\left\{P_{max}^{2-\alpha_2} - P_o^{2-\alpha_2}\right\}}$$

$$(A2.4b)$$

The contribution of the term

$$\frac{A_2}{\alpha_2 - 2}\ P_o^{2-\alpha_2}$$

$$(A2.5)$$

to P_{tot} varies between 0 and about 15%; we shall ignore this term. With the aid of eqs. (3.31a), (3.31c) and (3.32) we can deduce that

$$\frac{P'_{tot} - P_{tot}}{P'_{tot}} = \left\{P_o^{2-\alpha'_1} - (p'_{min})^{2-\alpha'_1}\right\}^{-1} \times$$

$$(A2.6a)$$

$$\times \left[\frac{P_o^{2-\alpha'_1}}{2-\alpha'_1+\Delta\alpha}\Delta\alpha + (p'_{min})^{2-\alpha'_1}\left|\frac{(2-\alpha'_1)\ f_p^{2-\alpha'_1}}{2-\alpha'_1+\Delta\alpha}\left(\frac{f_p\ p'_{min}}{P_o}\right)^{\Delta\alpha} - 1\right|\right]$$

for $\alpha_1 \neq 2$ and $\alpha_1' \neq 2$; for $\alpha_1' = 2$ and $\Delta\alpha \neq 0$ one finds

$$\frac{P'_{tot} - P_{tot}}{P'_{tot}} = 1 - \frac{1}{\Delta\alpha\ \ln\left(\dfrac{P_o}{P'_{min}}\right)}\left\{1 - \left(\frac{f_p\ p'_{min}}{P_o}\right)^{\Delta\alpha}\right\}$$

$$(A2.6b)$$

APPENDIX 3: PULSE OVERLAPPING.

In this appendix we will estimate the probability that pulses overlap.
To simplify the calculation we make the following assumptions which agree not with the experimental results of the secs. 3.6 and 3.7.
1) All pulses have the same duration τ , where

$$\tau = < \tau_B > \qquad \text{and} \qquad \tau \ll T_{rev} \qquad (A3.1)$$

T_{rev} is the time duration of the reversal of the magnetization of the sample. In all measurements we find

$$\frac{\sum_k \Theta_k \ z(\Theta_k) \ \Delta \Theta_k}{\sum_j \tau_{B,j} \ z(\tau_{B,j}) \ \Delta \tau_{B,j}} \ \gg \ 1 \qquad (A3.1a)$$

This ratio varies between 30 and 1000, for most samples it is about 300.
2) The pulses start at random during the reversal time. The number of Barkhausen pulses per reversal is $N_{tot/2}$ with

$$N_{tot} / 2 \ \gg \ 1 \qquad (A3.2)$$

Here N_{tot} is the number of pulses per hysteresis loop. For a time interval t_a with

$$t_a / T_{rev} \ \ll \ 1 \qquad (A3.3)$$

the probability that k pulses with length τ lie entirely or partially in the interval t_a is given by the probability that k pulses start in the interval $t_a + \tau$. According to [A3.1] this is given by

$$P(k, t_a + \tau) = \frac{\{\lambda(t_a + \tau)\}^k}{k!} \ \exp\{-\lambda(t_a + \tau)\} \qquad (A3.4)$$

where
$$\lambda = \frac{N_{tot}/2}{T_{rev}}$$
(A3.5)

The probability that k pulses occur in the interval τ, i.e. k pulses start in the interval 2τ, follows from eq. (A3.4)

$$P(k, 2\tau) = \frac{(2\lambda\tau)^k}{k!} \exp(-2\lambda\tau)$$
(A3.6)

If $k > 1$ then pulse overlapping occurs in the time interval τ:

$$P(pulse\ overlapping) = P(k > 1, 2\tau)$$
(A3.7)

where
$$P(k > 1, 2\tau) = 1 - P(0, 2\tau) - P(1, 2\tau)$$
(A3.8)

so that we find

$$P(k > 1, 2\tau) = 1 - (1 + 2\lambda\tau)\exp(-2\lambda\tau)$$
(A3.9)

A more important quantity is the ratio between the probability that pulse overlapping occurs in the interval τ and the probability that only one pulse start in the interval 2τ. For some samples $P(k > 1, 2\tau)/P(k = 1, 2\tau)$ have been calculated. The results are presented in table A3.1. All pulses are assumed to occur in the steep part of the hysteresis loop; so we use for T_{rev} a typical value of 0.2s.

TABLE: A3.1

sample	$d_m(Å)$	$z(\tau_B)$	τ_o	$<\tau_B> = \tau$	λ	$\dfrac{P(k > 1, 2\tau)}{P(k = 1, 2\tau)}$
B197.3	2380	$3\times10^{-4}\ \tau_B^{-2.2}$	7×10^{-5}	7.1×10^{-6}	3700	2.6×10^{-2}
B289.35	437	$5.4\times10^{-3}\ \tau_B^{-1.9}$	2×10^{-4}	1.1×10^{-5}	2000	2.1×10^{-2}
S725.36	455	$2.4\times10^{-2}\ \tau_B^{-1.6}$	5×10^{-4}	2.6×10^{-5}	250	6.3×10^{-3}

The value of $<\tau_B>$ is determined from the measurements of $z(\tau_B)$ using $\delta_2 = 0$ and $(\tau_{B,det})_{min} = 2\times10^{-6}$s. For N_{tot} we used the measured value.

In the Barkhausen process a large number of pulses occur with $\tau_B < (\tau_{B,det})_{min}$. Therefore we have calculated also $P(k > 1, 2\tau)$ using a minimum pulse time τ_B of 10^{-7} s. This is listed in Table A3.2 for the same samples as used in table A3.1.

TABLE: A3.2

sample	$<\tau_B>=\tau$	λ	$\dfrac{P(k>1,2\tau)}{P(k=1,2\tau)}$
B197.3	4.4×10^{-7}	1.6×10^5	4.2×10^{-2}
B289.35	1.0×10^{-6}	3×10^4	3.0×10^{-2}
S725.36	4.4×10^{-6}	1.6×10^3	7.1×10^{-3}

From this simplified model calculations it is clear that the probability of pulse overlapping is so small that we can safety neglect this effect in our investigation (see also sec. 4.4, fig. 4.8).

A3.1   A. Papoulis, " Probability, Random Variables and Stochastic Processes", McGraw Hill, New York, 1965, p. 73.

SUMMARY AND CONCLUSIONS.

The present thesis deals with an investigation into
the magnetic Barkhausen effect in thin magnetically uni-
axial films with a thickness larger than 900 Å, having a
two-dimensional magnetic domain structure. The remagnet
ization process in the easy direction was caused solely
by domain wall motion. The Barkhausen process, i.e. the dis-
continuous domain wall motion due to inhomogeneities in
the magnetic material, was studied when the hysteresis
loop was traced in the easy direction. Examination of the
samples used enabled a relationship to be established be-
tween the Barkhausen noise and the micromagnetic behaviour.

Investigated were a large number of samples whose
coercive field and strength of uniaxial anisotropy were
varied and the film thickness was in addition varied be-
tween 420 and 2800 Å. The structure of the magnetic do-
main wall changes with its thickness. Thicker films (i.e.
ones with a thickness in excess of 900 Å) contain Bloch
walls with a high stiffness whereas in thinner films
(i.e. ones with a thickness between 400 and 900 Å) flexible
cross-tie walls occur. Hence we are able in the samples
to assess the effect of the wall structure on the Bark-
hausen effect. For this purpose we have investigated the
Barkhausen effect both in the time domain and in the fre-
quency domain: the frequency-density function of the
parameters of the Barkhausen effect have been determined
(chapter 3) and the spectral noise intensity has been
measured (chapter 6).

Our measurements (sec. 3.4) have revealed that there is a relationship between the time τ_B and the size p of a Barkhausen jump. The Barkhausen jumps in a sample obey a relationship of the form $p \propto \tau_B^{\varkappa}$. In our samples two values of $\varkappa$, i.e. $\varkappa = 2$ and $\varkappa = 1.5$ were dominant. The experiments showed that in thicker films (with a thickness between 400 and 900 Å) usually the value $\varkappa = 1.5$ is found. From a comparison between the experimentally found $\varkappa$ values with the wall structure (sec. 2.2.3) occurring in samples of different thickness it follows that in magnetic films with Bloch walls, the Barkhausen process can be characterized by $\varkappa = 2$ and in films with cross-tie walls by $\varkappa = 1.5$.

In chapter 5 the process of domain wall pinning is outlined and models are established for the Barkhausen jumps of a domain wall. For a process, in which the wall motion stops due to the finite radius of curvature of the flexible wall (sec. 5.5) the model provides the relation $p = K \tau_B^{1.5}$ (stiffness-dominated wall motion). For a process at which the motion of a rigid wall stops owing to wall pinning (sec. 5.6) if can be deduced from the model that the relation $p = K \tau_B^2$ must be valid (pinning dominated wall motion). These models completely account for the most frequently occurring $\varkappa$ values measured in sec. 3.4: the cross-tie wall behaves as a flexible one and hence yield $\varkappa = 1.5$; to the Barkhausen jumps of a rigid Bloch wall the model of sec. 5.6 applies, consequently, in a sample having this wall structure we find $\varkappa = 2$.

Chapter 4 presents measurements of the Barkhausen jumps along the hysteresis loop which are compared with similar measurements carried out on bulk samples by other investigators. In thin films the Barkhausen effect along the loop is almost identical to that in bulk samples. In this chapter we also discuss the stationarity of the Barkhausen noise, which has been investigated for the

first time. Our measurements have revealed that the sig-
nal can be considered stationary provided that the sus-
ceptibility is almost constant.

In chapter 6 the measured frequency-density functions
are used for calculating the spectral noise intensity of
the Barkhausen signal. The noise spectra thus calculated
are in reasonable agreement with the measured spectral
noise intensities. From the model of a Barkhausen jump
(sec. 5.3) it can be inferred that the cut-off frequency
f_o of the spectrum should have the same trend as a func-
tion of film thickness as the wall mobility μ which has
indeed been found experimentally.

SAMENVATTING EN CONCLUSIES.

In dit proefschrift worden de resultaten weergegeven van
een onderzoek aan het magnetische Barkhausen-effect in
dunne films van nikkel ijzer (80% Ni, 20% Fe). Deze mag-
netisch uniaxiale films hebben een twee-dimensionale mag-
netische domeinstructuur. Het onmagnetisatie proces in de
gemakkelijke richting vindt volledig plaats door domein-
wandbeweging. Het Barkhausenproces, i.e. de discontinue
domeinwandbeweging ten gevolge van inhomogeniteiten in
het magnetisch materiaal, werd onderzocht tijdens het
doorlopen van de hysteresislus in de gemakkelijke richting.
In deze preparaten is het mogelijk een verband te leggen
tussen de Barkhausen ruis en het micromagnetisch gedrag.

Een groot aantal preparaten werd onderzocht waarvan het
coërcitief veld en de sterkte van de uniaxiale anisotropy
varieerden. Bovendien varieerde de filmdikte tussen 420
en 2800 Å. Als functie van de dikte verandert de struc-
tuur van de magnetische domeinwand. In de dikkere films
(met een dikte groter dan 900 Å) komen Blochwanden voor,
die een grote wandstijfheid bezitten en in dunnere films
(met een dikte tussen 400 Å en 900 Å) komen flexibele
cross-tiewanden voor. We kunnen dus in deze samples de
invloed van de wandstructuur op het Barkhausen-effect
onderzoeken. Hiervoor hebben we het Barkhausen-effect zo-
wel in het tijddomein als ook in het frequentiedomein on-
derzocht: de frequentiedichtheids-functies van de para-
meters van het Barkhausen-effect zijn bepaald (hoofdstuk
3) en de spectrale ruisintensiteit is gemeten (hoofdstuk 6).

Uit onze metingen (par. 3.4) volgt dat een relatie aanwe-
zig is tussen de duur τ_B en de grootte p van een Bark-
hausensprong. De Barkhausensprongen in een preparaat vol-
doen aan een relatie van de vorm: $p \propto \tau_B^{\varkappa}$. In onze prepa-
raten overheersen twee waarden van $\varkappa$,nl. $\varkappa = 2$ en $\varkappa = 1.5$.
De experimenten tonen aan dat in dikkere films (met een
dikte groter dan 900 Å) de waarde $\varkappa = 2$ en in dunnere
films (met een dikte tussen 400 Å en 900 Å) de waarde
$\varkappa = 1.5$ meestal wordt gevonden. Uit een vergelijking van
de experimenteel gevonden $\varkappa$ waarden met de wandstructuur
(par. 2.2.3), welke in samples van verschillende dikte
voorkomt, volgt dat in de magnetische films met Bloch-
wanden het Barkhausen-proces gekarakteriseerd kan worden
door $\varkappa = 2$ en in films met cross-tiewanden door $\varkappa = 1.5$.

In hoofdstuk 5 is het proces van de domeinwandpinning glo-
baal beschreven en zijn er modellen opgesteld voor de Bark-
hausensprongen van een domeinwand. Voor een proces, waar-
bij de wandbeweging stopt t.g.v. de eindige wandkromming
van een buigzame wand (par. 5.5) geeft het model de vol-
gende relatie $p = K \tau_B^{1.5}$ (stiffness-dominated wall motion).
Voor een proces, waarbij de beweging van een stijve rechte
wand stopt t.g.v. wandpinning (par. 5.6) volgt uit het mo-
del dat de relatie $p = K \tau_B^2$ moet gelden (pinning-dominated
wall motion). Deze modellen verklaren volledig de in par.
3.4 gemeten, meest voorkomende $\varkappa$ waarden: de cross-tiewand
gedraagt zich als een flexibele wand en geeft dus $\varkappa = 1.5$;
voor de Barkhausensprongen van een starre Blochwand geldt
het model van par. 5.6, in een preparaat met deze wand-
structuur vinden we dus $\varkappa = 2$.

In hoofdstuk 4 zijn metingen van de Barkhausensprongen
langs de hysteresislus gepresenteerd en vergeleken met
soortgelijke metingen van andere onderzoekers aan bulk
samples. Het Barkhausen effect langs de lus gedraagt zich
in dunne films vrijwel hetzelfde als in bulk samples. In
dit hoofdstuk is ook voor het eerst de stationairiteit van
het Barkhausen-effect experimenteel onderzocht. Uit onze

metingen volgt dat het signaal als stationair beschouwd
kan worden zolang de susceptibiliteit vrijwel constant is.

In hoofdstuk 6 zijn de gemeten frequentiedichtheidsfunc-
ties gebruikt voor de berekening van de spectrale ruis-
intensiteit van de Barkhausen ruis. De aldus berekende
ruisspectra stemmen goed overeen met de gemeten spectrale
ruisintensiteiten. Uit het model van een Barkhausensprong
(zie par. 5.3) volgt dat de afsnijfrequentie f_o van het
spectrum eenzelfde verloop als functie van de filmdikte
moet hebben als de wandbewegelijkheid μ. Dit is inderdaad
experimenteel ook gevonden.

CURRICULUM VITAE

19 dec. 1946   Geboren te Wieringen.

1960-1966   Gymnasium β gevolgd aan het Murmellius
Gymnasium te Alkmaar.

1966-1973   Studie aan de Technische Hogeschool te
Delft, alwaar op 8 maart 1973 het docto-
raal examen electrotechnisch ingenieur
werd behaald (met lof). Afstudeerwerk
onder leiding van Prof.Dr.Ir.S.Middelhoek
met als onderwerp "Bubbles domains in (112)
Gd I Garnet Slabs".

1 april 1973 -   Wetenschappelijk medewerkster bij de
1 juli 1977   Technische Hogeschool Eindhoven. Werkzaam
in de vakgroep Electrotechnische Materiaal-
kunde onder leiding van Prof.Dr.F.N.Hooge.

1 juli 1977 -   Wetenschappelijk medewerkster bij het
heden   Natuurkundig Laboratorium van de N.V.
Philips Gloeilampenfabrieken te Eindhoven.
Werkzaam in de groep Magnetic Devices on-
der leiding van Dr.Ir.W.F.Druyvesteyn.

27 october 1978 In het huwelijk getreden met
Ir. Luit Wieringa.

DANKBETUIGING

behorende bij het proefschrift van

N.J. Wiegman

I   Het voordeel van de hogere toelaatbare temperatuur in
    vermogenskunststofkabels van vernet (cross-linked)
    polyetheen t.o.v. gewoon polyetheen moet bij ligging
    in de grond vooral gezocht worden in zijn vermogen om
    kortsluitstromen en kortdurende piekbelastingen beter
    te weerstaan en eigenlijk niet in de hogere toelaat-
    bare continue belasting.

    - J.Th.J. Beeren, A.F.G. Jacobs, J. Vermeer, G.M.L.M. van de Wiel,
      Elektrotechniek 56, 1978, p. 579-587.

II Magnetisch geladen wanden kunnen hoogstwaarschijnlijk
    niet voorkomen in orthorhombische-granaatfilms. Het
    feit dat orthorhombische granaatfilms hierdoor onge-
    schikt zouden kunnen zijn voor propagatie van magne-
    tische bubbles met behulp van geïmplanteerde structuren
    vormt geen enkele beperking voor de toepassing in
    hoogfrequent bubblegeheugens.

    - E.H.L.J. Dekker, N.J. Wiegman, K.L.L. van Mierloo,
      R. de Werdt, J.Appl.Phys. 50, 1979, p.2277-2279
    - A.H. Bobeck, S.L.Blank, A.D. Butherus, F.J. Caik,
      W. Strauss, Bell Syst.Techn.J. 58, 1979, p.1453-1540.

III Het vernetten van polyetheen kabels voor het midden-
    spanningsgebied d.m.v. hete stikstof (dry curing)
    i.p.v. met hete stoom (steam curing) vormt een beter
    fabricageproces, waarbij bovendien het indringen van
    vocht in de isolatie tijdens het fabricageproces gro-
    tendeels wordt vermeden. Dit laatste wordt echter bij
    de huidige opbouw van de kunststofkabels ten onrechte
    als verkoopargument gebruikt.

    - M. Aaltonen, Wire J. 11, juni 1978, p.64-68
    - J.A. Wiersma, Electra (Parijs) 55, dec. 1977, p.25-38.

IV De doorbraak bij de toepassing van Röntgenstraling in lithografische processen voor submicron structuren wordt bemoeilijkt door het fundamentele probleem dat de massa-absorptiecoëfficient van de lakken en van het transparante deel van het masker van dezelfde orde van grootte zijn.

V   Door de snelle toename van de pakkingsdichtheid van conventionele bubblegeheugens en de extra problemen die opgelost moeten worden bij de geheugens die gebruik maken van bubbleroosters valt het te betwijfelen of het zinvol is aan bubbleroostergeheugens te werken zolang met de conventionele geheugens nog grotere pakkingsdichtheden bereikt kunnen worden.

VI Het komt veelvuldig voor dat bij warmte-isolatie van gebouwen de spouw zodanig opgevuld wordt met isolerend materiaal dat er geen voldoend dikke luchtlaag tussen isolatie en buitenmuur blijft bestaan. In deze gevallen is het twijfelachtig of op den duur de aanwezigheid van de spouwmuurisolatie nog enige energiebesparing oplevert.

VII De relatie tussen de grootte en de tijdsduur van Barkhausensprongen hangt in dunne Ni-Fe films af van de structuur van de magnetische domeinwand.
    - Hoofdstuk 5 van dit proefschrift.

VIII Het storende effect van Barkhausenruis in devices kan verminderd worden door het vergroten van het aantal magnetische domeinen of door ervoor te zorgen dat wandbeweging niet plaats kan vinden.

IX In verband met de verkeersveiligheid dient de ontgrendeling van de autogordels gestandaardiseerd te worden.

X   Voor het verkrijgen van informatie over het micro-
scopische magnetisatie proces is het meten van de
spectrale ruisintensiteit van het Barkhausen-effect
een weinig zinvolle bezigheid.
Hoofdstuk 6 van dit proefschrift.

XI   Het effect van de wet op gelijke beloning van man
en vrouw wordt wat betreft de werkende gehuwde vrouw
ernstig aangetast door de grote ongelijkheid in de
positie van echtgenoten in de Nederlandse belasting
wetgeving.

Waalre, 6 November 1979